様式 2-4-1

日米科学技術協力事業「脳研究」分野
グループ共同研究実施報告書　　〔研究分野：　　〕

１．グループ共同研究代表者
所属機関・職名・氏名
群馬大学大学院医学系研究科・教授・白尾　智明

２．研究課題名

中枢神経シナプス後部におけるグルタメート受容体のアクチン細胞骨格依存性集積機構

３．日本側グループ組織（代表者及び分担者の所属・職・氏名）
代表者　群馬大学医学部・教授・白尾智明
分担者　群馬大学医学部・助教授・関野祐子
分担者　群馬大学医学部・助手・山崎博幸
分担者　群馬大学医学部・大学院生・小林千穂
分担者　北里大学医療衛生学部生理学・教授・佐治真理
分担者　北里大学医療衛生学部生理学・助手・緒方雅則

４．米国側グループ組織（代表者及び分担者の所属・職・氏名）
代表者　ニューヨーク大学神経科学センター・準教授・Chiye Aoki
分担者　マサチューセッツ工科大学脳認知科学講座・準教授・Yasunori Hayashi

５．研究期間　平成１５年　４月　１日～平成１８年　３月３１日

６．研究の概要，成果及び意義（1000 字）
シナプス可塑性は認知・学習の神経機構の重要な素過程である。シナプス後部のグルタメート受容体の制御機構はその中心をなすものと考えられ、従来より集中的に研究が行われてきた。また、形態的シナプス可塑性との関連で樹状突起スパインの細胞骨格に関する研究が進んできた。これらの研究は、細胞骨格の変化が直接グルタメート受容体のシナプス後部膜へのトラフィッキングに重要な役割を果たしうることを示唆している。ドレブリン A は神経細胞特異的なアクチン結合蛋白であり、樹状突起スパインの唯一の細胞骨格であるアクチン細胞骨格の特徴を決定している。本研究では、生体脳におけるドレブリン A の機能を免疫電子顕微鏡および薬理学的に解析し、その結果を培養系を用いたドレブリン A 機能の解析結果と総合して、ドレブリン A およびドレブリン A 結合アクチン細胞骨格の NMDA 型グルタミン酸受容体の集積機構における役割を解明することを目指した。生体動物脳を用いた実験から（1）ドレブリン A の樹状突起膜直下への集積がシナプス形成の最初期に起きること（JCN,2005）、（2）ドレブリン A はシナプス部においては、興奮性シナプス後部にのみ出現し、興奮性シナプス前部や抑制性シナプスに存在しないこと（JCN. 2005）、（3）ドレブリン A はコントロール動物では興奮性シナプスの約 3／4 に出現し、その割合は NMDA 型グルタメート受容体を阻害すると有意に増加すること（Neurosci. 2006）、（4）ドレブリン A 陽性スパインは大型のスパインが多いこと（論文作成中）がわかった。また、培養細胞を用いた実験から、（1）ドレブリン A を幼弱細胞に発言させてもスパイン形成は誘導されず、その代わり巨大なフィロポディア（メガポディア）が形成されること（MCN, 2005）、（2）成熟神経細胞でドレブリン A 発現を阻害すると神経活動依存性の NMDA 型グルタミン酸受容体のシナプス集積（Synaptic Scaling）が抑制されること（JNC, 2006）を見出した。これらの結果は、ドレブリン A およびドレブリン A 結合型のアクチン細胞骨格と NMDA 型グルタメート受容体の間には

相互の強い制御機構があることを示唆している。近年、Synaptic Scaling はシナプスの長期的な変化ばかりでなく短期的なシナプス可塑性における役割も示唆されている。本研究で明らかとなったグルタメート受容体のシナプス後部膜へのトラフィッキング機構におけるアクチン細胞骨格系の役割は、シナプス可塑性ばかりでなくシナプス形成の基本メカニズム解明に寄与するとともに、高次神経機能障害の診断、治療への応用の可能性が考えられる。

7．その他（実施上の問題点，特記事項等）

無し

◎参考資料があれば，添付ください。
論文別刷り（PDF ファイル）４編

1. Aoki, C., Sekino, Y., Hanamura, K., Fujisawa, S., Mahadomrongkul, V., Ren, Y., and Shirao, T. "Drebrin A is a Postsynaptic Protein that Localizes in vivo to the Submembranous Surface of Dendritic Sites Forming Excitatory Synapses" ***J. Comp. Neurol***. 483: 383-402 . (2005)
2. Mizui, T., Takahashi, H., Sekino, Y., and Shirao, T. "Overexpression of drebrin A in immature neurons induces the accumulation of F-actin and PSD-95 into dendritic filopodia, and the formation of large abnormal protrusions." ***Mol. Cell. Neurosci.*** 30: 149 – 157 (2005)
3. Fujisawa, S., Shirao, T., Aoki, C. "In vivo, competitive blockade of NMDA receptors induces rapid shape change of post-synaptic spines and F-actin reorganization within dendritic spines of adult rat cortex." ***Neuroscience*** 140:1177-1187 (2006)
4. Takahashi, H., Mizui T. and Shirao, T. "Downregulation of drebrin A expression suppresses synaptic targeting of NMDA receptors in developing hippocampal neurons" ***J. Neuochem*** 97(s1):110-115 (2006)

THE JOURNAL OF COMPARATIVE NEUROLOGY 483:383–402 (2005)

Drebrin A Is a Postsynaptic Protein That Localizes In Vivo to the Submembranous Surface of Dendritic Sites Forming Excitatory Synapses

CHIYE AOKI,[1]* YUKO SEKINO,[2,3] KENJI HANAMURA,[2] SHO FUJISAWA,[1] VEERAVAN MAHADOMRONGKUL,[1] YONG REN,[2] AND TOMOAKI SHIRAO[2]*
[1]Center for Neural Science, New York University, New York, New York 10003
[2]Department of Neurobiology and Behavior, Gunma University Graduate School of Medicine, Maebashi, Gunma 371-8511, Japan
[3]Core Research for Evolution Science and Technology, Japan Science and Technology Corporation, Kawaguchi 332-0012, Japan

ABSTRACT

Drebrin A is a neuron-specific, actin binding protein. Evidence to date is from in vitro studies, consistently supporting the involvement of drebrin A in spinogenesis and synaptogenesis. We sought to determine whether drebrin A arrives at the plasma membrane of neurons, in vivo, in time to orchestrate spinogenesis and synaptogenesis. To this end, a new antibody was used to locate drebrin A in relation to electron microscopically imaged synapses during early postnatal days. Western blotting showed that drebrin A emerges at postnatal day (PNd) 6 and becomes progressively more associated with F-actin in the pellet fraction. Light microscopy showed high concentrations of drebrin A in the synaptic layers of the hippocampus and cortex. Electron microscopy revealed that drebrin A in these regions is located exclusively in dendrites both neonatally and in adulthood. In adulthood, nearly all of the synaptic drebrin A is within spines forming asymmetric excitatory synapses, verified by γ-aminobutyric acid (GABA) negativity. At PNd7, patches of drebrin A immunoreactivity were discretely localized to the submembranous surfaces of dendrites forming slight protrusions—protospines. The drebrin A sites exhibited only thin postsynaptic densities and lacked axonal associations or were contacted by axons that contained only a few vesicles. Yet, because of their immunoreactivity to the NR2B subunit of *N*-methyl-D-aspartate receptors and immunonegativity of axon terminals to GABA, these could be presumed to be nascent, excitatory synapses. Thus, drebrin A may be involved in organizing the dendritic pool of actin for the formation of spines and of axospinous excitatory synapses during early postnatal periods. J. Comp. Neurol. 483:383–402, 2005.

Indexing terms: synaptogenesis; F-actin; NR2B; NHDA receptor; cortex; hippocampus; electron microscopy; spinogenesis; proto-spines

Drebrins are F-actin binding proteins, first identified by their surging expression during synaptogenesis (Shirao et al., 1988; Shirao, 1995). Two isoforms of drebrin occur in mammals—drebrin E (embryonic form) and drebrin A (adult form; Shirao and Obata, 1986; Shirao et al., 1989; Hayashi et al., 1998), generated by alternative mRNA splicing from a single gene (Kojima et al., 1993). Both are expressed in neurons, but only drebrin A is neuron-specific (Shirao and Obata, 1986). Their cellular distributions have been studied using a monoclonal antibody, M2F6, that recognizes both the adult and embryonic isoforms. Within non-neuronal cells, drebrin E colocalizes with actin stress fibers along sites adhering to the substratum (Asada et al., 1994; Peitsch et al., 1999), while in cultured neurons, drebrins E and A localize to spines (Shirao et al., 1987; Hayashi et al., 1996), together with F-actin (Takahashi et al., 2003). Transfection of non-neuronal cells with drebrin A-cDNA leads to enhanced adhesion of these cells to the substratum (Ikeda et al.,

Grant sponsor: Ministry of Education, Science, Sports, and Culture of Japan; Grant number: Grants-in-Aid 12053209; Grant number: Japan Foundation for Aging and Health; Grant sponsor: National Institutes of Health; Grant number: R01-NS41091; Grant number: R01-EY13145; Grant number: P30 EY13079.

Drs. Aoki and Sekino contributed equally to this work.

*Correspondence to: Chiye Aoki, Center for Neural Science, New York University, 4 Washington Place, New York, NY 10003. E-mail: chiye@cns.nyu.edu or Tomoaki Shirao, Dept. of Neurobiology and Behavior, Gunma University Graduate School of Medicine, 3-39-22, Showamachi, Maebashi, 3718511. E-mail: tshirao@med.gunma-u.ac.jp

Received 5 July 2004; Revised 24 September 2004; Accepted 27 September 2004

DOI 10.1002/cne.20449

Published online in Wiley InterScience (www.interscience.wiley.com).

1995) and the appearance of neurite-like processes (Shirao et al., 1992), while transfection of cultured hippocampal neurons with drebrin A-cDNA causes dendritic spines to elongate (Hayashi and Shirao, 1999). These observations indicate that drebrin A may be involved in neurite extension and spine formation. Within cultured neurons, the arrival of drebrin A in spines precedes the arrival of PSD-95, and suppression of drebrin A using antisense oligonucleotide prevents the formation of PSD-95 clusters within spines (Takahashi et al., 2003). These more recent observations indicate that the molecular maturation of protospines into mature spines may be governed by the formation of drebrin A–actin complexes.

The two drebrin isoforms can be distinguished by using Western blots. Within the cortex and the hippocampus, drebrin E is the major isoform expressed in rat brains at postnatal day 7 (PNd7) and the slightly larger drebrin A isoform becomes more prevalent by PNd21 (Hayashi et al., 1998). These observations suggest a rapid conversion of drebrin isoforms during the phase of spine and synapse formation. Might the embryonic isoform, drebrin E, be involved in the initial formation of protospines or filopodia, with the adult isoform, drebrin A, taking over the subsequent steps to govern the molecular maturation of protospines? If so, one would predict that drebrin A appears only after the establishment of morphologically identifiable spine heads and that drebrin A remains in spines after synapses have become established.

In this study, the emergence of drebrin A within intact cortex and hippocampus was examined by using a newly generated antibody, DAS2. Unlike its predecessor, M2F6, DAS2 recognizes drebrin A selectively and does not recognize drebrin E. Also, unlike DAS1, the previously made anti-drebrin A antibody (Shirao et al., 1994), DAS2 is compatible with immunocytochemistry. Using DAS2, electron microscopy was used to analyze the distribution of drebrin A in relation to newly forming synapses. Within the cortex and hippocampus of postnatal day (PNd) 7 rats, newly forming presumptive synapses could be distinguished from well-established excitatory synapses, based on the scarcity of vesicles within the abutting axons, absence of postsynaptic densities (PSDs), and/or absence of spine necks. Adult tissue was also sampled for determining whether drebrin A occurs exclusively at asymmetric excitatory synapses or across a mixture of excitatory, inhibitory, and neuromodulatory synapses.

MATERIALS AND METHODS

Animals

For the light and electron microscopic studies, Wistar rats were purchased from Charles River and bred in the NYU animal center in accordance with the guidelines published in the NIH Guide for the Care and Use of Laboratory Animals. For the biochemical analyses, male Wistar rats at PNd 0, 2, 4, 6, 8, 10, 12, 14, 16, 18, and 20, and at 15-weeks postnatal were used. These Wistar rats were housed in the animal center of Gunma University Graduate School of Medicine.

All experiments were carried out according to the Animal Care and Experimentation Committee of Gunma University, Showa Campus and of New York University.

Subcellular fractionation

Animals were deeply anesthetized with ether inhalation and the specified brain regions were removed. Each tissue was homogenized by sonication in 10 volumes of 5 mM Tris-HCl, pH 7.5, 150 mM NaCl, 0.5 mM dithiothreitol, 1% NP-40, and protease inhibitors (1 μM leupeptin, 250 μM phenylmethyl sulfonyl fluoride, 2 μM pepstatin), yielding the crude fraction. The crude fraction was then centrifuged at 200,000 × *g* for 60 minutes at 4°C (Optima TLX Ultracentrifuge, Beckman Instrument, Fullerton, CA), so as to bring down the F-actin in the pellet fraction but to retain actin monomers (G-actin) in the supernatant (Fox, 1985; Crosbie et al., 1991). The supernatant thus obtained was considered a mixture of the cytosolic fraction plus some portion of the membranous proteins solubilized by NP-40. The pellet was washed once and suspended directly with the sodium dodecyl sulfate (SDS) sample buffer in preparation for Western blotting. For extraction experiments, the pellet was again homogenized by sonication in 10 volumes of the high salt buffer containing 1 M NaCl and was then centrifuged at 200,000 × *g* for 60 minutes at 4°C.

Use of the three anti-drebrin antibodies in Western blots to characterize the developmental changes in the expression of drebrin isoforms across brain regions

For the detection of specific isoforms of drebrin, the Western blot membranes were probed with the M2F6 monoclonal antibody (Medical and Biological Laboratories, Japan), previously shown to recognize both the E and the larger A isoforms (Shirao et al., 1994). Alternatively, the expression level of drebrin A was probed using the polyclonal antibody DAS1, which recognizes the amino acid sequences unique to the A isoform: 319–335, 342–353, and 354–363 (Shirao et al., 1994).

Because DAS1 was shown not to be compatible with immunocytochemistry, a new polyclonal antibody, DAS2, was generated for the present study. DAS2 was directed against peptide Phe-Ile-Lys-Ala Ser-Asp-Ser-Gly-Pro-Ser-Ser-Ser (residues 325–336) that is also unique to the adult form of drebrin (Shirao et al., 1992). DAS2 was purified by epitope selection, using the above polypeptide.

Proteins from equal wet weights of tissue were separated by polyacrylamide SDS gel electrophoresis and transferred to an Immobilon-P membrane (Millipore, Bedford, MA). Detection of immunoreactive bands was made using the ECL Western Blotting analysis system (Amersham, Buckinghamshire, UK). Further details of the methods appear elsewhere (Hayashi et al., 1998).

For quantitative analysis, signals were densitometrically quantified by the NIH-Image analysis system. Data were statistically analyzed by the Student's *t* test. All of the data were presented as a mean ± SEM.

Preparation of tissue for light and electron microscopy

Nine adult and 10 PNd7 Wistar rats were transcardially perfused with a mixture of aldehydes for fixation. All fixatives contained 0.1 M phosphate buffer (PB, pH 7.4) and 4% paraformaldehyde. For three of the adults and four of the neonates, 1% glutaraldehyde was added to the fixative. For two of the adults and three of the neonates, 3% acrolein was added to the fixatives. Slabs of brains

were sectioned in the sagittal or coronal plane, using a Vibratome, and fixation was terminated by reacting free-floating sections with 1% sodium borohydride made in 0.1 M PB. Sections were stored at 5°C, free-floating in a solution consisting of 0.9% sodium chloride (saline), 0.01 M phosphate buffer (pH 7.4), and 0.05% sodium azide (PBS–azide) to prevent bacterial growth.

Immunocytochemistry

The silver-intensified gold (SIG) was chosen as the label to optimize subcellular localization of drebrin A, while the horseradish peroxidase–diaminobenzidine (HRP-DAB) reaction product was used to maximize detection of drebrin A (Aoki et al., 2000). For both labeling procedures, sections were first treated to terminate the aldehyde fixation by immersing in a solution consisting of 1% hydrogen peroxide mixed in 0.1 M PB at room temperature for 30 minutes. These sections were incubated in a solution consisting of 0.01 M PB, saline (0.9% NaCl), and containing 1% bovine serum albumin (BSA) to minimize background immunolabeling and 0.05% sodium azide to minimize bacterial growth in the buffer. After preincubating sections for a minimum of 30 minutes, free-floating sections were incubated in the primary antibody solution, consisting of a 1:1,000 dilution of DAS2 in PBS–BSA–azide. The incubation was for 1 to 4 days at room temperature, under constant, gentle agitation. For immunolabeling that used the HRP reaction product as the label, the standard ABC Elite kit from Vector was used. For sections immunolabeled using SIG as the label, sections were incubated in a solution containing a 1:100 dilution of colloidal gold (0.8 nm) -conjugated goat anti-rabbit IgG, produced by Aurion (EM Sciences). The electron microscopy-grade silver-intensification kit (IntenSEM, Amersham) was used to enlarge the gold particles to sizes detectable by electron microscopy. Further details were as described previously (Aoki et al., 2000).

To determine whether the drebrin A-immunoreactive sites are contacted by glutamatergic or γ-aminobutyric acid (GABA)ergic terminals, two ultrastructural immunocytochemical tests were performed. One was to probe for the coexistence of drebrin A with the NR2B subunit of *N*-methyl-D-aspartate (NMDA) receptors along the postsynaptic membrane. The other was to probe for the presence of GABA within the axons positioned presynaptically to the drebrin A-site. The immunodetection of GABA and the NR2B subunits followed Phend's postembedding gold immunolabeling procedure (PEG; Phend et al., 1995) but with slight modifications, as described previously (Erisir et al., 2001; Fujisawa and Aoki, 2003). The NR2B subunit antibody was purchased from Upstate Technology (New York) and used at a dilution of 1:40. The rabbit anti-GABA antibody was purchased from Sigma and used at a dilution of 1:1,000.

Controls for immunocytochemistry

Specificity of the drebrin A antibody, DAS1, has been published previously (Shirao et al., 1994). Selectivity of the new anti-drebrin A antibody, DAS2, to drebrin A was determined by verifying that the antibody recognized a single band in Western blots (Fig. 1, right) corresponding to the upper of the two bands recognized by the monoclonal antibody, M2F6. In a previous study, the two bands recognized by M2F6 were shown to be drebrin E (lower band) and drebrin A (upper band; Shirao et al., 1994).

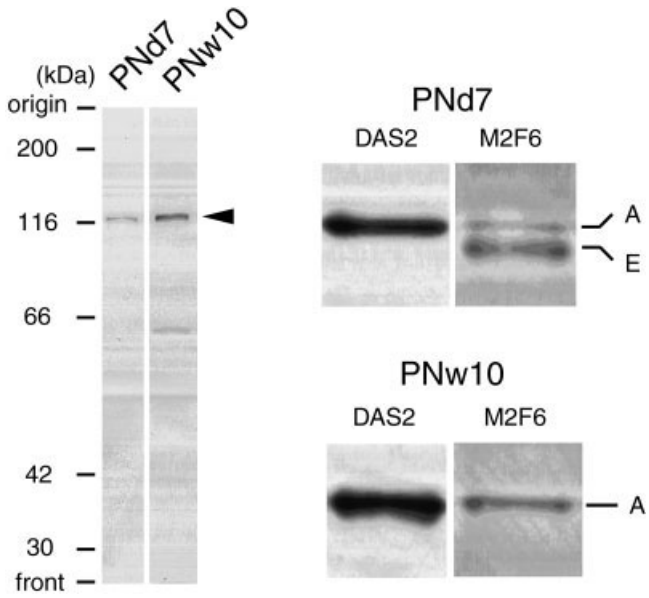

Fig. 1. Specificity of the new drebrin A antibody, DAS2 as revealed by Western blotting. The protein extract equivalent to 0.20 mg of wet weight tissue was analyzed by Western blotting. Left column: Western blot analysis using 8% gel showed that DAS2 antibody recognized a single band (arrowhead), both in postnatal day 7 (PNd7) and postnatal week 10 (PNw10) rat hippocampi. Right column: Top panel is a Western blot of PNd7 rat hippocampus using 5% gel. The monoclonal antibody M2F6 detected a faint band of drebrin A (A, upper band) in addition of major band of drebrin E (E, lower band), as reported earlier (Shirao et al., 1989; Imamura et al., 1992). DAS2 antibody recognized drebrin A but not drebrin E. Bottom panel: Western blot of PNw10 hippocampus. Both of M2F6 and DAS2 antibodies detected a single band.

Within homogenates prepared from hippocampi of PNd7 and postnatal week 10 (PNw10), the new DAS2 antibody did not recognize any protein band other than drebrin A (left column of Fig. 1).

Further controls for immunocytochemistry were performed using sections that were semiadjacent to the ones used for immunocytochemistry. The control sections were treated exactly as described under the Immunocytochemistry section above, except that the primary antibody was omitted. This resulted in complete elimination of immunoreactivity for drebrin A, GABA, and the NR2B subunit of NMDA receptors. In addition, preadsorption control for the DAS2 antibody was performed. As noted above, DAS2 was purified by epitope selection, using the synthetic polypeptide corresponding to the amino acid sequence unique to drebrin A. The same synthetic peptide was added to the DAS2 antibody solution at a concentration of 1 mg/ml at 37°C for 1 hour to preadsorb the primary antibody. The preadsorption caused great reduction of immunoreactivity within semiadjacent sections (further details described under the Results section).

Specificity of GABA labeling was further verified electron microscopically, based on the abundance of PEG within axon terminals forming axosomatic symmetric synapses and the relative scarcity of PEG with axon terminals forming asymmetric axospinous synapses (less than 1/30th of the colloidal gold/terminal content observed at symmetric synapses). This outcome was similar to the

results shown previously from this laboratory (Erisir et al., 2001) and by others (Megias et al., 2001).

Viewing of immunocytochemically stained sections

Sections were mounted on slides, coverslipped, and viewed using the light microscope. For electron microscopy, sections were further fixed using 1% osmium tetroxide, embedded in Embed 812, ultrathin-sectioned, and viewed under the JEOL 1200XL electron microscope. HRP-labeled sections were viewed without counterstaining, so as to optimize detection of low levels of reaction products along the membrane. SIG-labeled sections were counterstained with Reynold's lead citrate, because SIG labels could still be identified against the contrast-enhanced images of the neuropil. Images were captured both on film and digitally by using the Hamamatsu CCD camera from AMT (Boston, MA).

Ultrastructural analysis

Samples from the neocortex and hippocampus of five adult brains and four neonatal brains were collected for ultrastructural analyses, using an electron microscope. Digitally captured images were used to quantify the areal density of synaptic junctions and of immunolabeled processes, using the Hamamatsu CCD camera and the data acquisition system of AMT.

Processes were identified as axon terminals, based on the presence of vesicles and absence of microtubules. Conversely, dendritic shafts were identified by the absence of vesicles and, most often, also by the presence of microtubules. The putatively postsynaptic sites within neonatal tissue were identified by their juxtaposition to processes that were more clearly identifiable as axonal processes.

Where possible, junctions were identified as symmetric vs. asymmetric, based on the absence vs. presence, respectively, of PSDs. Junctions were also identified as forming on a dendritic shaft vs. a spine. The spines were distinguished from shafts, based on the absence of mitochondria or of microtubules or of vesicles in the cytoplasm.

The morphological criteria used to judge a synapse as mature and asymmetric were as follows: Parallel alignment of the dendritic and axonal plasma membranes; a collection of vesicles that are closely bounded by the plasma membrane or clustered near the presynaptic plasma membrane; presence of the PSD; and narrowing of the neck, if the synapse was on a spine. All of the axospinous junctions within adult tissue exhibited all of these characteristics, whereas few within PNd7 tissue exhibited all of these characteristics. This finding indicated that our criteria were useful for discriminating immature from mature synapses. Most of the asymmetric synapses of PNd7 tissue showed one or more of the following features: spine heads in which the neck was not narrowed; PSDs that are detectable but thin; and presynaptic profiles with only a few vesicles, most of which were at sites removed from the junction. Intercellular junctions exhibiting any of these features were categorized as presumptive immature synapses.

In neonatal tissue only, processes sometimes came in direct contact and were immunolabeled at contact sites but neither side could be identified as axonal or dendritic. These were categorized as junctional but were excluded from the "presumptive immature synapse" category. Protrusions along the plasma membrane of dendrites for which the axonal partner could not be identified were referred to as nonjunctional protospines and also excluded from the presumptive immature synapse category.

Within adult tissue, synapses on dendritic shafts and somata sometimes lacked PSDs. These were categorized as symmetric synapses. Within PNd7 tissue, only those synapses exhibiting more than four vesicles near the cleft, yet lacking PSDs, were categorized as symmetric and mature.

The synapse categories described above are congruent with previously accepted categories for symmetric (inhibitory) and asymmetric (excitatory) synapses within adult and developing tissue (Purpura and Pappas, 1972; Vaughn, 1989; Harris, 1999; Megias et al., 2001; Marty et al., 2002; Peters, 2002; Minelli et al., 2003).

Quantitative analysis of synapses

Quantitative analysis of HRP-labeled adult tissue was performed upon immunolabeled synaptic profiles collected from 36 nonoverlapping fields, with each field encompassing 12.25 μm^2. We determined the proportion among the encountered synapses that were or were not labeled, labeled pre- or postsynaptically, at an asymmetric or a symmetric synapse, and formed on a dendritic spine or a dendritic shaft. Quantitative analysis of HRP-labeled PNd7 tissue was performed similarly, by categorizing the randomly encountered synapses from 26 nonoverlapping fields into groups that were or were not labeled, labeled pre- or postsynaptically, at a symmetric or an asymmetric synapses, and with immature or mature morphological features.

Further quantitative analysis was performed for the cortex. Comparisons across the two ages (PNd7 vs. adult) was made by dividing the encountered synapses randomly into 10 groups for the PNd7 tissue and into 13 groups for the adult tissue, calculating the percentage of synapses encountered (mature or immature) for each group that were immunolabeled or not immunolabeled. Unpaired *t* test (two-tailed) was performed to determine whether the mean percentage value of unlabeled synapses was different across the two ages.

Quantitative analysis of the proximity of drebrin A immunoreactivity to the plasma membrane

The nondiffusible immunolabel, SIG, was used to analyze the proximity of drebrin A immunoreactivity to the plasma membrane. SIG-labeled tissue were sampled from two PNd7 and two adult brains. The proximity of SIG particles to the plasma membrane was assessed by measuring the distance, in nanometers, from the center of the silver grains to the inner surface of plasma membranes. The proximity of SIG particles to the plasma membrane, relative to the diameter of the immunolabeled profiles, was also assessed. Histograms were prepared, based on 250 SIG particles collected from 39 nonoverlapping fields of adult tissue and 80 SIG particles collected from 14 nonoverlapping PNd7 tissues.

Photomicrograph presentation

Images were captured digitally by using AMT System's CCD camera or directly on electron microscopy negatives. The captured images were cropped, contrast-enhanced when needed, and labeled to identify structures using the Adobe Photoshop software (version 6.0).

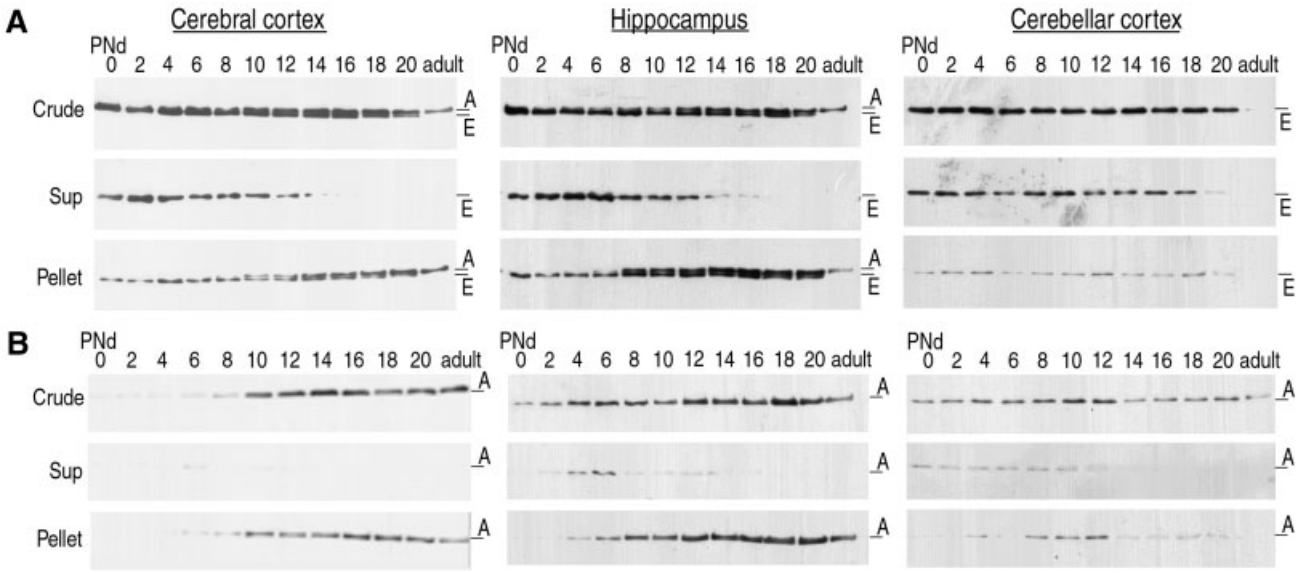

Fig. 2. Developmental changes in drebrin isoforms and subcellular distribution in rat brain as revealed by Western blotting. The supernatant and pellet fractions were obtained from the crude fraction of rat brain at various developmental stages from postnatal day (PNd) 0 to adult (postnatal week 15, PNw15) by centrifugation at 200,000 × *g*. Each fraction, equivalent to 0.23 mg of wet weight tissue, was analyzed in Western blot for the presence of drebrin A and drebrin E. **A:** The drebrin isoforms A and E are detected using the monoclonal antibody M2F6. **B:** The drebrin A-band was detected by using an antibody, DAS1, directed against the amino acid sequence unique to drebrin A (Shirao et al., 1994). Left column is cerebral cortex; middle column is hippocampus; and right column is cerebellar cortex. Details of the procedure appear under the Materials and Methods section.

RESULTS

Developmental change of drebrin isoform expression

We analyzed the developmental change of drebrin isoform expression in the cerebral cortex, hippocampus, and cerebellum. Western blot analysis showed that the expression level of drebrin E in the cortex was relatively constant during the first 2 weeks after birth, based on measurements of immunoreactivity of the lower band using the monoclonal antibody M2F6 (lower band in Crude of Fig. 2A, left column). Immunoreactivity of the lower band decreased gradually and was hardly detectable in adulthood. A similar developmental expression pattern of drebrin was observed in the hippocampus (Crude of Fig. 2A, middle column). In comparison, drebrin E decreased more slowly in the cerebellar cortex (Crude of Fig. 2A, right column) than in the cerebral cortex and or in the hippocampus.

The expression of drebrin A in the cerebral cortex, measured using M2F6 (upper band in Crude of Fig. 2A, left column) or using the drebrin A-specific antibody, DAS1 (Crude of Fig. 2B, left column), increased sharply at around PNd10. The expression of drebrin A also increased in the hippocampus at around the same age (Crude of Fig. 2B, middle column). In the cerebellar cortex, M2F6 barely detected drebrin A throughout development (Crude of Fig. 2A, right column). A faint band for drebrin A, recognized by DAS1, increased at around PNd10 but soon decreased and never showed such sharp increases as was seen for the cerebral cortex or the hippocampus (Crude of Fig. 2B, right column).

Disappearance of drebrin from the supernatant fraction in parallel with neuronal development

To assess the subcellular distribution of drebrin isoforms during postnatal development, homogenates, prepared in the presence of the mild nonionic detergent, NP-40, were fractionated into the supernatant and the pellet fractions by centrifugation. Drebrin E and drebrin A in homogenates of the cortex, the hippocampus, and the cerebellum were analyzed by Western blot. The supernatant was interpreted to be cytoplasmic or membranous, whereas the pellet was interpreted to be bound to organelles, possibly including F-actin (Fox, 1985; Crosbie et al., 1991).

Drebrin E. Before PNd12, drebrin E in cortex was detected in both the supernatant and pellet, using the monoclonal antibody M2F6. However, the protein level in the supernatant fraction decreased rapidly at around PNd14 and was no longer detectable by PNd20 (Sup of Fig. 2A, left column). On the other hand, the level of drebrin E in the pellet fraction was relatively constant until PNd20 (Pellet of Fig. 2A, left column). This developmental change in the subcellular distribution of cortical drebrin E was observed also for the hippocampus and the cerebellar cortex, although the change in the cerebellar cortex was not as sharp (middle and right columns of Fig. 2A).

Drebrin A. The emergence of drebrin A was detectable using the monoclonal antibody M2F6 (Fig. 2A). To investigate the appearance of drebrin A more directly, a polyclonal antibody, DAS1, that recognizes only drebrin A (and not drebrin E; Shirao et al., 1994) was used for the

Western blotting. A faint band of drebrin A in cortex was detected in both the supernatant and the pellet fractions at around PNd6. After PNd10, drebrin A in the cortex was barely detectable in the supernatant fraction but clearly was observed in the pellet fraction (Fig. 2B, left column). Drebrin A in the pellet increased in parallel with postnatal development.

The developmental change in the subcellular distribution of drebrin A in the hippocampus was similar to that in the cerebral cortex. Although drebrin A in the pellet fraction increased in parallel with development, drebrin A in the supernatant fraction disappeared after PNd14 (Fig. 2B, middle column). On the other hand, in the cerebellum, drebrin A in both the supernatant and the pellet fractions decreased after PNd14 (Fig. 2B, right column). Two regions—the cortex and the hippocampus—which showed particularly prominent developmental changes in the amount of drebrin A were chosen for further analysis of the cellular and subcellular distribution of drebrin A.

Light microscopy

Drebrin A immunoreactivity was analyzed throughout the cortical areas and hippocampus of PNd7 and adult tissue, using the newly generated antibody, DAS2 (Fig. 3). All three fixation conditions yielded similar patterns of immunolabeling and, thus, will not be described separately.

PNd7 cortex. PNd7 cortices exhibited a diffuse but darkened band that was midway between the pial surface and the white matter (Fig. 3). At a higher magnification (Fig. 4A1), it was evident that these bandings corresponded to delicate immunolabeling of perikaryal cytoplasm. Immunoreactive primary dendrites emanated horizontally from these perikarya within layer 5. Based on the size and the prominence of their apical dendrite that extended into layer 1 (white arrows in Fig. 4A1), these perikarya were identifiable as layer 5 pyramidal neurons. Layer 1 contained smaller puncta (<0.5 μm in diameter), immediately dorsal to the point where apical dendrites of the layer 5 pyramidal neurons formed tufts (white arrows in Fig. 4A1). The apical tufts and small puncta together formed an intense band within layer 1 (Fig. 3A). The most ventral, immunoreactive band within the cortex (SP in Fig. 3A) consisted of immunolabeled neurons residing immediately dorsal to the corpus callosum. These were multipolar, nonpyramidal neurons of the subplate (also referred to as layer 6b; Fig. 4A2). Some of the immunoreactive processes in this layer appeared long, varicose, and more intensely labeled than were the perikarya in the same tier (white arrows in Fig. 4A2).

Adult cortex. In place of the dark banding that corresponded to layer 5 of the PNd7 cortex, drebrin A immunoreactivity was most dense in layer 1 (Figs. 3A, 4C). At higher magnifications, it became evident that immunoreactivity consisted of uniformly sized puncta, less than 0.5 μm in diameter (Fig. 4B1–3). These puncta were distributed throughout the neuropil but were not detectably associated with the main trunks of dendrites (white arrows in Fig. 4B2,B3) or with neuronal perikarya (white asterisks in Fig. 4B3). Sections immunolabeled using the preadsorbed DAS2 showed complete elimination of the small puncta, whereas the diffuse labeling within the nucleus remained.

PNd7 and adult hippocampus. Labeling of the hippocampus resembled the pattern seen in the cortex. As seen for the PNd7 layer 5 pyramidal neurons, pyramidal neurons in the CA1–CA3 fields and the granule cells in the dentate gyrus exhibited prominent, continuous labeling within dendritic branches at PNd7 (Fig. 3B,C). Also, as seen for the adult cortex, the adult CA1 exhibited high density of immunolabeled puncta, and these puncta were not detectable over the primary dendrites' trunks or neuronal perikarya (Fig. 3D). The immunoreactive puncta were of markedly heightened density in the stratum lacunosum moleculare.

Immunolabeled puncta in stratum lucidum of the CA3 field also were fine, and these coalesced along the surface of major dendritic trunks of the CA3 pyramidal neurons (Fig. 3F). Puncta were even more intense in the stratum oriens of the CA3 field (Fig. 3F). In contrast to the adult cortex, adult pyramidal neurons in the CA3 field and granule cells in the dentate gyrus also retained the neonate-like form of labeling, i.e., continuous labeling within dendrites (Fig. 3E).

The puncta seen in adult tissue matched the sizes of spine heads, and the laminar distribution of the puncta matched the reported laminar distribution of excitatory synapses (Petralia and Wenthold, 1992; Megias et al., 2001; Levy and Aoki, 2002). These puncta were eliminated completely when the DAS2 antibody was preadsorbed. This observation indicated that the puncta reflected discrete, specific immunolabeling. We surmised that the differences seen between the two ages could reflect alteration in the subcellular distribution of drebrin A, as was indicated by the light microscopic and biochemical results, i.e., from the cytoplasm and plasma membrane of dendritic trunks and perikarya to spines. To determine whether drebrin A was localized to the cytoplasm of perikarya and dendritic trunks at PNd7 and became distributed more distally to spine heads in adulthood, electron microscopy was performed. Electron microscopy was also used to analyze the distribution of drebrin A in relation to the newly forming and well-established synaptic junctions within single PNd7 tissue.

Electron microscopy

For electron microscopic analyses, adult cortex and hippocampus were analyzed first, because it was easier to identify axons, dendritic shafts, and dendritic spines within adult tissue than in PNd7 tissue. Within the adult tissue, we aimed to establish whether drebrin A occurred pre- or postsynaptically or on both sides of synapses. The following morphological criteria were used to identify synapses as asymmetric: presence of vesicles, typically clustered into a group of 10 or more, near the synaptic cleft; thick coating along the intracellular surface of the other profile, recognized as the PSD. These were presumed to be excitatory, based on earlier studies that used immunoreactivity of synapses to AMPA and NMDA receptor subunits as indicators (Petralia and Wenthold, 1992; Aoki et al., 1994; Farb et al., 1995; Aoki, 1997; He et al., 1998). In the present study, we also verified that the presynaptic terminals of asymmetric synapses were consistently GABA-negative, based on PEG immunolabeling for GABA upon a subset of grids (Fig. 5A).

Twenty-three percent of the adult cortical synapses lacked PSDs. These will be referred to as symmetric and were presumed to be inhibitory or modulatory (Purpura and Pappas, 1972; Megias et al., 2001; Marty et al., 2002; Peters, 2002; Minelli et al., 2003). Immunolabeling for

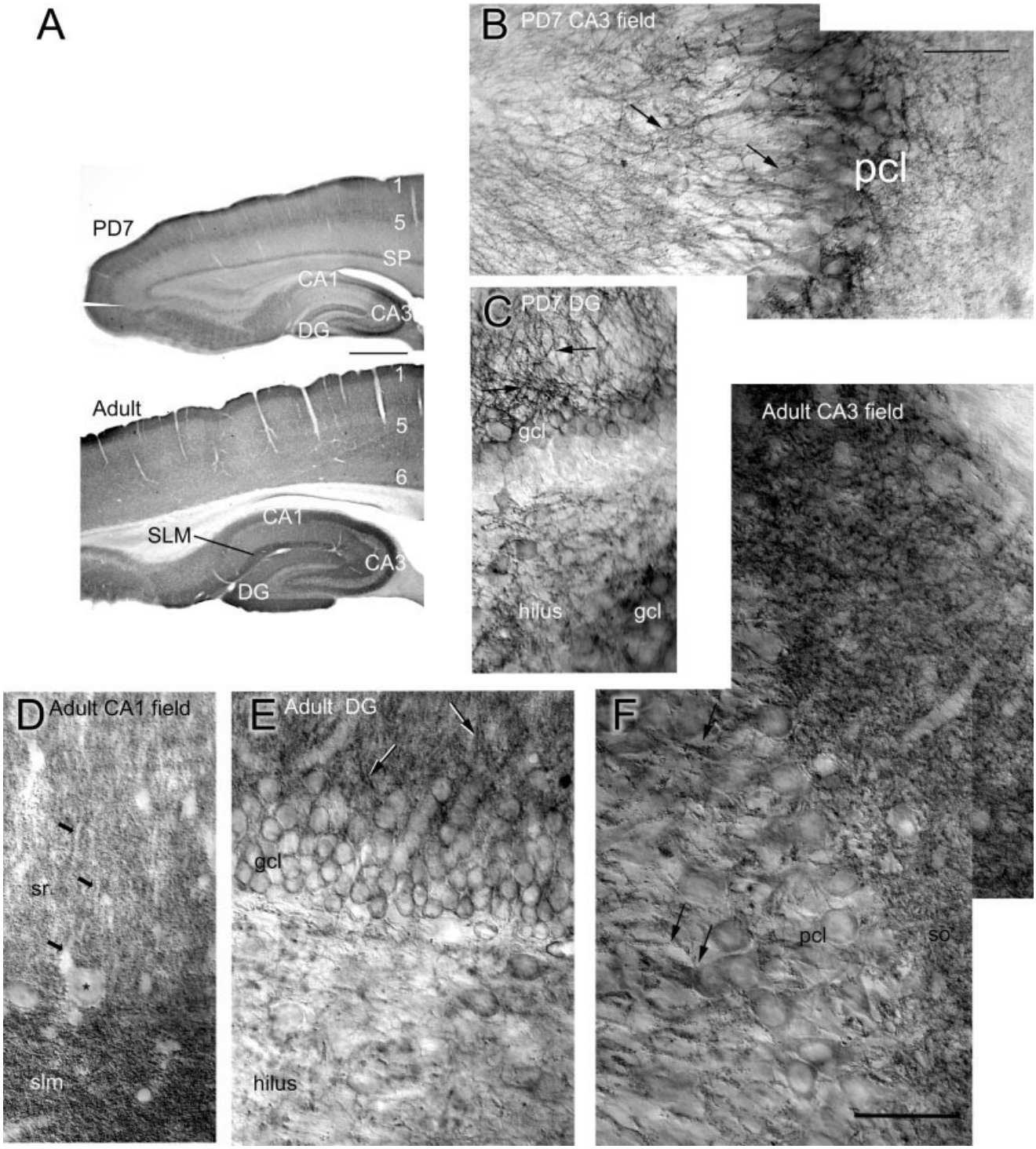

Fig. 3. Drebrin A immunoreactivity within postnatal day (PNd) 7 and adult cortex and the hippocampal formation. **A:** Sagittal sections show the overall distribution of drebrin A immunoreactivity, as revealed using the new drebrin A-specific antibody DAS2. At both ages, drebrin A immunoreactivity is particularly intense in the CA3 field of the hippocampus, the infrapyramidal leaf of the dentate gyrus (DG), and layer 1 of cortex. At PNd7 but not in adult, banding is also evident in the upper blade of the dentate gyrus as well as layers 5 and the subplate (SP) of cortex. In adulthood, but not at PD7, the stratum lacunosum moleculare (SLM) shows high concentration of immunoreactivity. **B,C:** Montages of light photomicrographs showing details of drebrin A immunoreactivity in the hippocampus of a PNd7 brain. **D–F:** Montages from an adult brain. At this magnification, it is evident that drebrin A immunoreactivity undergoes a laminar shift during development. At PNd7, immunoreactivity is intense in the perikaryal cytoplasm (labeled "pcl" for the pyramidal cell layer and "gcl" for the granule cell layer). Equivalent levels of immunoreactivity can be traced into the dendrites (arrows). In contrast, within the adult hippocampal formation, immunoreactivity is barely detectable within the cell bodies (asterisk), but is more intense within the synaptic layers. Immunolabeling is not contiguous, as seen in PNd7 brain but, instead, consists of high densities of puncta. D: Within the synaptic layers of the CA1 field (sr = stratum radiatum), the cytoplasm of apical dendrites' shafts appears unlabeled (arrows). Note the particularly intense labeling of puncta in the stratum lacunosum moleculare (slm). F: In stratum lucidum of the CA3 field, it is evident that these puncta aggregate along dendritic shafts (arrows). At both ages, immunoreactive puncta occur more dispersed in the hilus of the dentate gyrus. These dispersed puncta in the hilus are larger than the puncta coating dendrites. Most likely, these are cross-sectioned dendritic shafts. DG, dentate gyrus; gcl, granule cell layer; pcl, pyramidal cell layer; SLM, stratum lacunosum moleculare; so, stratum oriens; sr, stratum radiatum; sp, subplate. Scale bars = 1 mm in A, 50 μm in B,F (applies to B–F).

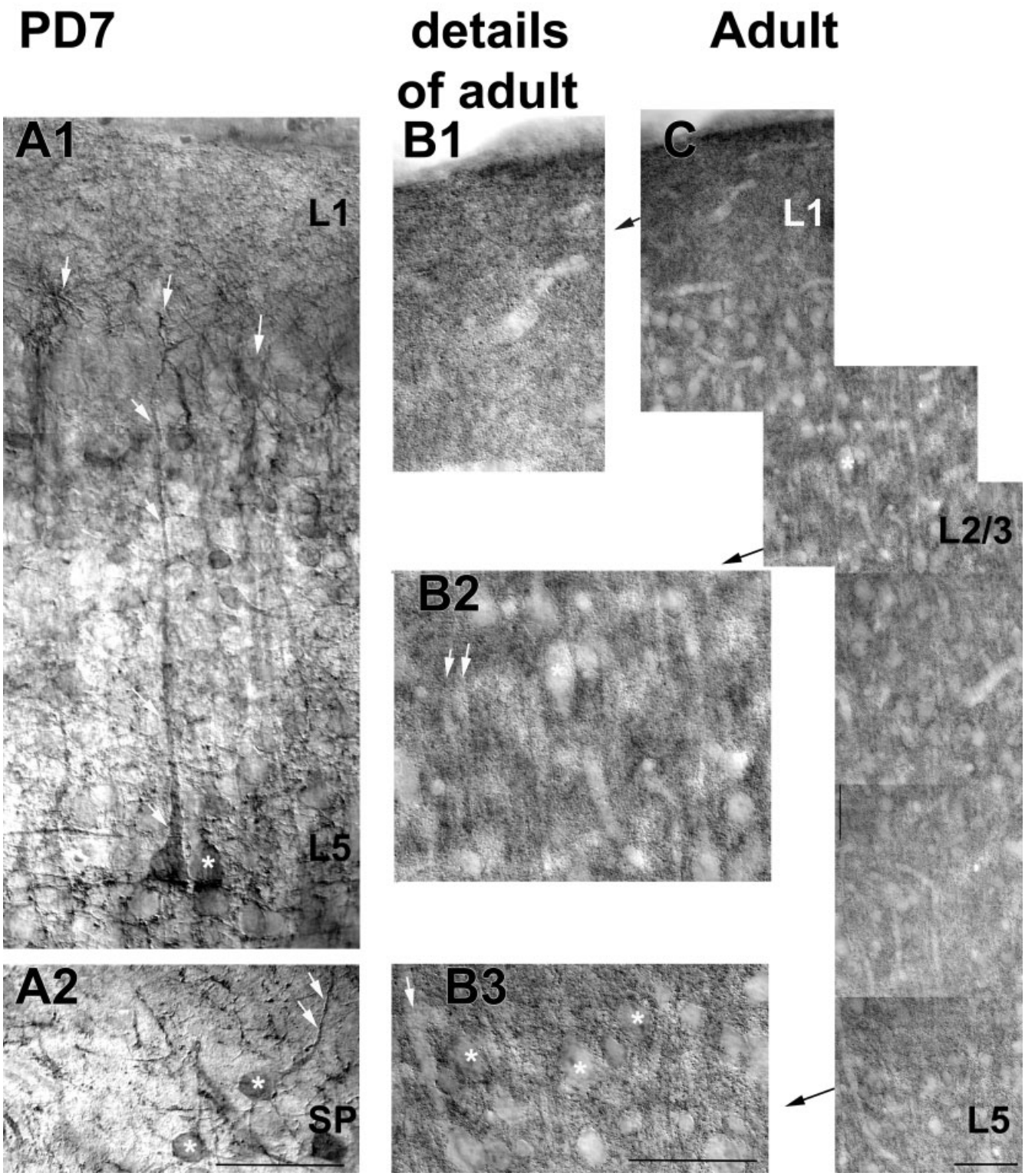

Fig. 4. Details of immunoreactivity in the neocortex at postnatal day (PNd, PD) 7 and in adulthood. **A1:** A montage showing drebrin A immunoreactivity in and surrounding a layer-5 pyramidal cell of PNd7 somatosensory cortex. The vertically oriented white arrows point to immunoreactivity within tufts of apical dendrites at the base of layer 1 (L1). Immunoreactivity continues along the apical dendrite of one cell that can be followed down to layer 5 (five angled, white arrows). The soma of this and the immediately neighboring cell (asterisk) show evenly distributed immunolabeling within the cytoplasm. **A2:** The subplate (SP, also referred to as layer 6b) of the same cortical tissue. Drebrin A immunolabeling is moderate within somata (asterisks) and more intense within dendrites (white arrows). **B1,B2,B3:** The middle column shows neuropil labeling of adult cortex, photographed and shown at the same magnification as that of the PNd7 tissue. In contrast to the PNd7 tissue, immunoreactivity is absent from the somata (asterisks in B3) but, instead, is distributed throughout the neuropil in the form of puncta. The white angled arrows point to examples of dendritic shafts, revealed by the absence of immunoreactivity.**C:** The right column shows a montage of the same adult neocortex, reduced in magnification to show the layers continuously. At this magnification, the unlabeled perikarya, embedded within the synaptic neuropil of the gray matter, are easily detectable from layers 2 through 5 (L1, L2/3, L5). All photomicrographs were obtained from sections immunolabeled using the newly generated drebrin A-specific antibody DAS2. Scale bars = 50 μm in A2 (applies to A1,A2), B3 (applies to B1–B3), C.

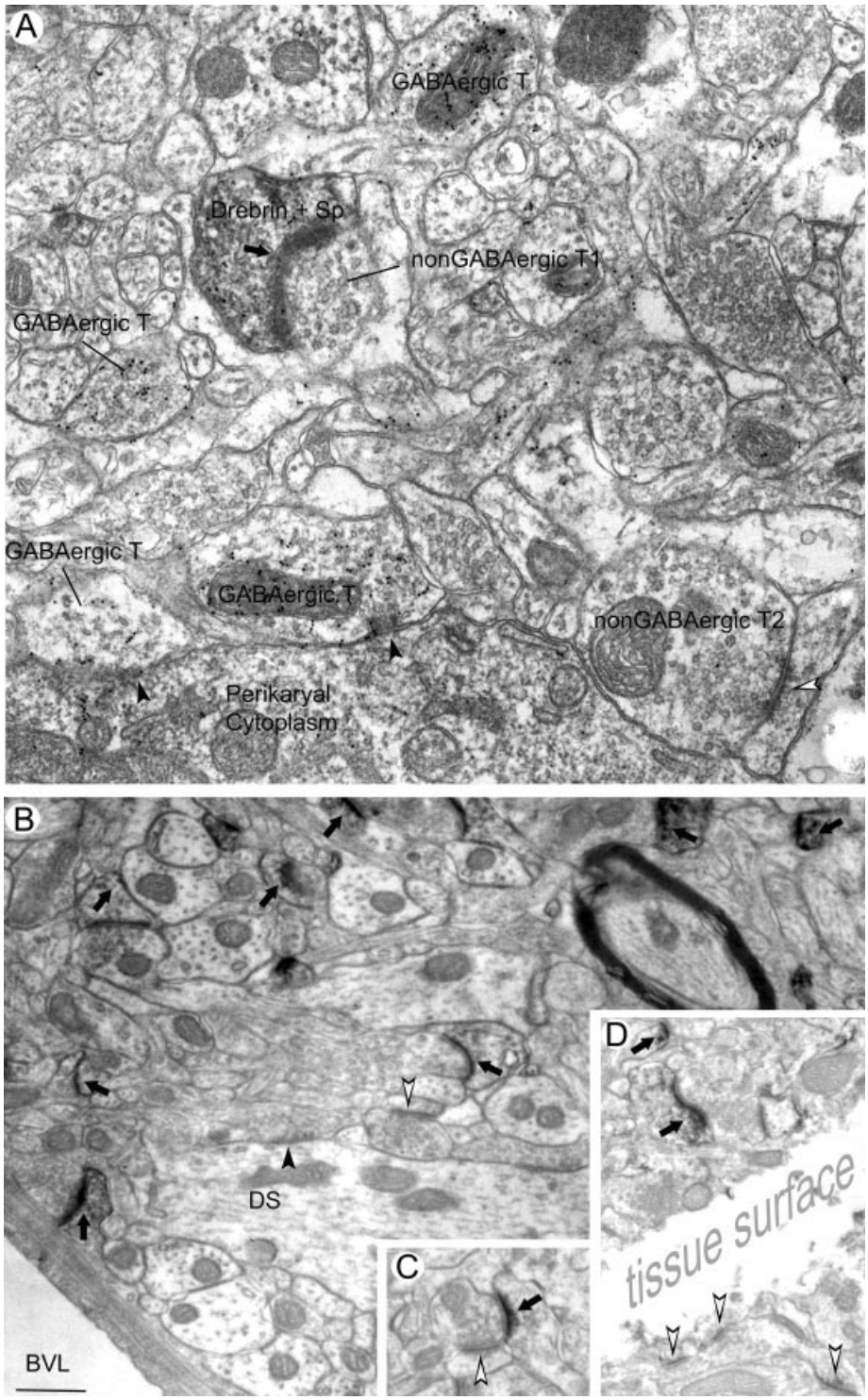

Fig. 5. Electron microscopic localization of drebrin A in adult cortex and hippocampus. A–D: Horseradish peroxidase–diaminobenzidine was used as the label to visualize drebrin A sites stratum oriens of the CA1 field of hippocampus (A,B) and in layer 6 of adult somatosensory cortex (C,D). All photomicrographs were obtained from sections that were immunolabeled using the new drebrin A-specific antibody DAS2. **A:** In A, only, immunoreactivity to γ-aminobutyric acid (GABA) is also shown by the postembedding immunogold labeling procedure (PEG) and also shows an absence of drebrin A labeling along somatic, symmetric synapses (filled arrowheads). These are inhibitory axosomatic synapses, as evidenced by the immunoreactivity of the axon terminal to GABA (GABA-T). In contrast, an asymmetric, axospinous synaptic junction immediately above the GABA-Ts is drebrin A immunoreactive on the postsynaptic side (arrow). Immunoreactivity appears diffusely within the spine cytoplasm (Drebrin + Sp). Based on the thickness of the postsynaptic density and the absence of GABA in the presynaptic terminal (nonGABA-T1), this synapse is likely to be glutamatergic and excitatory. Another spine to the right is unlabeled for drebrin A (open arrowhead), even though it is postsynaptic to a non-GABAergic terminal (nonGABAergic T2, probably glutamatergic). **B:** An adjacent ultrathin section from the hippocampus is shown. Drebrin A immunoreactivity is more intense, because this tissue has not undergone the osmium-extraction step required for the PEG shown in A. B also shows an unlabeled symmetric synapse (filled arrowhead, at the dendritic shaft, DS), an unlabeled asymmetric synapse (open arrowhead, on a spine), and many more drebrin A-immunolabeled asymmetric synapses on spine heads (arrows). BVL, blood vessel lumen. **C:** Two asymmetric synapses associated with a single axon terminal, one of which is immunolabeled (right, arrow) and the other of which is unlabeled (left, arrowhead). **D:** Heterogeneous labeling among spine heads, all located at the resin-tissue interface and, therefore, expected to have received optimal exposure to immunoreagents. Arrows point to immunolabeled spines' postsynaptic densities, whereas the arrowheads point to unlabeled asymmetric synapses. Scale bar = 500 nm in B (applies to A–C); 565 nm for D.

TABLE 1. Ultrastructural Characteristics of Synapses in Relation to Drebrin A: Adult Cortex (190 encountered synapses)

Asymmetric 147				Symmetric 43			
Labeled 111		Unlabeled 36		Labeled 3		Unlabeled 40	
Spinous 106	On shaft 5	Spinous 29	On shaft 7	Spinous 0	On shaft 3	Spinous 0	On shaft 40

TABLE 2. Ultrastructural Characteristics of Synapses in Relation to Drebrin A: Adult Hippocampus (179 encountered synapses)

Asymmetric 150				Symmetric 29			
Labeled 102		Unlabeled 48		Labeled 0		Unlabeled 29	
Spinous 99	On shaft 3	Spinous 44	On shaft 4	Spinous 0	On shaft 0	Spinous 0	On shaft 29

GABA by the PEG procedure upon a subset of grids verified that axon terminals forming symmetric synapses were GABAergic (Fig. 5A).

All three fixation conditions used for the study yielded excellent preservation of the ultrastructure and antigenicity, thereby allowing for sampling of synapses at surface-most regions of tissue, where penetration by immunoreagents would be the greatest. The proportion of encountered synapses with detectable levels of labeling did not differ greatly across the layers. Thus, the immunolabeling features described below apply to all layers.

Adult tissue, labeled using HRP-DAB: Asymmetric synapses are drebrin A-positive on the postsynaptic side. Twenty nonoverlapping fields along the tissue-resin interface were sampled from the adult cortical tissue, covering 245 μm^2 of the neuropil, mostly from the infragranular layers. 77% of the encountered synaptic profiles (147 of 190) were identifiable as asymmetric (Table 1) and of these, 76% (111 of 147) were detectably immunolabeled for drebrin A (Table 1). Drebrin A immunoreactivity was never on the presynaptic side. An analogous survey was performed for the adult hippocampus, using 14 nonoverlapping fields, spanning 171.5 μm^2 of the neuropil, mostly from the infrapyramidal leaf of the dentate gyrus. A total of 179 synapses were encountered and of these 84% (150 of 179) were asymmetric (Table 2) and of these, 68% (102 of 150) were immunolabeled for drebrin A (Table 2). Again, immunoreactivity was strictly on the postsynaptic side.

Unlabeled asymmetric junctions occurred immediately adjacent to immunolabeled asymmetric synapses (Fig. 5). A striking example of the juxtaposition of immunolabeled and unlabeled synapses is shown in Figure 5C. Here, the two synapses are immediately adjacent to one another and receiving inputs from a single presynaptic terminal. Juxtaposition of labeled and unlabeled asymmetric synapses occurred even along the extreme edges of tissue (Fig. 5D), where large portions of the dendritic shafts were visibly cut open by the Vibratome knife. Such observations indicated that lack of immunoreactivity to drebrin A cannot be explained entirely by failure of immunoreagents to penetrate tissue. Rather, these observations indicated that asymmetric synapses of adult cortices and hippocampi vary in drebrin A content.

Analysis of the tissue immunolabeled using the preadsorbed DAS2 antibody indicated further that the labeling of asymmetric synapses was specific: the percentage of asymmetric synapses that were detectably immunolabeled was reduced from approximately 80% down to 7%, accompanied by a markedly reduced intensity of immunolabeling within the individual spines.

Large subset of the drebrin A-immunoreactive asymmetric synapses is axospinous. The great majority of immunolabeled synaptic junctions with thick PSDs in the cortex (95%, 106 of 111) and hippocampus (97%, 99 of 102) were axospinous (Fig. 5A; Tables 1, 2). On the other hand, asymmetric junctions on dendritic shafts of cortex also were drebrin A immunoreactive (5 of 12 in cortex, 3 of 7 in hippocampus; Tables 1, 2), indicating that spinous location was not a strict requirement for the presence of drebrin A. Conversely, more than half of the asymmetric synaptic junctions on shafts were unlabeled, as opposed to approximately one third to one-quarter of the axospinous asymmetric synaptic junctions that were unlabeled, indicating that drebrin A is preferentially clustered within spines.

Symmetric synapses have low amounts or no drebrin A. All of the symmetric synapses were on dendritic shafts and almost all of these were unlabeled for drebrin A (40 of 43 in cortex; 29 of 29 in hippocampus; black arrowheads in Fig. 5A). The three immunolabeled synapses on shafts that appeared symmetric may actually have been asymmetric synapses that were not sectioned at a favorable plane to reveal the presence of PSDs.

Neonatal tissue, labeled using HRP-DAB: Drebrin A occurs in dendrites, not axonal growth cones. Within neonatal tissue, labeling was apparent along the intracellular surface of plasma membranes. Considering the diffuse nature of HRP-DAB label in general, the immunoreactivity was surprisingly discrete, occurring as small patches that were immediately opposed to sites contacted by axons. These processes exhibiting drebrin-A immunoreactive patches were identifiable as dendrites, based on the smooth but irregular contour, large diameter, absence of vesicles, and occasional abutting with profiles identifiable as axonal. Not all dendrites exhibited clear arrays of microtubules (compare Fig. 6B,C, which shows no microtubules, with Fig. 6D, which shows microtubule arrays clearly). Axons, in turn, were identified based on the presence of a few vesicles. Typically, these vesicles were gathered at sites removed from the junctional membrane (Fig. 6A, synapse 2 in Fig. 6D, Fig. 6E). Only 1 of the 149 encountered synapses exhibited drebrin A immunoreactivity in a profile that was judged to be possibly axonal.

Drebrin A appearance precedes synapse formation. Unlike the adult tissue, drebrin-A immunoreactivity was present in profiles lacking any features identifiable as synaptic (Fig. 6B). Where spine-like protrusions could be detected, these appeared incompletely formed, in that the neck was still nearly as wide as the spine head (Fig 6A, right, and synapse 1 in Fig. 6D). In addition, those that appeared to be junctional were still immature, because the

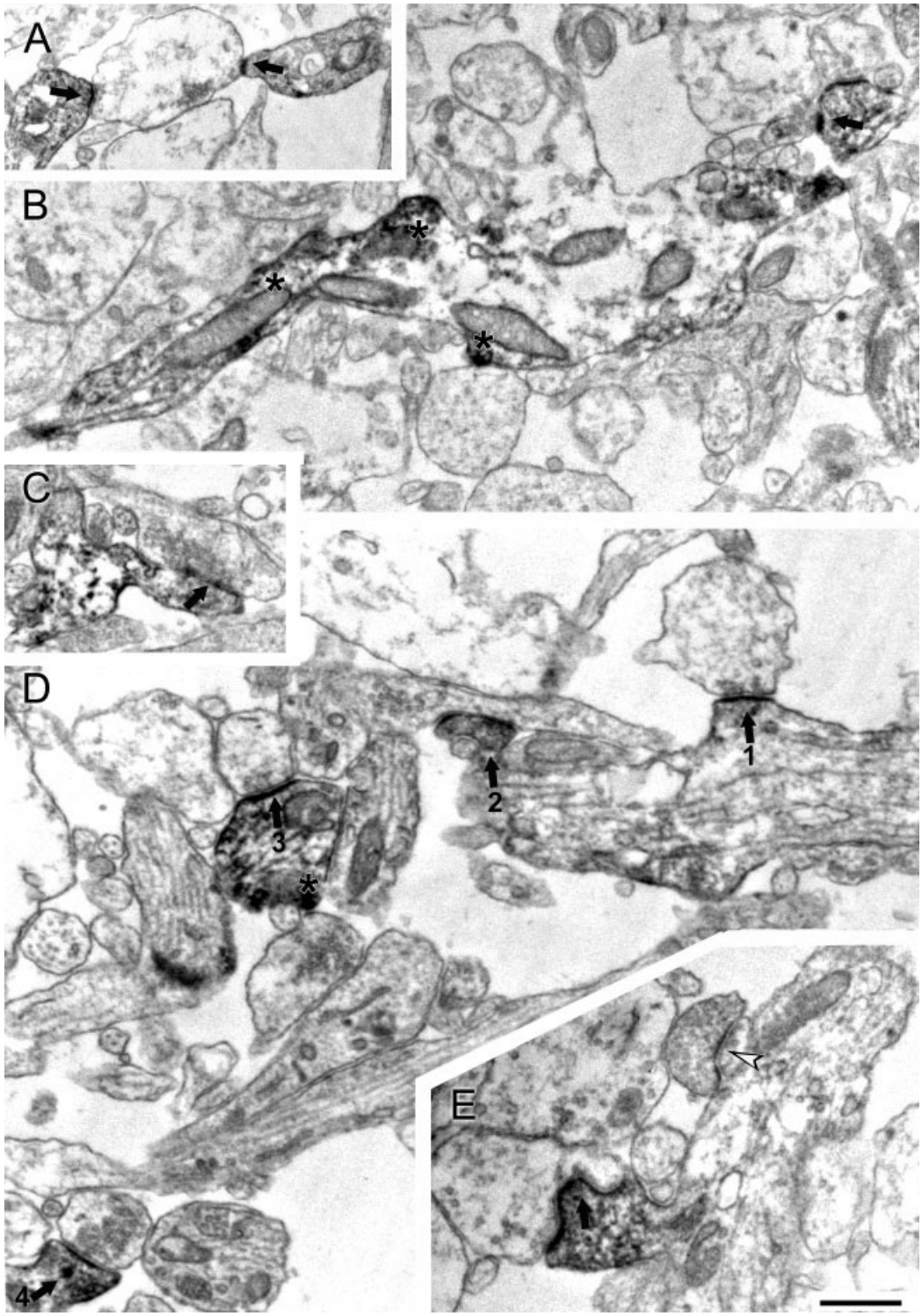

Fig. 6. Ultrastructural localization of drebrin A in postnatal day (PNd) 7 cortex. Horseradish peroxidase–diaminobenzidine was used to detect the presence of drebrin A. **A:** A large-caliber axon that is largely devoid of vesicles, yet synaptically associated with two dendritic processes. Of the two small clusters of vesicles, only one is at a synapse. The synapse showing a slight indentation of the plasma membrane, perhaps an early sign of spine neck formation, lacks vesicles presynaptically. Both synapses show accumulation of drebrin A immunoreactivity along the postsynaptic membrane (arrows). **B:** A dendrite lacking morphologically identifiable synapses. Drebrin A immunoreactivity has accumulated along small protrusions (asterisks). **C:** A well-established spine head forming a synapse with an axon. The axon contains a moderate number of vesicles that are clustered at the synaptic junction, and the postsynaptic membrane (arrow) is slightly immunoreactive. Drebrin A immunoreactivity is more intense along the nonsynaptic portions of the plasma membrane. The nonsynaptic portions of the dendrite contain no detectable microtubules and also exhibit plasma membranes with irregular contours. **D:** A dendrite containing well-defined microtubules. Drebrin A immunoreactivity is evident along a slight protruding portion of the shaft (synapse 1) and along a spine with narrow neck (synapse 2) but whose presumably "presynaptic" profile shows no vesicle clustering near the juxtaposed portion of membrane. Drebrin A immunoreactivity is also associated with a dendritic shaft forming an asymmetric synapse (synapse 3) opposite of another protuberance (asterisk) and another dendritic protuberance (synapse 4) whose presynaptic element shows adult-like vesicle clustering. **E:** A dendrite bearing a spine that stains strongly for drebrin A. The neurite with which this immunoreactive spine is associated shows only a few vesicles, scattered widely and away from the juxtaposed portion of the plasma membrane. In contrast, the other presynaptic element associated with an unlabeled spine (arrowhead) of the same dendrite contains a large cluster of vesicles. Scale bar = 500 nm in E (applies to B–E); 650 nm for A.

TABLE 3. Ultrastructural Characteristics of Synapses in Relation to Drebin A: PNd7 Cortex (149 Encountered Synapses)

Asymmetric 93				Symmetric 56			
Labeled 40		Unlabeled 53		Labeled 18		Unlabeled 38	
Mature 2	Immature 38	Mature 4	Immature 49	Mature 0	Immature 18	Mature 0	Immature 38

PNd, postnatal day.

PSDs were often absent (left arrow in Fig. 6A, Fig. 6C) and the putatively presynaptic profile contained either no vesicle near the junctional membrane (Fig. 6A,D), only a few vesicles (right synapse with straight arrow in Fig. 6A, synapse 1 of Fig. 6D, Fig. 6E), or many more vesicles that were removed from the junctional membrane (synapse 2 in Fig. 6D). We noted that some dendritic profiles showed more intense drebrin A immunoreactivity in the nonjunctional portions than in the synaptic portions (e.g., Fig. 6C).

Majority of asymmetric synapses are immature and unlabeled for drebrin A. Quantitative analysis was performed upon neonatal cortex, categorizing synapses either as newly formed, immature, and presumed to be synaptic, or as mature. The number of vesicles, detectability of PSDs and narrowness of spine necks were used as criteria to distinguish between the two categories. Those intercellular contact sites lacking both the PSDs and vesicles were categorized as nonsynaptic. Twenty-six nonoverlapping fields were surveyed from which were found 149 synaptic profiles (labeled and unlabeled, asymmetric and symmetric) and 31 nonsynaptic immunolabeled profiles. Ninety-six percent of these profiles appeared immature, using the above criteria. Unlike the adult tissue, in which the majority of synapses were immunolabeled (114 of 190), only a minority (58 of 149) of the synaptic junctions encountered in PNd7 cortex were drebrin A immunoreactive (Labeled, symmetric + asymmetric; Table 3). This difference across the ages was statistically significant ($58 \pm 4\%$ for adults, $31 \pm 4\%$ for PNd7 tissue; $P < 0.0005$, two-tailed unpaired t test). Among the synapses identifiable as asymmetric, the majority of those in the PNd7 cortex (53 of 93) were also unlabeled, as opposed to the adult cortex, for which only 36 of the 147 asymmetric synapses were unlabeled (Table 3). This difference across the ages was statistically significant ($59 \pm 8\%$ for PNd7; $23 \pm 5\%$ for adult; $P < 0.005$, two-tailed unpaired t test).

Larger proportion of the presumptive immature symmetric synapses is immunolabeled for drebrin A. Another notable departure from adult tissue was the prevalence of drebrin A at symmetric junctions. Thirty-two percent (18 of 56) of the presumptive immature symmetric synapses in PNd7 cortex were immunolabeled (Table 3). Compared with the adult tissue, many more of the neonatal synapses were classified as symmetric, due to the absence of the PSDs (38% for PNd7-tissue, 23% for adult tissue; Table 3). Most likely, many of these were glutamatergic synapses in which the PSD had not yet assumed their mature thick form and in which the spine necks had not yet narrowed (Aoki et al., 1994; Aoki, 1997).

Two PEG immunolabeling results supported the above presumption that neonatal synapses exhibiting drebrin A are excitatory. One was that the axons identifiable to be presynaptic to the drebrin A-positive dendritic membrane were almost always GABA-negative (more than 90% of the drebrin A-positive synapses encountered, an example shown in Fig. 7), with some of the exceptions consisting of dendrites receiving convergent inputs from multiple axons that included GABA-positive ones. The second was that dendritic membranes, revealed to be drebrin A-positive by the SIG label (detailed below), also were immunopositive for the NR2B subunit of NMDA receptors (an example shown in Fig. 8).

Adult tissue, immunolabeled for drebrin A using SIG, exhibit dendritic localizations. Another set of tissue was immunolabeled using SIG, so as to be able to analyze the distribution of drebrin A within postsynaptic profiles. Although light microscopy indicated only low amounts of drebrin A in perikarya and dendritic trunks, electron microscopy revealed discrete labeling along the intracellular surface of perikarya (data not shown). These immunoreactive sites of perikaryal plasma membranes were not synaptic. The immunoreactive patches of the membrane typically occurred adjacent to arrays of endoplasmic reticulum.

Synaptic labeling with SIG was exclusively postsynaptic and at asymmetric synapses. The proportion of synapses labeled (30 of 51 or 59%) was lower than that seen using HRP-DAB (111 of 147 or 76%), indicating that many more synapses may have expressed drebrin A but at amounts too low to be detectable by the less-sensitive SIG procedure. Nevertheless, the SIG-labeled tissue could be used to reveal more precise information regarding the intracellular distribution of drebrin A. Drebrin A was detected immediately adjacent to PSDs (Fig. 9B). However, more often, SIG particles within dendrites occurred along membranous portions removed from PSDs (Fig. 9A), indicating that a larger pool of drebrin A exists at nonjunctional sites.

Neonatal tissue, labeled using SIG, shows enrichment of drebrin A at presumptive immature synapses. Neonatal tissues were also subjected to drebrin-A immunolabeling using SIG. As expected, the proportion of synaptic profiles labeled by the SIG label was less, compared with the HRP-DAB labeling. Nevertheless, the SIG labeling resembled the DAB labeling's developmental pattern, in that the proportion of synapses labeled was less at PNd7 (9 of 31 or 29%) than in adulthood (59%).

The SIG procedure revealed an additional feature regarding drebrin A, namely that the presumptive immature synapses are more frequently labeled than are the synapses with relatively more established morphological characteristics. Some of the immunoreactive sites showed no intercellular specializations, whereas other immunoreactive sites were synapses with distinctively immature features (arrowheads in Fig. 10). In contrast, mature synapses with clearly identifiable PSDs in the immediate vicinity were frequently unlabeled (open arrows in Fig. 10). Over the scanned area, only 1 of the 24 mature synapses encountered within PNd7 tissue was immunolabeled by SIG, in contrast to 9 of the 21 presumptive immature synapses encountered that were immunolabeled. These observations indicated that the amount of

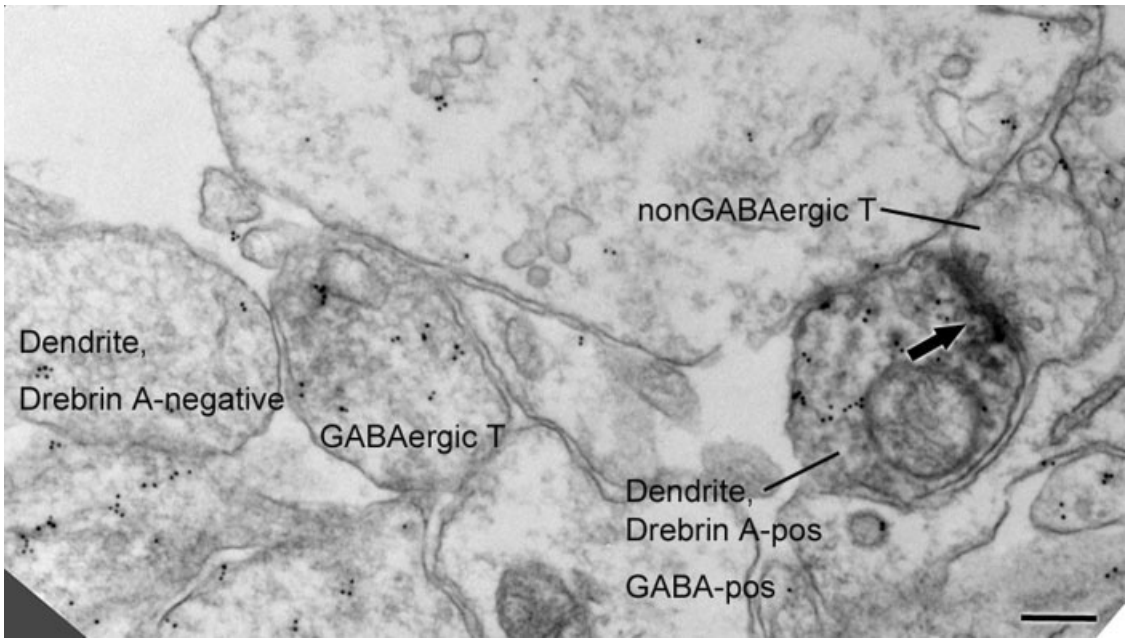

Fig. 7. Drebrin A is postsynaptic to γ-aminobutyric acid (GABA) -negative terminals of postnatal day (PNd) 7 tissue. At PNd7, dendrites rarely exhibit axospinous asymmetric synapses, thereby making the distinction between excitatory and inhibitory synapses more difficult than for adult tissue. The section shown here was dually labeled for drebrin A (by horseradish peroxidase–diaminobenzidine [HRP-DAB]) and for the inhibitory neurotransmitter, GABA by the postembedding gold immunolabeling procedure (PEG). The 10-nm colloidal particles reflect GABA immunoreactivity. GABA immunoreactivity is detectable in one profile that appears to be an axon terminal (GABAergic T), based on the presence of a few vesicles. This profile is juxtaposed to a drebrin A-negative profile that is likely to be a dendrite. In contrast, the dendrite to the right is HRP-DAB–labeled for drebrin A (Drebrin A-pos) and is also immunoreactive for GABA (GABA-pos). However, its presynaptic terminal is completely devoid of 10-nm colloidal gold particles, indicating that is it non-GABAergic (nonGABAergic T). The arrow points to the postsynaptic membrane over which drebrin A accumulates. Scale bar = 200 nm.

drebrin A expressed at single synapses varied, with mature synapses exhibiting relatively less than the newly forming ones. Examples were seen where two axons converged upon a single postsynaptic profile, with each axon abutting a distinct spine head (Fig. 10B). Here, too, drebrin A immunoreactivity was more robust within the less mature spine head, so identified by the absence of PSD and absence of vesicle clusters within the abutting portion of the axon.

Although the SIG labeling for drebrin A was not strictly along the postsynaptic membrane (small arrows in Fig. 10), it appeared to be biased toward the inner surface of the dendritic plasma membrane, rather than being distributed evenly in the cytosol. Quantitative analysis of SIG particle positions showed that the above impressions regarding the membranous bias of labeling were valid. The 331 SIG particles encountered within the 46 nonoverlapping surveyed fields were collected from two PNd7 and two adult brains; 20% of the SIG particles occurred directly on the membrane, and 45% remained within 50 nm from the plasma membrane. This distance corresponded to the 0 to 10% distance from the plasma membrane, relative to the diameter of the profiles (Fig. 11). This proximity of drebrin A sites to the membrane was relatively more prominent for the PNd7 tissue. Specifically, 56% of the SIG particles for one PNd7 tissue occurred within the 10% distance from the plasma membrane, and the corresponding value for the other PNd7 tissue was 64%. Both of these values were greater than the value obtained for the two adult tissue—40% and 41% (Fig. 11). However, data from more animals will need to be collected before we can be certain about the age-dependent differences.

Western blotting reveals developmental loss of drebrin A in the supernatant. The electron microscopic observation showing association of drebrin A with the intracellular surface of the plasma membrane prompted us to further quantify the subcellular distribution of drebrin. To this end, Western blotting was performed to obtain quantitative measures of drebrin in the supernatant (mostly free cytosolic, but also including drebrin associated with the membrane) and in the pellet (mostly associated with F-actin and microsomes) fractions (Fox, 1985; Crosbie et al., 1991). Based on the developmental data obtained from Western blotting (Fig. 2), PNd8 was taken as the representative ages of the neonatal stage (where a large portion of the drebrin is still in the E-isoform), whereas PNd16 was taken as the representative, youngest adult-like stage, in which the A-isoform dominates.

Quantitative analysis of drebrin content in the PNd8 and PNd16 cortices was performed by measuring the intensity of Western blots, using the M2F6 monoclonal antibody that could recognize both the E and A isoforms (Fig. 12). In agreement with the decline of both the A and E isoforms of drebrin in the supernatant during development, the total drebrin intensity (drebrin A + drebrin E) in the supernatant fraction at PNd16 significantly decreased to 17.9 % of that at PNd8 ($P < 0.001$). In comparison, there was no significant difference in the actin intensity in the supernatant fraction between PNd8 and

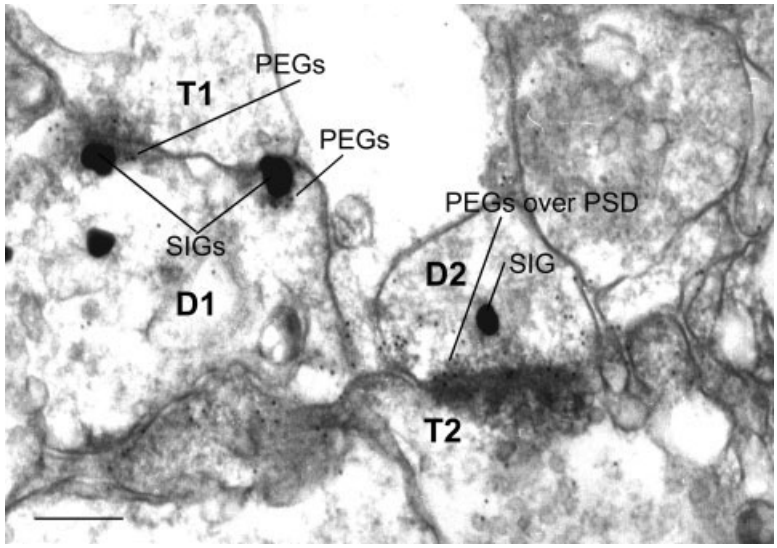

Fig. 8. Coexistence of drebrin A with the NR2B subunit of *N*-methyl-D-aspartate receptors at the postsynaptic membrane of a postnatal day (PNd) 7 dendrite. D1 to the left exhibits silver-intensified colloidal gold particles (SIG), reflecting immunoreactivity for drebrin A. Two of the SIG particles occur along the intracellular, postsynaptic membrane surface. Immediately adjacent to each of the SIG particles, two to four postembedding gold immunolabeling procedure (PEG) particles occur, reflecting the presence of low levels of NR2B subunits. The presynaptic terminal T1 contains only a few vesicles. In contrast, the terminal, T2, forming the adjacent synapse contains many vesicles, and the postsynaptic membrane of D2 exhibits a thick postsynaptic density (PSD). At least 12 PEG particles occur over the postsynaptic density, indicating the prevalence of NR2B subunits. This postsynaptic membrane does not show detectable levels of drebrin A. Instead, drebrin A immunoreactivity is slightly removed from the postsynaptic membrane. Scale bar = 200 nm.

PNd16. Also, in the crude homogenate or the pellet fraction, drebrin intensity did not change significantly between PNd8 and PNd16.

Based on previously published results, we surmised that the pellet fraction prepared after centrifugation at 200,000 $\times$ *g* represented the association of drebrin with F-actin (Ishikawa et al., 1994). Earlier studies had established that high salt could extract actin binding proteins from F-actin pellets (Glenney et al., 1982; Yamashiro-Matsumura and Matsumura, 1985). When this same procedure was used on our pellet fractions, a large portion of drebrin A was extracted from the pellet and entered the supernatant fraction (Fig 13). This outcome indicated that a large portion of drebrin A in the pellet was bound to the cytoskeleton and most likely to F-actin and microsomes and not to the plasma membrane.

DISCUSSION

The present study revealed a clear-cut segregation of drebrin A to postsynaptic sides of asymmetric synapses within mature cortex and hippocampus. During the phase of active synaptogenesis, drebrin A was present at the submembranous zone of dendritic plasma membranes before the formation of PSDs or spine heads, and also before the aggregation of vesicles presynaptically. This observation is consistent with results from our previous in vitro study, indicating that clustering of drebrin A precedes the formation of spines (Takahashi et al., 2003). Contrary to the presumptions we held before this ultrastructural study, our new observations indicate that drebrin E, *together with drebrin A*, are involved in the initial formation of protospines, rather than the involvement of drebrin E, alone. Moreover, the present ultrastructural study was able to verify that drebrin A occurs at membranous sites that were positively identifiable as synaptic, based on the emergence of a few vesicles, PSDs, and/or aggregation of glutamate receptor subunits there. The biochemical results indicate that the phase of synaptogenesis is paralleled by the increasing association of drebrin A with the pellet fraction containing actin. Below, we discuss the possibility that drebrin A may be involved in organizing the dendritic pool of actin for the formation of at least some of the spines and axospinous excitatory synapses.

Drebrin A is postsynaptic for excitatory synapses

The segregation of drebrin A to the postsynaptic side was clearer than it was for any of our previous observations of synaptic proteins, including the glutamatergic receptors (Aoki et al., 1994; Farb et al., 1995) and PSD-95 (Aoki et al., 2001). This was so, even though the immunolabeling for glutamatergic receptor subunits and PSD-95 faced similar technical limitations. We also noted absence of drebrin A at almost all of the mature symmetric synapses. Symmetric synapses are sites for inhibitory inputs, indicated by the clustering of $GABA_A$ receptor subunits, proteins such as gephyrin for the anchoring of these subunits and contacts formed by GABAergic axon terminals (reviewed by Fritschy and Brunig, 2003). Symmetric synapses also are associated with axons releasing neuromodulators, such as the monoamines and acetylcholine (Descarries, 1991).The segregation of labeling between symmetric and asymmetric synapses indicates that drebrin A is involved in the formation of at least some of the excitatory synapses but not of the GABAergic or purely modulatory synapses. Whether or not another organizer of F-actin occurs at GABAergic synapses remains unknown.

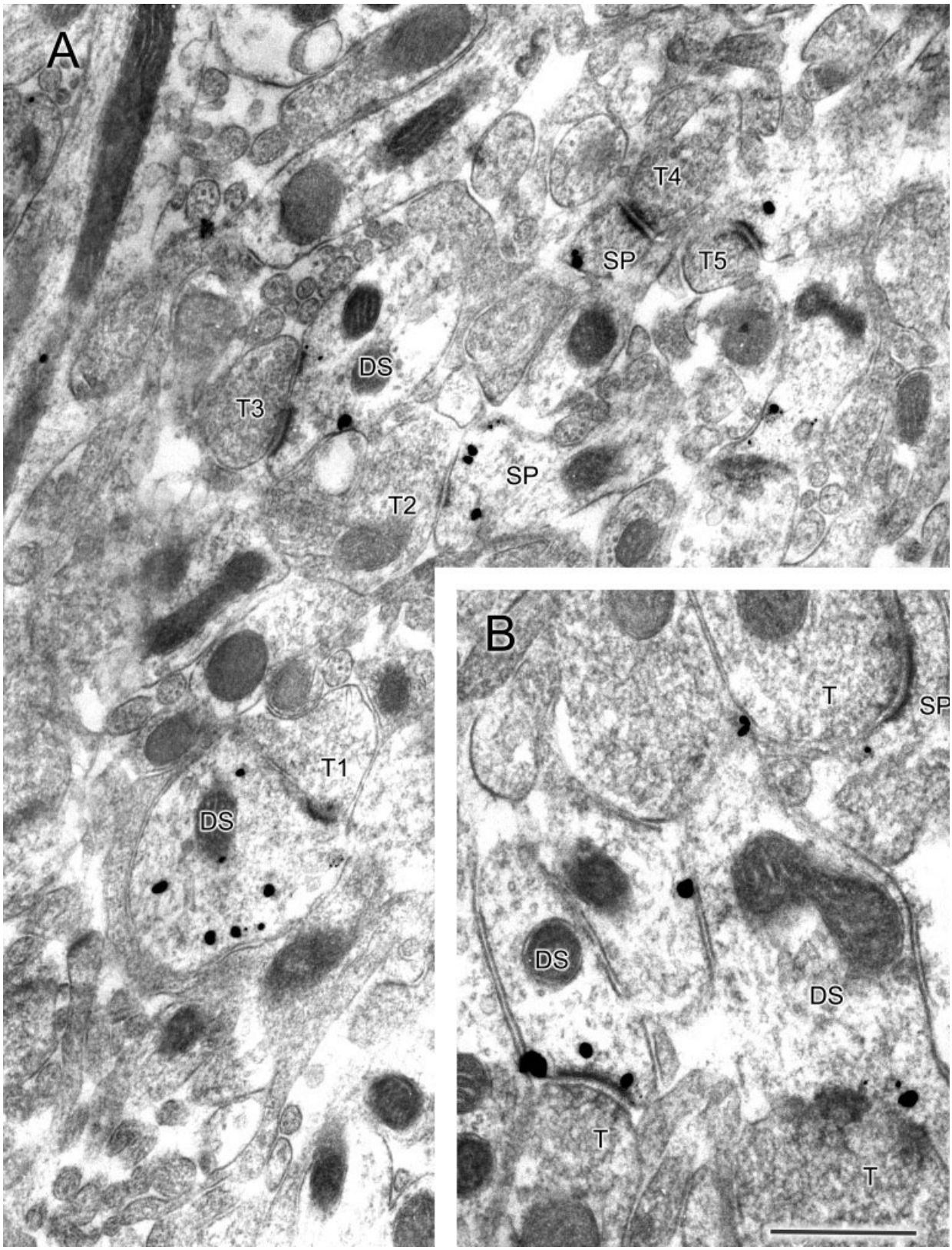

Fig. 9. Drebrin A in the synaptic neuropil of the molecular layer of the adult infrapyramidal dentate gyrus. Silver-intensified colloidal gold particles (SIG) were used to detect drebrin A. **A:** Five synapses, all asymmetric and associated with immunoreactivity to drebrin A on the postsynaptic side, only. The postsynaptic side is indicated as DS for dendritic shafts or as SP for spines, whereas the presynaptic profiles are indicated as T for terminal. At synapses formed with terminals T1, T2 and T3, the SIG particles occur along nonsynaptic portions of the plasma membrane and at the periphery of the postsynaptic density (PSD). At these synapses and all others, SIG particles occur in the cytoplasm as well. **B:** Three more synapses, two of which exhibit SIG particles discretely along the postsynaptic membrane. Additional SIG particles occur at nonjunctional sites. Scale bar = 666 nm in B; 500 nm for A.

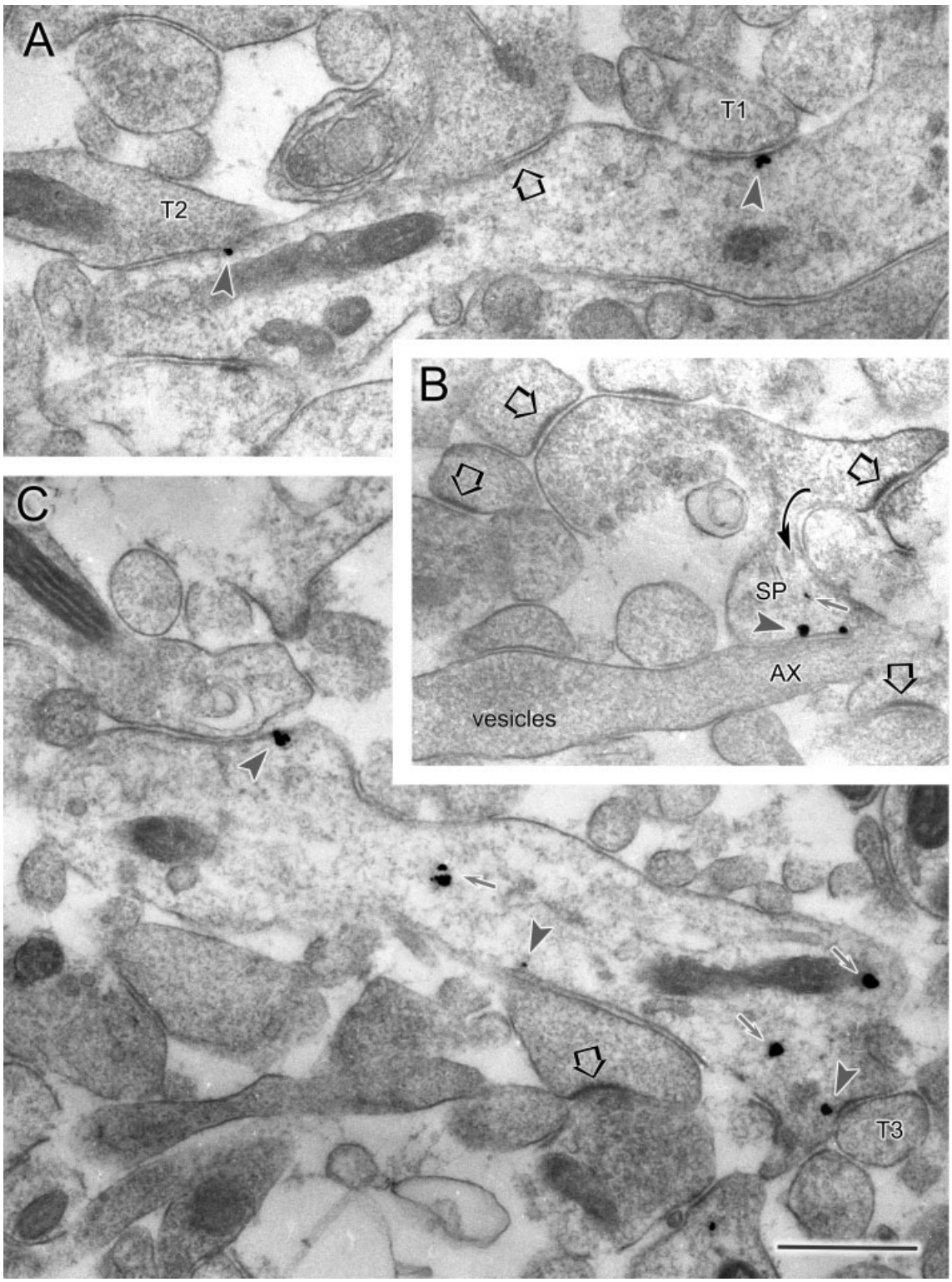

Fig. 10. Drebrin A in the molecular layer of postnatal day (PNd) 7 infrapyramidal dentate gyrus. Silver-intensified colloidal gold particles (SIG) were used as the label to detect the presence of drebrin A. **A:** Selective labeling along junctional portions of the plasma membrane. The arrowhead to the right shows SIG particles associated with a morphologically identifiable synapse (T1 marks the presynaptic terminal), whereas the SIG particle to the left shows no association with postsynaptic densities (PSDs). The immediately adjacent profile, T2, appears to be an axon terminal, indicating that this site is an immature synapse. The open arrow in the middle (and in other panels) points to a well-differentiated synapse lacking SIG particles. **B:** Three SIG particles occurring within a spine head (SP) lacking a PSD (arrowhead points to membranous SIG; small arrow to a cytoplasmic SIG). The immediately adjacent profile is an axon (Ax), as is evident by the cluster of vesicles in the same profile, toward the left. The same filopodia branches (curved arrow) from a more well-established but unlabeled spine with PSD (open arrows). **C:** A dendrite with irregular contours, no apparent microtubules, and containing six clusters of SIG particles. SIG occurs discretely along the plasma membrane forming a protuberance (arrowhead to the left) and contacting an axon. The arrowhead in the center points to an SIG particle along the plasma membrane that lacks apparent association with any axon. The arrowhead to the right points to the SIG particle associated with a portion of the plasma membrane beginning to form a PSD adjacent to an axon terminal, T. Arrows point to SIG particles in the cytoplasm, away from the plasma membrane. Scale bar = 500 nm in C (applies to A–C).

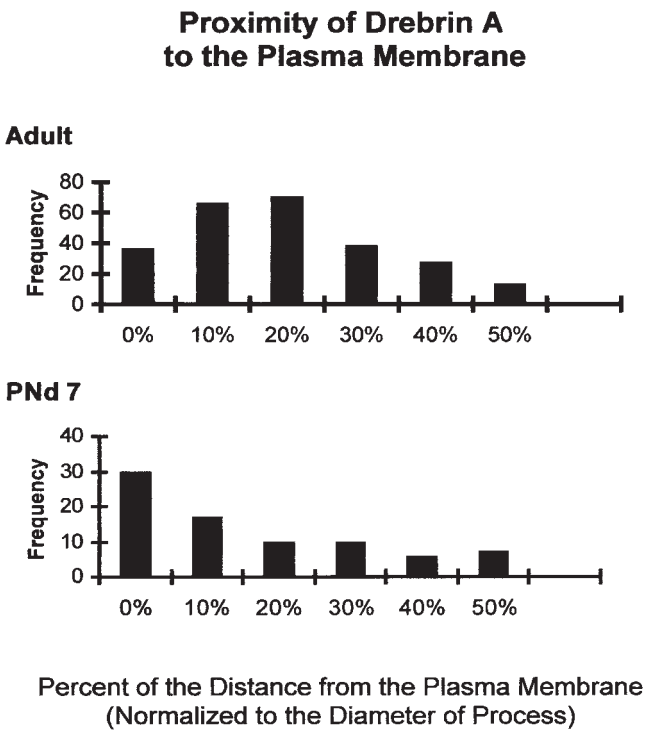

Fig. 11. Histograms showing the distribution of silver-intensified colloidal gold (SIG) particles in relation to the plasma membrane. The percentage values on the x-axis depict distances from the plasma membrane, normalized to the diameter of the profile in which the SIG particles are found. The y-axis depicts frequency of encounters at these varying distances from the membrane. Zero percent denotes SIG occurring at the plasma membrane. The encountered SIG particles were tallied from two postnatal day 7 and two adult hippocampal tissues.

Because GABAergic synapses occur at nonspinous portions of the plasma membrane, these synapses may not require F-actin binding proteins. Alternatively, a counterpart to an F-actin binding protein like drebrin may still be required at GABAergic synapses for the sake of receptor clustering and anchoring.

It has been shown previously that asymmetric synapses increase progressively in the neuropil during early postnatal development and that the spines emerge from stubby protospines along dendritic shafts after dendritic filopodia have disappeared (Vaughn, 1989; Harris, 1999; Jontes et al., 2000). Based on these observations, we surmise that PSDs convert from thin to thick during ontogeny, thereby converting synapses with symmetric appearances along protospines into those with asymmetric appearances at the spine heads. Our past (Aoki et al., 1994; Aoki, 1997) and present dual PEG immunocytochemical localization of glutamatergic receptor subunits corroborate this finding, because these receptors are found on synapses with very thin PSDs early on, and at progressively thicker PSDs in later weeks and in adulthood. The association of drebrin A with symmetric synapses at PNd7 and with asymmetric synapses in adulthood is likely to reflect drebrin A's association with newly formed glutamatergic synapses and of its persistence there during varying phases of maturation, rather than the switching of drebrin A from inhibitory to excitatory synapses during development. In support of this idea, drebrin A immunoreactivity was absent from symmetric synapses that had begun to acquire some of the morphological characteristics of mature GABAergic synapses (e.g., large cluster of vesicles that are associated along the presynaptic membrane; clearly defined microtubules within the postsynaptic dendrite, GABA immunoreactivity within the terminal). Drebrin A may be useful for identifying immature excitatory synapses before they acquire the more obvious morphological features. Studies are under way to determine whether the arrival of drebrin A to the dendritic membrane precedes arrival of NMDA receptor subunits or is linked to NMDA receptor recruitment.

Drebrin A arrives at dendritic membranes before synaptogenesis

By using both SIG and DAB as immunolabels for electron microscopy, we show that drebrin A appears at the earliest phase of synaptogenesis. Although neither label can be used to reveal the absolute values of drebrin A concentrations at junctions, the SIG label could be used to assess the relative concentration of antigens in the proximity of synaptic junctions. Our observations of tissue immunolabeled using HRP-DAB and SIG as the label indicate that the *proportion* of synaptic junctions lacking drebrin A immunoreactivity is greater at PNd7 than in adulthood. It has been reported that the turn-over rate of spines is higher in neonatal brain than in adult brain (Lendvai et al., 2000). It may be that drebrin A plays a role not only at the beginning of synaptogenesis and spinogenesis but also in the maintenance of spines. Once a spine loses drebrin A, that spine may be cleared from the neuropil more rapidly. If so, then the higher turnover rate of spines neonatally may be a consequence of a larger proportion of spines having lost drebrin A. Further experiments are needed to link physiological characteristics of spines to the presence of drebrin A and of the cause–effect relationship between spine turnover and drebrin A content.

Possible role of Drebrin A in neonatal cortex and hippocampus

In this study, we show that the rapid increase of drebrin A is paralleled by the disappearance of drebrin from the supernatant fraction at PNd8. Because we prepared crude homogenates in the presence of a mild detergent, NP-40, we expect the supernatant fraction to contain proteins that are free in the cytosol or solubilized from the membrane. Although G-actin (actin monomers) occurs in high amounts in the supernatant, we know that drebrin does not associate with actin monomers (Ishikawa et al., 1994). Thus, drebrin in the supernatant could represent free drebrin and those loosely attached to the plasma membrane. This interpretation agrees well with the SIG labeling PATTERN, which showed membranous labeling for drebrin A more at PNd7 than in adulthood. The drebrin appearing in the supernatant may be the correlate of ultrastructurally observed junctional and nonjunctional drebrin at flat portions and shallow protrusions (protospines) along intracellular surfaces of dendritic membranes.

The extraction experiment shows that drebrin's association with the pellet is ionic and nonmembranous. The best candidate for an element contained within pellets

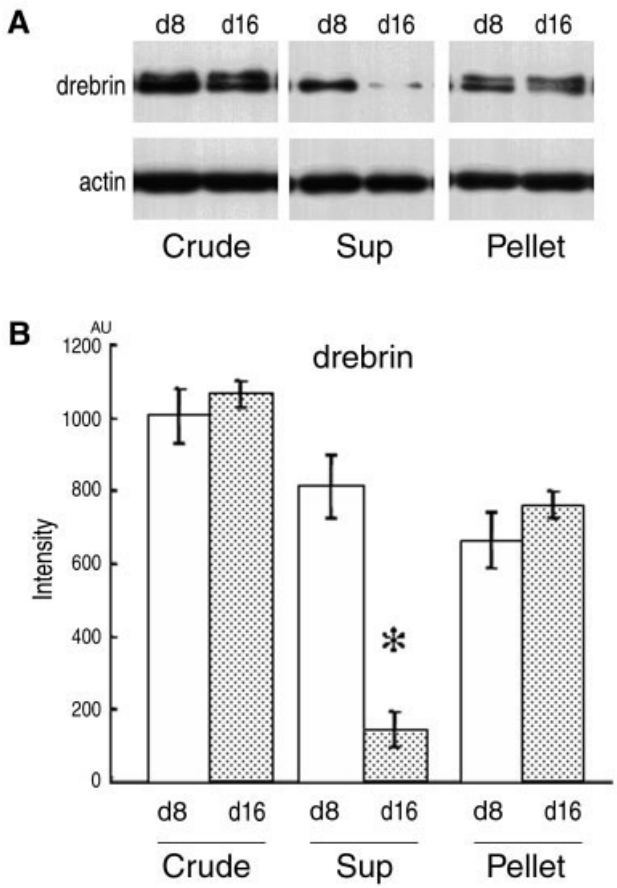

Fig. 12. Densitometric analysis of drebrin in each subcellular fraction. Each fraction equivalent to 0.23 mg of wet weight tissue was quantitatively analyzed in Western blots for drebrin content. Drebrin content was measured as intensity in Western blots from the crude, supernatant, and pellet fractions of postnatal day (PNd) 8 and PNd16 cortex homogenates. Panel **A** shows an example of a Western blot using M2F6 monoclonal antibody directed against drebrin and β-actin immunostaining used for comparison. Drebrin intensity in the supernatant fraction at PNd16 (d16) was significantly less than that at PNd8 (d8, n = 4, $*P < 0.001$, *t* test). Drebrin intensity in the crude and pellet fractions did not change during the same developmental period (n = 4; $P = 0.42$ for crude fraction; n = 4; $P = 0.30$ for the pellet fraction). AU, Arbitrary unit. Error bars indicate SEM. Histograms show mean values ± SEM.

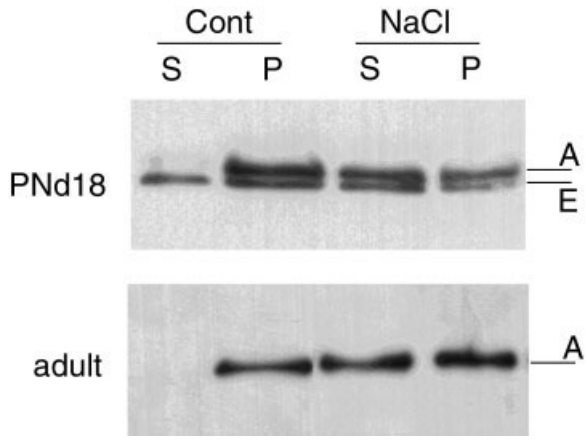

Fig. 13. Drebrin is bound to the cytoskeleton in the pellet. Crude fractions were prepared from cerebral cortices of postnatal day (PNd) 18 (upper panel) and adult rats (lower panel) and was the centrifuged at 200,000 × *g* for 60 minutes at 4°C. The resultant pellet was then homogenized in high-salt buffer and recentrifuged. Proteins in each fraction equivalent to equal amount of wet weight tissue (0.23 mg) were analyzed by Western blot using the M2F6 antibody. Note that intense bands in the supernatant fraction appeared in the high-salt buffer. A, drebrin A; E, drebrin E.

that can provide ionic and nonmembranous association is the cytoskeletal matrix (Glenney et al., 1982; Yamashiro-Matsumura and Matsumura, 1985), of which F-actin is the main constituent within mature spines (Matus, 2000). Drebrin associated with F-actin in the pellet may be the component involved in the formation of spines from the shallow protrusions (protospines).

How does drebrin A associated with F-actin promote spine formation? In vitro assays have shown that drebrin reduces the association of F-actin with α-actinin and tropomyosin, possibly by binding competitively to these latter proteins' binding sites to actin (Shirao and Sekino, 2001). Because α-actinin mediates cross-linking and bundling of actin filaments, the consequence of drebrin binding to F-actin within the submembranous zone would be to relax the actin cytoskeletal matrix, thereby allowing for shape changes to take place. Flexibility is exactly what would be needed for the formation and retraction of dendritic filopodia, enabling actin-based shape changes to occur there.

Our recent and older observations indicate that drebrin A may also play a role at the initial event of synaptogenesis, that is, contact between an axon and a dendrite, even before it plays a role in spine formation. The new observation supporting this idea is that drebrin A immunoreactivity could be found along the flat submembranous surfaces of dendrites and at protospines. This finding is corroborated by earlier studies analyzing the role of drebrin upon intercellular adhesion of cells grown in culture. Specifically, Ikeda et al. (1996) observed that drebrin A transfection of fibroblasts led to the stabilization of adhesion plaques. The isoform drebrin E has been observed to interact with connexin at sites of functional GAP junctions within brain tissue (Butkevich et al., 2004) and also to occur at junctional plaques, defining a specific microfilament anchorage system in polar epithelial cells (Peitsch et al., 1999). There is additional evidence indicating that drebrin A may recruit synaptic proteins resident in spines. Interactions between PSDs and the postsynaptic cytoskeleton involve Shank, a scaffold protein (Naisbitt et al., 1999). Shank is reported to promote the maturation of dendritic spines by regulating the accumulation of spine-resident proteins, such as PSD-95, F-actin, and the NR1 subunit of NMDA receptors (Sala et al., 2001). This influence of Shank upon spine maturation, in turn, is dependent on its binding to Homer. We have shown that drebrin A, like Shank, promotes the accumulation of PSD-95 (Takahashi et al., 2003). Because Homer binds to drebrin A (Mizutani et al., 1999) as well as to Shank, drebrin A may facilitate the synaptic recruitment of Homer and Shank and, hence, the accumulation of PSD-95 and receptors for a coordinated maturation of spines and synapses.

Possible role of drebrin A in adulthood

The developmental increase of drebrin A's association with the pellet fraction and, thus, with actin indicates that drebrin A may continue to regulate dendritic shape in adulthood. Recent studies have permitted direct visualization of spines in vivo over a period of days. Such studies have shown that, indeed, spines undergo turnover throughout adulthood, with approximately 20% of those in the adult cortex disappearing within a day (Trachtenberg et al., 2002; Majewska and Sur, 2003). Spinogenesis is even more active in the hippocampus, with profound changes in spine density occurring every 4–5 days, in synchrony with the estrous cycle (Gould et al., 1990; Woolley et al., 1990; Leranth et al., 2004). The same studies and many others (Bonhoeffer and Yuste, 2002; Star et al., 2002; Konur and Yuste, 2004) have also shown that spine motility is dependent on synaptic activity (reviewed by Harris, 1999). Studies are planned that will examine the impact of overexpression and loss of expression of drebrin A and/or drebrin E upon spine and synapse formation.

ACKNOWLEDGMENTS

We thank Dr. Robert Levy for critical reading of the article and for helpful discussions.

LITERATURE CITED

Aoki C. 1997. Postnatal changes in the laminar and subcellular distribution of NMDA-R1 subunits in the cat visual cortex as revealed by immuno-electron microscopy. Brain Res Dev Brain Res 98:41–59.

Aoki C, Venkatesan C, Go CG, Mong JA, Dawson TM. 1994. Cellular and subcellular localization of NMDA-R1 subunit immunoreactivity in the visual cortex of adult and neonatal rats. J Neurosci 14:5202–5222.

Aoki C, Rodrigues S, Kurose H. 2000. Use of electron microscopy in the detection of adrenergic receptors. Methods Mol Biol 126:535–563.

Aoki C, Miko I, Oviedo H, Mikeladze-Dvali T, Alexandre L, Sweeney N, Bredt DS. 2001. Electron microscopic immunocytochemical detection of PSD-95, PSD-93, SAP-102, and SAP-97 at postsynaptic, presynaptic, and nonsynaptic sites of adult and neonatal rat visual cortex. Synapse 40:239–257.

Asada H, Uyemura K, Shirao T. 1994. Actin-binding protein, drebrin, accumulates in submembranous regions in parallel with neuronal differentiation. J Neurosci Res 38:149–159.

Bonhoeffer T, Yuste R. 2002. Spine motility. Phenomenology, mechanisms, and function. Neuron 35:1019–1027.

Butkevich E, Hulsmann S, Wenzel D, Shirao T, Duden R, Majoul I. 2004. Drebrin is a novel connexin-43 binding partner that links gap junctions to the submembrane cytoskeleton. Curr Biol 14:650–658.

Crosbie R, Adams S, Chalovich JM, Reisler E. 1991. The interaction of caldesmon with the COOH terminus of actin. J Biol Chem 266:20001–20006.

Descarries L. 1991. Non junctional relationships of monoamine axon terminals in the cerebral cortex of adult rat. Volume transmission in the brain: novel mechanisms for neural transmission. Adv Neurosci 1:53–62.

Erisir A, Levey AI, Aoki C. 2001. Muscarinic receptor M(2) in cat visual cortex: laminar distribution, relationship to gamma-aminobutyric acidergic neurons, and effect of cingulate lesions. J Comp Neurol 441:168–185.

Farb CR, Aoki C, Ledoux JE. 1995. Differential localization of NMDA and AMPA receptor subunits in the lateral and basal nuclei of the amygdala: a light and electron microscopic study. J Comp Neurol 362:86–108.

Fox JE. 1985. Identification of actin-binding protein as the protein linking the membrane skeleton to glycoproteins on platelet plasma membranes. J Biol Chem 260:11970–11977.

Fritschy JM, Brunig I. 2003. Formation and plasticity of GABAergic synapses: physiological mechanisms and pathophysiological implications. Pharmacol Ther 98:299–323.

Fujisawa S, Aoki C. 2003. In vivo blockade of N-methyl-D-aspartate receptors induces rapid trafficking of NR2B subunits away from synapses and out of spines and terminals in adult cortex. Neuroscience 121:51–63.

Glenney JR Jr, Glenney P, Weber K. 1982. F-actin-binding and cross-linking properties of porcine brain fodrin, a spectrin-related molecule. J Biol Chem 257:9781–9787.

Gould E, Woolley CS, Frankfurt M, McEwen BS. 1990. Gonadal steroids regulate dendritic spine density in hippocampal pyramidal cells in adulthood. J Neurosci 10:1286–1291.

Harris KM. 1999. Structure, development, and plasticity of dendritic spines. Curr Opin Neurobiol 9:343–348.

Hayashi K, Shirao T. 1999. Change in the shape of dendritic spines caused by overexpression of drebrin in cultured cortical neurons. J Neurosci 19:3918–3925.

Hayashi K, Ishikawa R, Ye LH, He XL, Takata K, Kohama K, Shirao T. 1996. Modulatory role of drebrin on the cytoskeleton within dendritic spines in the rat cerebral cortex. J Neurosci 16:7161–7170.

Hayashi K, Suzuki K, Shirao T. 1998. Rapid conversion of drebrin isoforms during synapse formation in primary culture of cortical neurons. Brain Res Dev Brain Res 111:137–141.

He Y, Janssen WG, Morrison JH. 1998. Synaptic coexistence of AMPA and NMDA receptors in the rat hippocampus: a postembedding immunogold study. J Neurosci Res 54:444–449.

Ikeda K, Shirao T, Toda M, Asada H, Toya S, Uyemura K. 1995. Effect of a neuron-specific actin-binding protein, drebrin A, on cell-substratum adhesion. Neurosci Lett 194:197–200.

Ikeda K, Kaub PA, Asada H, Uyemura K, Toya S, Shirao T. 1996. Stabilization of adhesion plaques by the expression of drebrin A in fibroblasts. Brain Res Dev Brain Res 91:227–236.

Imamura K, Shirao T, Mori K, Obata K. 1992. Changes of drebrin expression in the visual cortex of the cat during development. Neurosci Res 13:33–41.

Ishikawa R, Hayashi K, Shirao T, Xue Y, Takagi T, Sasaki Y, Kohama K. 1994. Drebrin, a development-associated brain protein from rat embryo, causes the dissociation of tropomyosin from actin filaments. J Biol Chem 269:29928–29933.

Jontes JD, Buchanan J, Smith SJ. 2000. Growth cone and dendrite dynamics in zebrafish embryos: early events in synaptogenesis imaged in vivo. Nat Neurosci 3:231–237.

Kojima N, Shirao T, Obata K. 1993. Molecular cloning of a developmentally regulated brain protein, chicken drebrin A and its expression by alternative splicing of the drebrin gene. Brain Res Mol Brain Res 19:101–114.

Konur S, Yuste R. 2004. Developmental regulation of spine and filopodial motility in primary visual cortex: reduced effects of activity and sensory deprivation. J Neurobiol 59:236–246.

Lendvai B, Stern EA, Chen B, Svoboda K. 2000. Experience-dependent plasticity of dendritic spines in the developing rat barrel cortex in vivo. Nature 404:876–881.

Leranth C, Hajszan T, MacLusky NJ. 2004. Androgens increase spine synapse density in the CA1 hippocampal subfield of ovariectomized female rats. J Neurosci 24:495–499.

Levy RB, Aoki C. 2002. Alpha7 nicotinic acetylcholine receptors occur at postsynaptic densities of AMPA receptor-positive and -negative excitatory synapses in rat sensory cortex. J Neurosci 22:5001–5015.

Majewska A, Sur M. 2003. Motility of dendritic spines in visual cortex in vivo: changes during the critical period and effects of visual deprivation. Proc Natl Acad Sci U S A 100:16024–16029.

Marty S, Wehrle R, Alvarez-Leefmans FJ, Gasnier B, Sotelo C. 2002. Postnatal maturation of Na+, K+, 2Cl- cotransporter expression and inhibitory synaptogenesis in the rat hippocampus: an immunocytochemical analysis. Eur J Neurosci 15:233–245.

Matus A. 2000. Actin-based plasticity in dendritic spines. Science 290:754–758.

Megias M, Emri Z, Freund TF, Gulyas AI. 2001. Total number and distribution of inhibitory and excitatory synapses on hippocampal CA1 pyramidal cells. Neuroscience 102:527–540.

Minelli A, Alonso-Nanclares L, Edwards RH, DeFelipe J, Conti F. 2003. Postnatal development of the vesicular GABA transporter in rat cerebral cortex. Neuroscience 117:337–346.

Mizutani A, Shiraishi Y, Mikoshiba K, Furuichi T. 1999. Characterization of Cupidin-binding proteins. Soc Neurosci Abst 25:805.807.

Naisbitt S, Kim E, Tu JC, Xiao B, Sala C, Valtschanoff J, Weinberg RJ, Worley PF, Sheng M. 1999. Shank, a novel family of postsynaptic

density proteins that binds to the NMDA receptor/PSD-95/GKAP complex and cortactin. Neuron 23:569–582.

Peitsch WK, Grund C, Kuhn C, Schnolzer M, Spring H, Schmelz M, Franke WW. 1999. Drebrin is a widespread actin-associating protein enriched at junctional plaques, defining a specific microfilament anchorage system in polar epithelial cells. Eur J Cell Biol 78:767–778.

Peters A. 2002. Examining neocortical circuits: some background and facts. J Neurocytol 31:183–193.

Petralia RS, Wenthold RJ. 1992. Light and electron immunocytochemical localization of AMPA-selective glutamate receptors in the rat brain. J Comp Neurol 318:329–354.

Phend KD, Rustioni A, Weinberg RJ. 1995. An osmium-free method of Epon embedment that preserves both ultrastructure and antigenicity for post-embedding immunocytochemistry. J Histochem Cytochem 43: 283–292.

Purpura DP, Pappas GD. 1972. Structure and function of synapses. New York: Raven Press.

Sala C, Piech V, Wilson NR, Passafaro M, Liu G, Sheng M. 2001. Regulation of dendritic spine morphology and synaptic function by Shank and Homer. Neuron 31:115–130.

Shirao T. 1995. The roles of microfilament-associated proteins, drebrins, in brain morphogenesis: a review. J Biochem (Tokyo) 117:231–236.

Shirao T, Sekino Y. 2001. Clustering and anchoring mechanisms of molecular constituents of postsynaptic scaffolds in dendritic spines. Neurosci Res 40:1–7.

Shirao T, Obata K. 1986. Immunochemical homology of 3 developmentally regulated brain proteins and their developmental change in neuronal distribution. Dev Brain Res 29:233–244.

Shirao T, Inoue HK, Kano Y, Obata K. 1987. Localization of a developmentally regulated neuron-specific protein S54 in dendrites as revealed by immunoelectron microscopy. Brain Res 413:374–378.

Shirao T, Kojima N, Kato Y, Obata K. 1988. Molecular cloning of a cDNA for the developmentally regulated brain protein, drebrin. Brain Res 464:71–74.

Shirao T, Kojima N, Nabeta Y, Obata K. 1989. Two forms of drebrins, developmentally regulated brain proteins, in rat. Proc Jpn Acad 65: 169–172.

Shirao T, Kojima N, Obata K. 1992. Cloning of drebrin A and induction of neurite-like processes in drebrin-transfected cells. Neuroreport 3:109–112.

Shirao T, Hayashi K, Ishikawa R, Isa K, Asada H, Ikeda K, Uyemura K. 1994. Formation of thick, curving bundles of actin by drebrin A expressed in fibroblasts. Exp Cell Res 215:145–153.

Star EN, Kwiatkowski DJ, Murthy VN. 2002. Rapid turnover of actin in dendritic spines and its regulation by activity. Nat Neurosci 5:239–246.

Takahashi H, Sekino Y, Tanaka S, Mizui T, Kishi S, Shirao T. 2003. Drebrin-dependent actin clustering in dendritic filopodia governs synaptic targeting of postsynaptic density-95 and dendritic spine morphogenesis. J Neurosci 23:6586–6595.

Trachtenberg JT, Chen BE, Knott GW, Feng G, Sanes JR, Welker E, Svoboda K. 2002. Long-term in vivo imaging of experience-dependent synaptic plasticity in adult cortex. Nature 420:788–794.

Vaughn JE. 1989. Fine structure of synaptogenesis in the vertebrate central nervous system. Synapse 3:255–285.

Woolley CS, Gould E, Frankfurt M, McEwen BS. 1990. Naturally occurring fluctuation in dendritic spine density on adult hippocampal pyramidal neurons. J Neurosci 10:4035–4039.

Yamashiro-Matsumura S, Matsumura F. 1985. Purification and characterization of an F-actin-bundling 55-kilodalton protein from HeLa cells. J Biol Chem 260:5087–5097.

ELSEVIER

MCN Molecular and Cellular Neuroscience

www.elsevier.com/locate/ymcne
Mol. Cell. Neurosci. 30 (2005) 149 – 157

Overexpression of drebrin A in immature neurons induces the accumulation of F-actin and PSD-95 into dendritic filopodia, and the formation of large abnormal protrusions

Toshiyuki Mizui,[a] Hideto Takahashi,[a] Yuko Sekino,[a,b,1,2] and Tomoaki Shirao[a,*,2]

[a]*Department of Neurobiology and Behavior, Gunma University Graduate School of Medicine, 3-39-22 Showa-machi, Maebashi 371-8511, Japan*
[b]*Core Research for Evolution Science and Technology, Japan Science and Technology Corporation, Kawaguchi, Japan*

Received 22 March 2005; revised 11 June 2005; accepted 30 June 2005
Available online 28 July 2005

Drebrin A is a neuron-specific F-actin binding protein, and plays a pivotal role in the spine formation. In this study, we expressed drebrin A tagged with green fluorescent protein (GFP-DA) in hippocampal neurons at 7–9 days in vitro when presynaptic terminals are not fully maturated. GFP-DA was accumulated in dendritic protrusions and formed large abnormal structures. Since these structures were similar to filopodia in terms of lack of MAP2 immunostaining, we named them "megapodia" meaning large dendritic filopodia. F-actin and PSD-95 were also accumulated in megapodia, and their amounts were significantly correlated with that of GFP-DA. However, the expression of GFP-DA did not result in the promotion of the morphological change from filopodia into spines. These results demonstrate that drebrin A accumulates spine-resident proteins via protein–protein interaction in filopodia, and suggest that the spine formation requires the concurrence of the increase of drebrin-A expression and the functional presynaptic contact.

Introduction

Dendritic spines are the postsynaptic reception regions of most excitatory synapses, and spine formation is fundamental to the development of neuronal networks (Harris, 1999; Harris and Kater, 1994; Yuste and Bonhoeffer, 2001). It has been reported that long thin protrusions from dendrites, dendritic filopodia, change into morphologically mature spines, such as mushroom or stubby spines (Dailey and Smith, 1996; Dunaevsky et al., 1999; Ziv and Smith, 1996). Previous studies suggested that the actin cytoskeleton controlled the shape of both filopodia and spines (Dunaevsky et al., 1999; Fischer et al., 1998). We have recently shown that the accumulation of spine-resident actin cytoskeleton occurs at the initial stage of the morphological change from filopodia to spines and that this accumulation is necessary for the synaptic targeting of PSD-95 (Takahashi et al., 2003). However, the molecular mechanisms that regulate the initial stage of spine formation are still unclear.

Drebrin is a major binding protein of F-actin in the brain (Asada et al., 1994; Ishikawa et al., 1994; Shirao and Obata, 1985) (for review, see Shirao, 1995; Shirao and Sekino, 2001). Drebrin inhibits the actin-binding activity of tropomyosin and α-actinin (Ishikawa et al., 1994), and suppresses actomyosin interactions (Hayashi et al., 1996). Drebrin A is a neuron-specific isoform (Kojima et al., 1993; Shirao et al., 1989; Shirao and Obata, 1986), and its expression is increased in parallel with synapse formation (Hayashi et al., 1998; Shirao et al., 1989; Shirao and Obata, 1986). In adult, drebrin A is a major drebrin isoform, and locates at dendritic spines (Hayashi et al., 1996; Shirao et al., 1987). Transfection experiments have shown that drebrin A expressed in fibroblasts remodels straight actin bundles into thick and winding bundles (Shirao et al., 1994). Overexpression of drebrin A in mature neurons resulted in the elongation of the spine length (Hayashi and Shirao, 1999). Thus, drebrin A regulates dendritic spine shapes by changing the actin cytoskeletal properties.

PSD-95 is a postsynaptic density protein that associates with receptors and cytoskeletal elements at synapses. The overexpression of PSD-95 induced the enlargement of spines, suggesting that PSD-95 regulates the spine formation (El-Husseini et al., 2000). However, we have shown that the accumulation of drebrin and F-actin in dendritic filopodia precedes that of PSD-95 during spine formation (Takahashi et al., 2003). In addition, suppression of drebrin-A expression in developing neurons attenuates not only the accumulation of drebrin and F-actin but also that of PSD-95. Furthermore, replenishment of drebrin-A expression rescues the accumulation of PSD-95. These data suggest that the increase of drebrin-A expression during neuronal development plays a pivotal

* Corresponding author. Fax: +81 27 220 8053.
E-mail address: tshirao@med.gunma-u.ac.jp (T. Shirao).
[1] Present address: Division of Neuronal Network, Inst. Med. Sci., Univ. Tokyo, Tokyo, Japan.
[2] These authors equally contributed to this work.
Available online on ScienceDirect (www.sciencedirect.com).

1044-7431/$ - see front matter © 2005 Elsevier Inc. All rights reserved.
doi:10.1016/j.mcn.2005.06.008

role in the initiation of the spine formation. If so, it would be expected that overexpression of drebrin A at an early developmental stage facilitates the accumulation of spine-resident proteins into filopodia, and promotes the formation of mature spines.

In this study, we expressed drebrin A tagged with enhanced green fluorescent protein (GFP-DA) in cultured hippocampal neurons at 7–9 days in vitro (DIV). We analyzed the effect of exogenously expressed drebrin A on the accumulation of F-actin and PSD-95, and its effect on the morphological change of dendritic filopodia.

Results

Formation of abnormal dendritic protrusions by expression of GFP-DA

To analyze morphological changes induced by drebrin A, we co-expressed GFP-DA and DsRed2 in neurons at 7–9 DIV. In these immature neurons, mature spines are seldom observed (Takahashi et al., 2003), and only trace amount of endogenous drebrin A is expressed although drebrin E, which is not neuron specific, is highly expressed (Hayashi et al., 1998; Shirao et al., 1989). Neurons co-expressing GFP-DA and DsRed2 (GD-DR neurons) formed abnormal large dendritic protrusions (arrows in Fig. 1), in which GFP-DA was highly accumulated. Similar abnormal protrusions were also observed around the cell soma (asterisks in Figs. 1A–C). DsRed2 images showed that these abnormal protrusions (arrows in Figs. 1A, E) were thick and long, and did not have a head-like structure that was a characteristic feature of the mature spine. In addition to abnormal protrusions, transfected cells also have normal filopodia (arrowheads in Fig. 1E). In comparison, control neurons expressing only DsRed2 (DR neurons) did not form any large protrusions similar to the abnormal protrusions of GD-DR neurons, although they formed normal dendritic filopodia (arrowheads in Fig. 1H).

Quantitative analyses showed that the density of dendritic protrusions of GD-DR neurons (36.9 ± 2.1 per 100 μm dendrite, n = 25 dendrites) was not different from that of DR neurons (36.0 ± 2.1 per 100 μm dendrite, n = 28 dendrites) (Fig. 2A). However, dendritic protrusions of GD-DR neurons were significantly longer and wider than those of DR neurons [the average length of dendritic protrusions of GD-DR neurons was 3.9 ± 0.1 μm (n = 600 protrusions) and that of DR neurons was 2.5 ± 0.05 μm (n = 518 protrusions); the average width of dendritic protrusions of GD-DR neurons was 1.1 ± 0.02 μm (n = 600 protrusions) and that of DR neurons was 0.7 ± 0.01 μm (n = 518 protrusions)] (Figs. 2B, C).

We classified dendritic protrusions into abnormal or normal protrusions using DsRed2 images: protrusions that were longer than 4 μm and wider than 1 μm were classified as abnormal protrusions (gray area in Figs. 2D, E); and all other dendritic protrusions were classified as normal protrusions. In GD-DR neurons, 17.5% of dendritic protrusions were abnormal protrusions. In comparison, only 0.8% of dendritic protrusions in control DR neurons were abnormal protrusions. The GFP-DA fluorescent intensity of abnormal dendritic protrusions (1336 ± 72.1 arbitrary

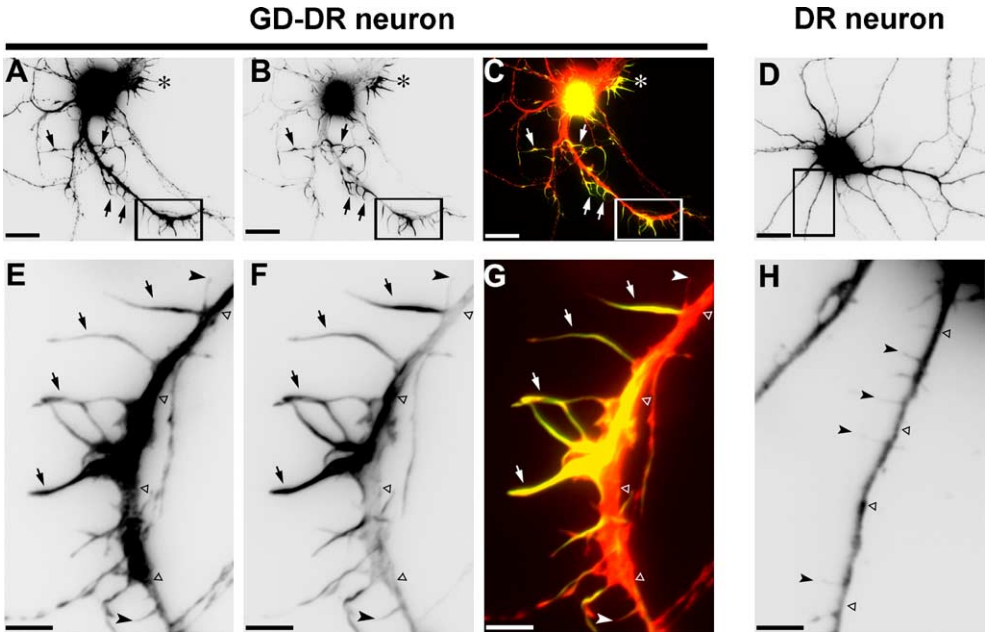

Fig. 1. Expression of GFP-DA in cultured hippocampal neurons at an early developmental stage. DsRed2 cDNA vector with GFP-DA vector or without it was microinjected into nuclei of neurons at 7 DIV, and the neurons were fixed at 9 DIV. (A–C, E–G) Neurons expressing GFP-DA and DsRed2 (GD-DR). (D and H) Control neurons expressing only DsRed2 (DR). Panels E–H are high-magnification images of the boxed region in panels A–D, respectively. Panels A, D, E, and H are DsRed2 images. Panels B and F are GFP-DA images. Panels C and G are merged images of GFP-DA (green) and DsRed2 (red) fluorescences. DsRed2 images (A and E) demonstrated that GD-DR neurons form abnormal dendritic protrusions (arrows) in addition to normal filopodia (arrowheads). Similar abnormal protrusions were also observed around the cell soma (asterisks) in panel A. Note that GFP-DA is highly accumulated in abnormal protrusions, which are observed yellow color in merged images (C and G). In control DR neurons (D and H), normal dendritic filopodia are observed (arrowheads), but no abnormal protrusions are observed. Scale bars: A–D are 20 μm; E–H are 5 μm. Open triangles indicate dendritic shafts.

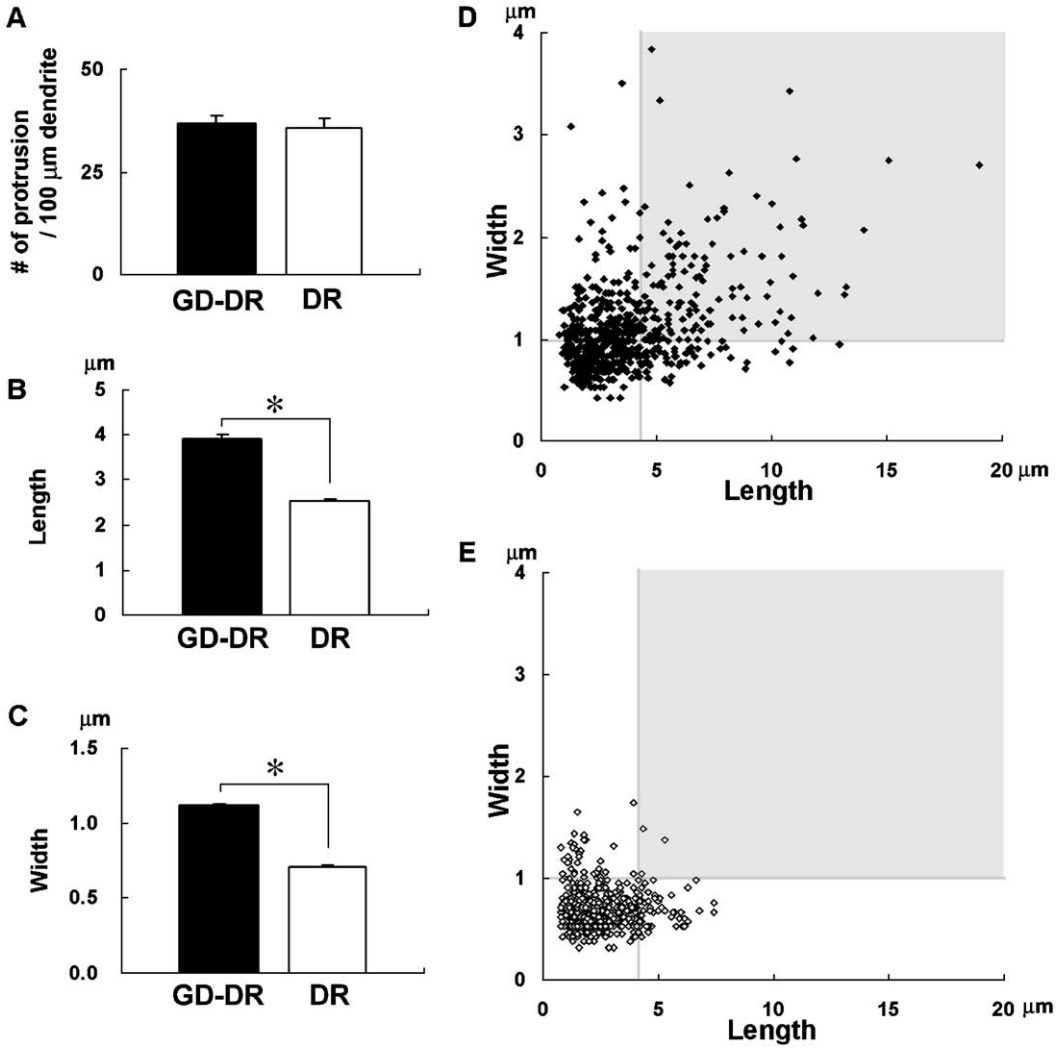

Fig. 2. Quantitative comparisons on the density, length, and width of dendritic protrusions between GD-DR neurons and control DR neurons. The density, length, and width of dendritic protrusions were manually measured using DsRed 2 images. (A) The density of dendritic protrusion of GD-DR neurons ($n = 25$ dendrites) is not different from that of control DR neurons ($n = 28$ dendrites). (B and C) The length (B) and the width (C) of dendritic protrusions of GD-DR neurons ($n = 600$ dendritic protrusions) were significantly higher than those of DR neurons ($n = 518$ dendritic protrusions) (*$P < 0.001$; t test). Histograms show means + SEM. (D and E) Scatter plots of dendritic protrusion length versus its width in GD-DR neurons (D) and in DR neurons (E). Protrusions in gray areas (length, >4 μm; width, >1 μm) are defined as abnormal.

units, $n = 141$) was significantly higher than those of normal protrusions (771 ± 48.2 arbitrary units, $n = 201$) and dendritic shafts (677 ± 78.3 arbitrary units, $n = 32$) in GD-DR neurons (Fig. 3). To analyze the effect of GFP-DA expression on the formation of abnormal dendritic protrusions in more mature neurons, which already have differentiated spines, we expressed GFP-DA in neurons at 21–23 DIV. In these more mature GFP-DA expressing neurons, only 1.3% of dendritic protrusions were abnormal protrusions.

We then analyzed effects of GFP-drebrin A expression on dendritic complexity using Sholl analysis, which quantifies the number of times the dendrites from a given neuron cross concentric circles of increasing diameter. We co-expressed GFP-DA and DsRed2 in neurons at 7–9 DIV, and immunostained them with anti-MAP2 antibody. The Sholl analyses using MAP2 immunofluorescence images showed no significant difference in dendritic complexity between DR neurons ($n = 15$ neurons) and GD-DR neurons ($n = 20$ neurons; t test) (Fig. 4).

Absence of MAP2 in the abnormal protrusions

In order to clarify whether the abnormal protrusions were similar to dendritic shafts or dendritic filopodia, we expressed GFP-DA or GFP in immature neurons, and immunostained them with anti-MAP2 antibody. In GFP-DA expressing neurons, MAP2 immunostaining was faintly observed in abnormal dendritic protrusions (arrows in Fig. 5A), in which GFP-DA was highly accumulated (arrows in Fig. 5B). Instead, intense MAP2 immunostaining was observed throughout dendritic shafts (open triangles in Fig. 5A), in which GFP-DA was observed discontinuously at the submembranous regions along dendrites (open triangles in Fig. 5B). These abnormal protrusions, in which GFP-DA was highly accumulated, were never observed upon axonal processes that did not have intense MAP2 immunostaining. The fluorescent intensity for MAP2 in the abnormal dendritic protrusions (277 ± 11.2, $n = 116$) was significantly lower than that in dendritic shafts (788 ± 81.6, $n = 28$) (Fig. 5C). In control GFP

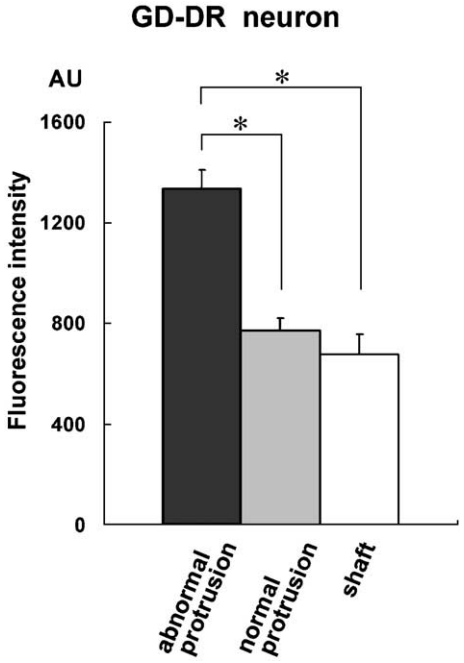

Fig. 3. Accumulation of GFP-DA in abnormal dendritic protrusions. GFP-DA and DsRed2 cDNA vectors were microinjected into nuclei of neurons at 7 DIV, and neurons were analyzed at 9 DIV. The GFP-DA fluorescent intensity of the abnormal dendritic protrusions (n = 141) was significantly higher than that of the normal protrusions (n = 201) (*P < 0.001; t test), and that of the dendritic shaft (n = 32) (*P < 0.001; t test). Histograms show means + SEM. AU, arbitrary unit.

expressing neurons, similar distribution pattern of MAP2 was observed. MAP2 immunostaining was faintly observed in dendritic protrusions and intensely observed in dendritic shafts (Figs. 5D, E). The fluorescent intensity for MAP2 in dendritic protrusions (244 ± 10.1, n = 264), which were identified by GFP images, was significantly lower than that in dendritic shafts (1020 ± 79.3, n = 15) (Fig. 5F).

Comparison of the amount of F-actin and PSD-95 between abnormal dendritic protrusions and normal dendritic filopodia

To examine whether F-actin is more highly accumulated in the abnormal protrusions than in normal dendritic filopodia, we labeled GFP-DA expressing neurons and neighboring control neurons with rhodamine-conjugated phalloidin. Dendritic filopodia in control neurons were weakly labeled (Fig. 6A), but abnormal protrusions in GFP-DA expressing neurons were intensely labeled (Figs. 6B–D). Quantitative analysis showed that RFPS (the ratio of the fluorescence intensity in dendritic protrusion to that in dendritic shaft) for F-actin of GFP-DA expressing neurons (3.58 ± 0.24, n = 208) was significantly higher than that of control neurons (0.65 ± 0.03, n = 326) (Fig. 6E).

Then, we analyzed the accumulation of PSD-95 in abnormal protrusions by immunocytochemistry. In control neurons, a faint punctate staining pattern for PSD-95 was observed mainly in dendritic shafts but seldom in dendritic filopodia (Fig. 6F). In GFP-DA expressing neurons, a similar punctate staining pattern for PSD-95 was observed in the abnormal dendritic protrusions in addition to dendritic shafts (Figs. 6G–I). Quantitative analysis showed that RFPS for PSD-95 of GFP-DA expressing neurons (1.31 ± 0.06, n = 208) was significantly higher than that of control neurons (0.45 ± 0.02, n = 113) (Fig. 6J).

Correlation of GFP-DA with F-actin and PSD-95 in the abnormal dendritic protrusions

In the abnormal dendritic protrusions, there were significant positive correlations in the fluorescent intensity between GFP-DA and F-actin (the correlation coefficient R = 0.803, n = 69) (Figs. 7A, B), and between GFP-DA and PSD-95 (R = 0.669, n = 115) (Figs. 7C, D). The linear regression analysis yielded a straight line between the intensities of GFP-DA and F-actin with an r^2 value of 0.644 and a slope of 0.87, and between those of GFP-DA and PSD-95 with an r^2 value of 0.448 and a slope of 0.14. In contrast, there was no significant correlation in the fluorescent intensity of the abnormal dendritic protrusion between GFP-DA and MAP2 (R = 0.235, n = 118) (Figs. 7E, F).

Effect of GFP-DA expression on presynaptic terminals

In order to clarify whether GFP-DA expression affects presynaptic terminals, we analyzed synapsin I clusters of control and GFP-DA expressing neurons at 7–9 DIV. In control neighboring neurons, most of synapsin I clusters were observed along dendrites (Fig. 8A). In GFP-DA expressing neurons, the distribution pattern of synapsin I clusters was similar to that in control neurons (Fig. 8B). Some, but not all, abnormal protrusions were associated with synapsin I clusters (Figs. 8C, D). Quantitative analysis demonstrated that the number of synapsin I clusters along dendrites of GFP-DA expressing neurons was not different with that of neighboring control neurons (Fig. 8E). As shown in Fig. 8F, the average area of synapsin I clusters along dendrites of GFP-DA expressing neurons (0.67 ± 0.07 μm^2, n = 6 dendrites) was similar

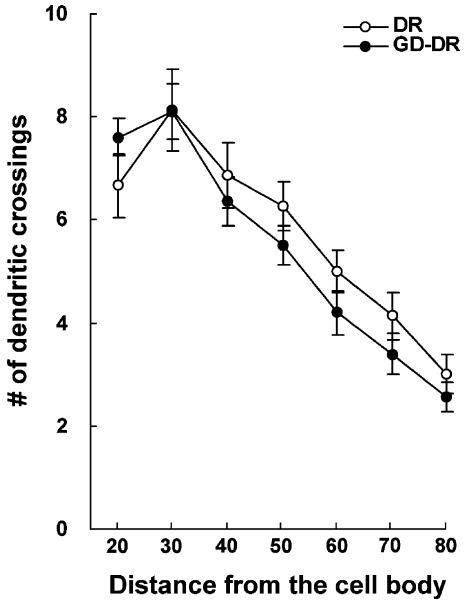

Fig. 4. Dendritic complexities of control DR neurons and GD-DR neurons. GD-DR neurons at 7–9 DIV were immunostained with anti-MAP2 antibody, and analyzed their dendritic complexity using Sholl analysis. DR neurons were used as control. The numbers of times the dendrites crossed concentric circles were not different between DR neurons (n = 15 neurons) and GD-DR neurons (n = 20 neurons; t test).

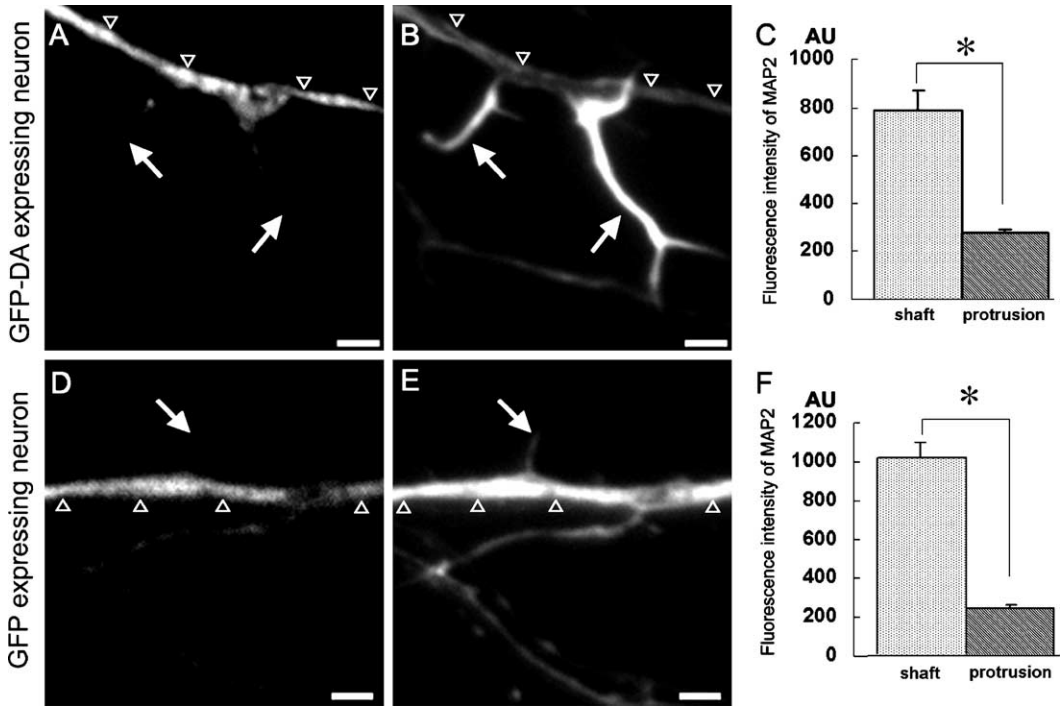

Fig. 5. Lack of MAP2 immunostaining in abnormal dendritic protrusions. GFP-DA vector was microinjected into nuclei of neurons at 7 DIV, and neurons were immunostained with anti-MAP2 antibody at 9 DIV. GFP vector was used as control. (A–C) GFP-DA expressing neuron. Fluorescence images of MAP2 (A) and GFP-DA (B) demonstrated that MAP2 was hardly observed in the dendritic protrusions in which GFP-DA is highly concentrated. Histogram (C) showed that the fluorescence intensity of MAP2 in dendritic shafts ($n = 28$) was significantly higher than that in dendritic protrusions ($n = 116$) ($^*P < 0.001$; t test). (D–F) Control neuron. Fluorescence images of MAP2 (D) and GFP (E) demonstrated that MAP2 was hardly observed in dendritic filopodia. Histogram (F) showed that the fluorescence intensity of MAP2 in dendritic shafts ($n = 15$) was significantly higher than that in dendritic filopodia ($n = 264$) ($^*P < 0.001$; t test). Arrows show dendritic protrusions. Open triangles show parent dendrites. Histograms show mean + SEM. Scale bars: 2 μm. AU, arbitrary unit.

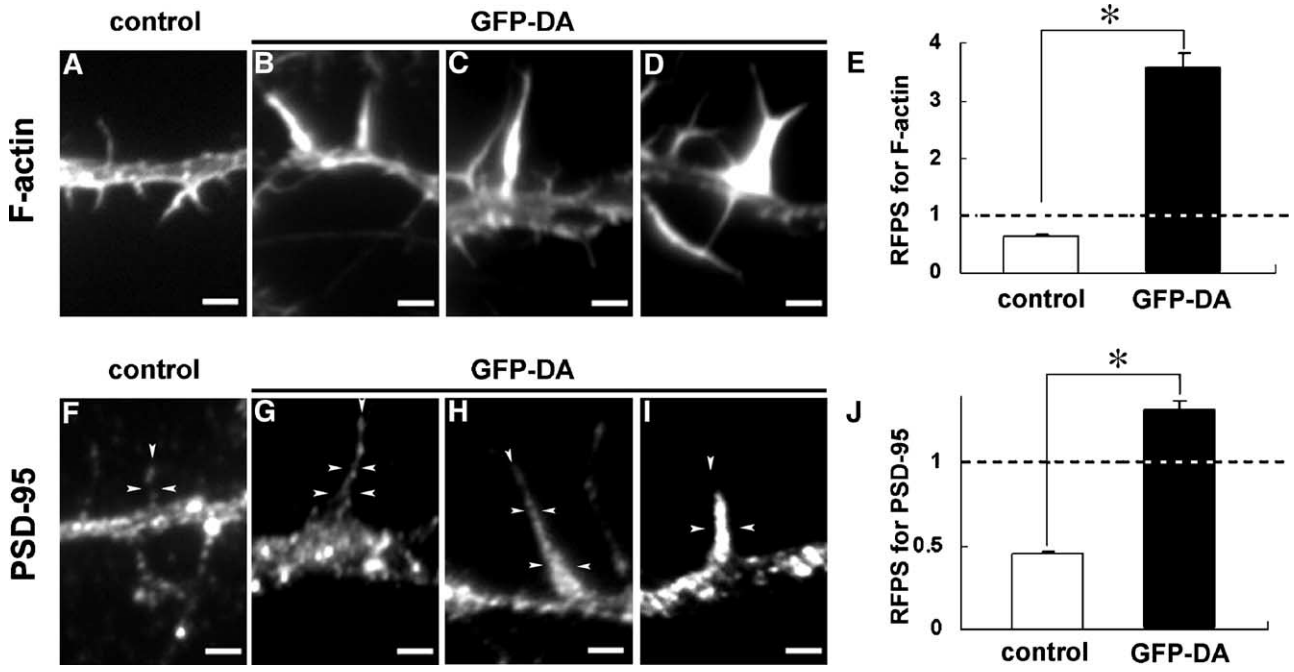

Fig. 6. Accumulation of F-actin and PSD-95 in abnormal dendritic protrusions. (A–D) Fluorescence images of F-actin in a control neighboring neuron (A) and in a neuron expressing GFP-DA (B–D). (E) Histogram showing the ratio of fluorescence intensity in dendritic protrusions to that in dendritic shafts (RFPS) for F-actin. (F–I) Fluorescence images of PSD-95 in a control neighboring neuron (F) and in a neuron expressing GFP-DA (G–I). (J) Histogram showing RFPS for PSD-95. Data showed that both RFPS for F-actin and PSD-95 of GFP-DA expressing neurons were significantly higher than those of control neurons ($^*P < 0.001$; t test). Dotted lines in panels E and J show the level that the fluorescence intensity of dendritic protrusion is equal to that of dendritic shaft. Scale bars: 2 μm. Histograms show means + SEM.

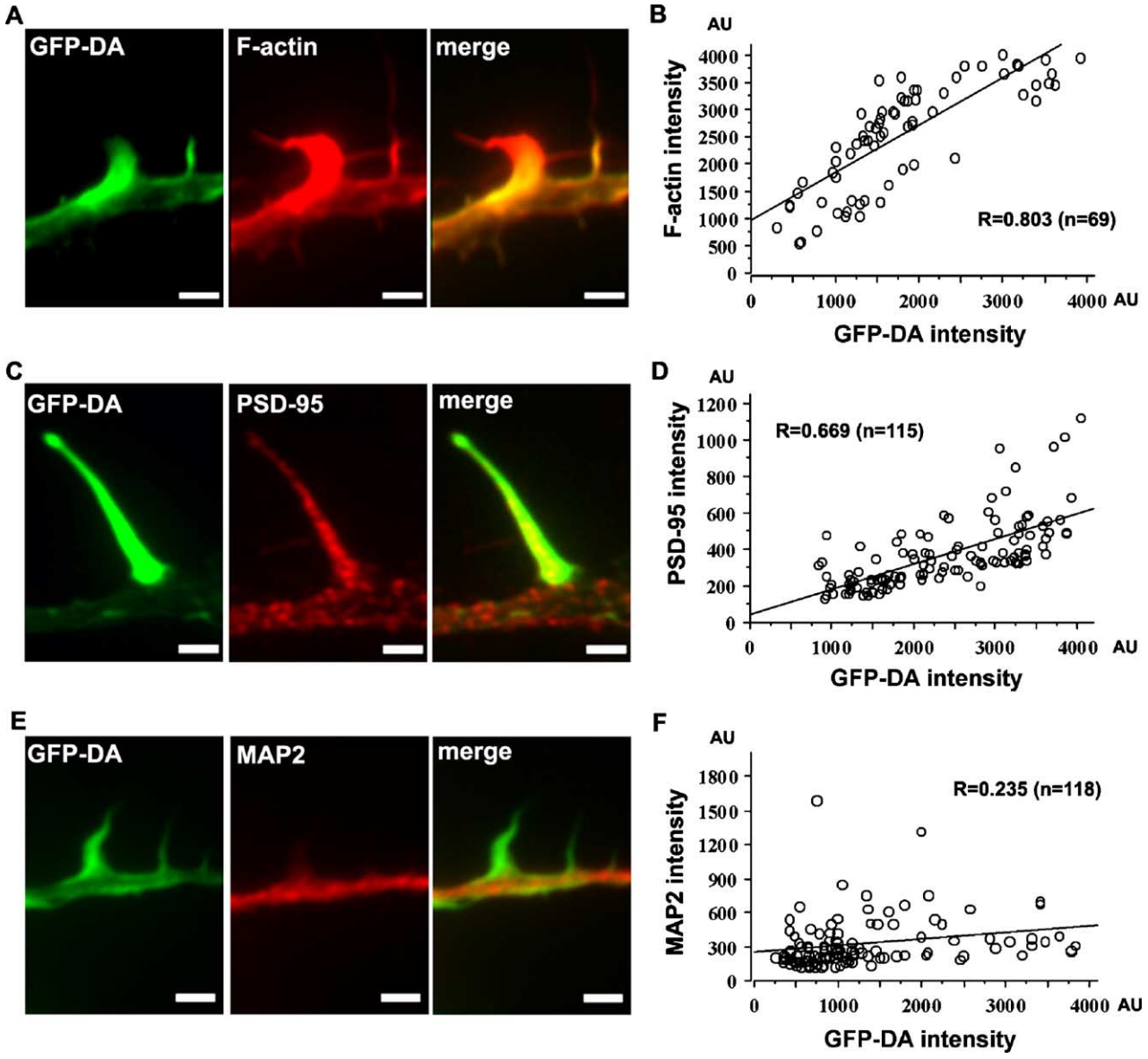

Fig. 7. Correlation of F-actin, PSD-95, and MAP2 levels with GFP-DA level. (A, C, E) Double fluorescence images of abnormal protrusions for GFP-DA and F-actin (A), for GFP-DA and PSD-95 (C), and for GFP-DA and MAP2 (E). (B, D, F) The correlations of GFP-DA and F-actin (B), of GFP-DA and PSD-95 (D), and of GFP-DA and MAP2 (F). The fluorescence intensity of GFP-DA is plotted on *x* axes (B, D, and F), and the fluorescence intensities of F-actin (B), PSD-95 (D), and MAP2 (F) are plotted on the *y* axes. There were significant positive correlations in the levels between GFP-DA and F-actin, and between GFP-DA and PSD-95. There was no significant correlation in the levels between GFP-DA and MAP2. Scale bars: 2 μm. AU, arbitrary unit.

to that of control neurons (0.68 ± 0.13 μm^2, n = 6 dendrites). Further, the average area of synapsin I clusters associated with abnormal protrusions of GFP-DA expressing neurons (0.74 ± 0.12 μm^2, n = 6 dendrites) was not significantly different from that along dendrites.

Discussion

We show here that the expression of GFP-DA in neurons at an early developmental stage results in the formation of abnormal large headless protrusions along dendrites. Expressed GFP-DA is highly accumulated in the abnormal protrusions, in which F-actin and PSD-95 are accumulated in correlation with the amount of GFP-DA. However, the expression of GFP-DA does not promote the morphological change from filopodia into spines. These results indicate that accumulation of spine-resident proteins in the filopodium is not sufficient for the spine formation.

The shape of abnormal protrusions is different from those of normal dendritic filopodia and spines. However, these abnormal protrusions are similar to dendritic filopodia in terms of the headless structure and the absence of MAP2 immunostaining. Hence, we name these abnormal protrusions “megapodia” meaning large dendritic filopodia. Sholl analysis demonstrates that the dendritic complexity of GFP-DA expressing neuron is not different from that of control neuron. This suggests that GFP-DA specifically affects megapodia formation but does not affect entire dendritic growth and arborization.

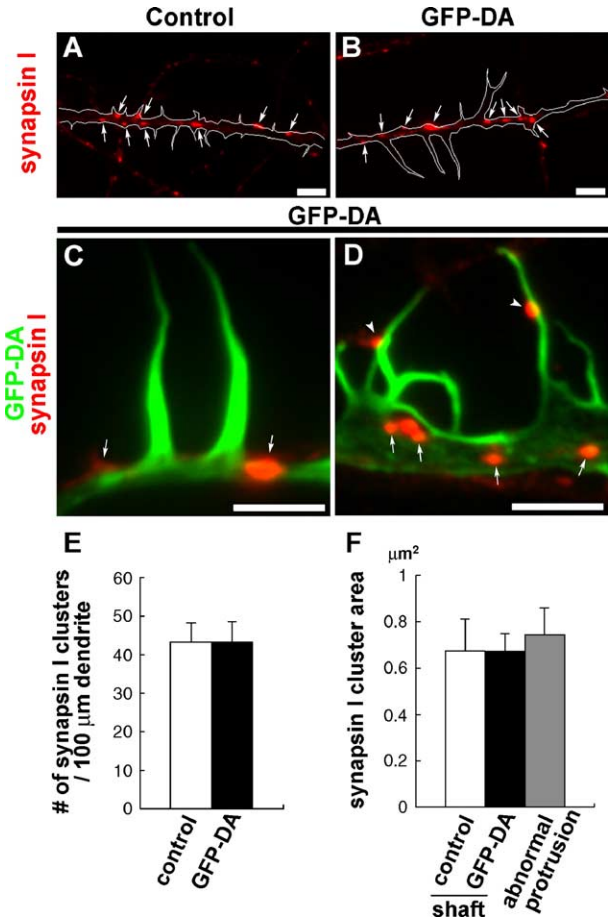

Fig. 8. Effect of GFP-DA expression on synapsin I clusters. (A and B) Low magnification of fluorescence images for synapsin I along dendrites of a control neighboring neuron (A) and of a GFP-DA expressing neuron (B). White lines indicate the contours of dendrites, which are determined with enhanced PSD-95 immunofluorescence image. (C and D) High magnification of double fluorescence images of abnormal protrusions for GFP-DA (green) and synapsin I (red) in GFP-DA expressing neurons. (E) The number of synapsin I clusters per 100-μm dendrites. There was no significant difference in the number of synapsin I clusters between control neurons (n = 12 dendrites) and GFP-DA expressing neurons (n = 12 dendrites, t test). (F) The area of synapsin I clusters. There was no significant difference in the synapsin I cluster area between control shafts (n = 6 dendrites), GFP-DA shafts (n = 6 dendrites), and abnormal protrusions (n = 6 dendrites, t test). Histograms show means + SEM. Scale bars: 5 μm.

Strong linear relationship between the amounts of F-actin and GFP-DA in megapodia indicates that drebrin A accumulates F-actin via direct protein–protein interaction. It is consistent with our previous finding that drebrin binds to actin filaments stoichiometrically in vitro (Ishikawa et al., 1994). Since the correlation coefficient R between the amounts of GFP-DA and PSD-95 is smaller than that of GFP-DA and F-actin, drebrin A probably accumulates PSD-95 via indirect protein–protein interaction. Expression of GFP-DA does not alter the density and size of synapsin I clusters along dendritic shafts. In addition, synapsin I clusters associated with megapodia are not bigger than those associated with dendritic shafts. These data indicate that upregulation of drebrin A during neuronal development in vivo directly relates to the formation of drebrin–actin complex in postsynaptic sites, and that this drebrin–actin complex enables PSD-95 to target at synapses.

Nevertheless, expression of GFP-DA in 7–9 DIV neurons does not promote the morphological maturation of filopodia into spines, and induce megapodia formation instead. In contrast, expression of GFP-DA in 21 DIV cortical neurons, which has many mature spines, results in the elongation of their spine lengths, but not in the megapodia formation (Hayashi and Shirao, 1999). Further, it has been reported that overexpression of PSD-95 in 12 DIV neurons promotes synapse maturation (El-Husseini et al., 2000).

What is the difference between our present finding and other previous findings? One possible explanation is the lack of functional presynaptic terminals at 7–9 DIV. Although it has been reported that synaptic vesicle marker proteins begin to increase in contact sites between axons and dendrites at 7 DIV, these presynaptic terminals hardly have functional synaptic vesicle turnover by 8–10 DIV (Renger et al., 2001). At 12–14 DIV, on the other hand, many functional presynaptic contacts on cultured neurons are observed (Renger et al., 2001). The lack of functional presynaptic contacts may cause megapodia formation. It is consistent to our present observation that the percentage of megapodia in total dendritic protrusions of GD-DR neurons at 21–23 DIV is less than 1/10 of that at 7–9 DIV. These indicate that spine formation requires the influence of presynaptic terminals in addition to the accumulation of drebrin A, F-actin, and PSD-95 at postsynaptic sites. However, we cannot rule out the possibility that lack of some other postsynaptic cytoskeletal molecules, such as αN-catenin, Shank, Homer, and SPAR (Abe et al., 2004; Pak et al., 2001; Sala et al., 2001), prevents spine formation.

In the elongated spines that are formed in mature neurons expressing GFP-DA, GFP-DA is highly concentrated in spine heads but not in spine necks (Hayashi and Shirao, 1999). This suggests that functional presynaptic contacts regulate the subcellular localization of drebrin A and its abundance at postsynaptic sites. When a functional presynaptic contact is absent, expressed GFP-DA may be over-accumulated through entire dendritic filopodia, and consequently dendritic filopodia may change into megapodia. Taken together, it is suggested that the spine formation requires the concurrence of the increase of drebrin-A expression and the functional presynaptic contact.

Experimental methods

Primary culture

Hippocampi were dissected from fetuses at embryonic day 18 (E18) from timed pregnant Wistar rats. Hippocampal cells were prepared by trypsinization and mechanical dissociation according to the methods described previously (Takahashi et al., 2003). Briefly, cell suspensions were plated at a density of 5000 cells/cm^2 on coverslips coated with poly-L-lysine and were incubated in Minimum Essential Medium (MEM) (Invitrogen, San Diego, CA) supplemented with 10% fetal bovine serum. After attachment of the cells, the coverslips were transferred into a culture dish containing a glial mono-layer sheet and maintained in serum-free MEM with a B27 supplement (Invitrogen). Cytosine β-D-arabinofuranoside (Sigma, St. Louis, MO) (10 μM) was added to the cultures at 4 DIV, to inhibit glial proliferation.

All animal experiments were carried out according to the Animal Care and Experimentation Committee, Gunma University,

Showa Campus (Maebashi, Japan). All efforts were made to minimize animal suffering and reduce the number of animals used.

cDNA microinjection

The construction of GFP-DA was described previously (Hayashi and Shirao, 1999). EGFP-C1 and DsRed2-C1 vectors (Clontech, Palo Alto, CA) were used as control. For transfection of these vectors into neurons, we used a microinjection method. Glass micropipettes (Femtotips; Eppendorf, Hamburg, Germany) were filled with Tris–EDTA buffer pH 8.0, which contained cDNA (0.5 μg/μl). We injected cDNA solution into nuclei of multipolar neurons at 7 DIV using a micromanipulator (Micromanipulator 5171; Eppendorf). At 2 days after the injection, the neurons were fixed and analyzed immunocytochemically.

Immunocytochemistry and fluorescent microscopy

Cells were fixed in 4% paraformaldehyde in phosphate-buffered saline pH 7.4 (PBS) at 4°C for 20 min. Fixed cells were permeabilized with 0.1% Triton X-100 in PBS for 5 min and incubated in blocking solution (3% bovine serum albumin in PBS) for 60 min. Then, the cells were incubated overnight at 4°C with a monoclonal antibody against PSD-95 (clone 7E3-1B8; Affinity BioReagents, Golden, CO), or against MAP2 (clone HM-2; Sigma). F-actin was detected with rhodamine-conjugated phalloidin (Molecular Probes, Eugene, OR). After washing with PBS for 30 min, the cells were incubated for 1 h at room temperature with secondary antibodies. Anti-mouse IgG antibodies labeled with rhodamine and with Cy5 (Chemicon, Temecula, CA) were used for detection of the monoclonal antibodies against MAP2 and against PSD-95, respectively. For analyzing Synapsin I clusters, some of neurons were further immunostained using rabbit polyclonal anti-synapsin I antibody (Chemicon) as primary antibody and anti-rabbit IgG antibodies labeled with Cy5 (Chemicon) as secondary antibody. After washing with PBS, the cells were mounted on glass slides with Perma Fluor mounting medium (Thermo Shandon, Pittsburgh, PA).

All fluorescent images of cells were obtained on a Zeiss Axioplan 2 microscope (Zeiss, Jena, Germany) equipped with a Cool Snap fx cooled CCD camera (Photometrics, Tucson, AZ), and operated with Meta Morph software (Universal Imaging, West Chester, PA) through a 63×, 1.4 numerical aperture objective lens (Zeiss). A filter set (86000 Sedat Quad; Chroma, Brattleboro, VT) was mounted in excitation and emission filter wheels (Ludl Electronic Products, Hawthorne, NY) on the microscope. All of the data were collected at 1300 × 1030 resolution at 12 bits/pixel. A single pixel in the image corresponded to a 106-nm square in the specimen plane. The images used for the comparison in this study were collected under an identical condition. Captured fluorescent images were analyzed using Meta Morph software. The signals of GFP and DsRed2 were obtained through the filters for FITC and rhodamine, respectively. We found no unsuitable fluorescent leakage of these signals through the other filters. Images for presentation were prepared using Adobe Photoshop software (Adobe Systems, San Jose, CA).

Quantification

For quantification, multipolar neurons (5–11 neurons) were selected from at least three separate cultures. The density, length, and width of dendritic protrusions were analyzed as described previously (Takahashi et al., 2003). The level of average fluorescent intensity at a dendritic protrusion or at a dendritic shaft was measured using Meta Morph software. For comparison of the amount of each protein between abnormal protrusions and normal dendritic filopodia, the ratio of the fluorescence intensity in dendritic protrusion to that in dendritic shaft (RFPS) was used.

For quantification of dendritic complexity, MAP2 immunofluorescence images of neurons were taken with 40× objective. The concentric sphere method of Sholl modified by Ma et al. (Sholl, 1953; Ma et al., 2003) was used to analyze dendritic complexity. Briefly, concentric spheres of a constant interval, 10 μm, were brought over each cell, and the cells were oriented with the center of soma as origin. Crossing of spheres were counted manually.

For quantification of the cluster number and area, clusters were defined as a staining region with a peak fluorescent level that was twofold greater than the averaged fluorescent level of dendrites. The contours of dendritic shafts were traced with enhanced immunofluorescence images. The clusters along dendritic shafts were automatically counted and measured by computer.

Statview v.5.0.1 software (SAS Institute, Cary, NC) was used for statistical analysis. Data were analyzed by unpaired Student's t test (with Welch's correction for unequal variance, if appropriate). To assess correlations between GFP-DA and other proteins, data were analyzed with Fisher's z transformation and linear regression analysis. All of the data were presented as a mean ± SEM. A P value < 0.001 was considered significant.

Acknowledgments

This work was supported by the Grants-in-Aid (12053209) for Scientific Research from the Ministry of Education, Science, Sports and Culture of Japan to TS and CREST grant to YS. The authors thank Dr. Kunihiko Obata for critical reading of the manuscript and for helpful comments. We thank Ms. Tomoko Takahashi for her excellent technical assistance.

References

Abe, K., Chisaka, O., Van Roy, F., Takeichi, M., 2004. Stability of dendritic spines and synaptic contacts is controlled by alpha *N*-catenin. Nat. Neurosci. 7, 357–363.

Asada, H., Uyemura, K., Shirao, T., 1994. Actin-binding protein, drebrin, accumulates in submembranous regions in parallel with neuronal differentiation. J. Neurosci. Res. 38, 149–159.

Dailey, M.E., Smith, S.J., 1996. The dynamics of dendritic structure in developing hippocampal slices. J. Neurosci. 16, 2983–2994.

Dunaevsky, A., Tashiro, A., Majewska, A., Mason, C., Yuste, R., 1999. Developmental regulation of spine motility in the mammalian central nervous system. Proc. Natl. Acad. Sci. U. S. A. 96, 13438–13443.

El-Husseini, A.E., Schnell, E., Chetkovich, D.M., Nicoll, R.A., Bredt, D.S., 2000. PSD-95 involvement in maturation of excitatory synapses. Science 290, 1364–1368.

Fischer, M., Kaech, S., Knutti, D., Matus, A., 1998. Rapid actin-based plasticity in dendritic spines. Neuron 20, 847–854.

Harris, K.M., 1999. Structure, development, and plasticity of dendritic spines. Curr. Opin. Neurobiol. 9, 343–348.

Harris, K.M., Kater, S.B., 1994. Dendritic spines: cellular specializations imparting both stability and flexibility to synaptic function. Annu. Rev. Neurosci. 17, 341–371.

Hayashi, K., Shirao, T., 1999. Change in the shape of dendritic spines caused by overexpression of drebrin in cultured cortical neurons. J. Neurosci. 19, 3918–3925.

Hayashi, K., Ishikawa, R., Ye, L.H., He, X.L., Takata, K., Kohama, K., Shirao, T., 1996. Modulatory role of drebrin on the cytoskeleton within dendritic spines in the rat cerebral cortex. J. Neurosci. 16, 7161–7170.

Hayashi, K., Suzuki, K., Shirao, T., 1998. Rapid conversion of drebrin isoforms during synapse formation in primary culture of cortical neurons. Dev. Brain Res. 111, 137–141.

Ishikawa, R., Hayashi, K., Shirao, T., Xue, Y., Takagi, T., Sasaki, Y., Kohama, K., 1994. Drebrin, a development-associated brain protein from rat embryo, causes the dissociation of tropomyosin from actin filaments. J. Biol. Chem. 269, 29928–29933.

Kojima, N., Shirao, T., Obata, K., 1993. Molecular cloning of a developmentally regulated brain protein, chicken drebrin A and its expression by alternative splicing of the drebrin gene. Mol. Brain Res. 19, 101–114.

Ma, X.M., Huang, J., Wang, Y., Eipper, B.A., Mains, R.E., 2003. Kalirin, a multifunctional Rho guanine nucleotide exchange factor, is necessary for maintenance of hippocampal pyramidal neuron dendrites and dendritic spines. J. Neurosci. 23, 10593–10603.

Pak, D.T., Yang, S., Rudolph-Correia, S., Kim, E., Sheng, M., 2001. Regulation of dendritic spine morphology by SPAR, a PSD-95-associated RapGAP. Neuron 31, 289–303.

Renger, J.J., Egles, C., Liu, G., 2001. A developmental switch in neurotransmitter flux enhances synaptic efficacy by affecting AMPA receptor activation. Neuron 29, 469–484.

Sala, C., Piech, V., Wilson, N.R., Passafaro, M., Liu, G., Sheng, M., 2001. Regulation of dendritic spine morphology and synaptic function by Shank and Homer. Neuron 31, 115–130.

Shirao, T., 1995. The roles of microfilament-associated proteins, drebrins, in brain morphogenesis: a review. J. Biochem. (Tokyo) 117, 231–236.

Shirao, T., Obata, K., 1985. Two acidic proteins associated with brain development in chick embryo. J. Neurochem. 44, 1210–1216.

Shirao, T., Obata, K., 1986. Immunochemical homology of 3 developmentally regulated brain proteins and their developmental change in neuronal distribution. Brain Res. 394, 233–244.

Shirao, T., Sekino, Y., 2001. Clustering and anchoring mechanisms of molecular constituents of postsynaptic scaffolds in dendritic spines. Neurosci. Res. 40, 1–7.

Shirao, T., Inoue, H.K., Kano, Y., Obata, K., 1987. Localization of a developmentally regulated neuron-specific protein S54 in dendrites as revealed by immunoelectron microscopy. Brain Res. 413, 374–378.

Shirao, T., Kojima, N., Nabeta, K., Obata, K., 1989. Two isoforms of drebrins, developmentally regulated brain protein, in rat. Proc. Jpn. Acad. 65, 169–172.

Shirao, T., Hayashi, K., Ishikawa, R., Isa, K., Asada, H., Ikeda, K., Uyemura, K., 1994. Formation of thick, curving bundles of actin by drebrin A expressed in fibroblasts. Exp. Cell Res. 215, 145–153.

Sholl, D.A., 1953. Dendritic organization in the neurons of the visual and motor cortices of the cat. J. Anat. 87, 387–406.

Takahashi, H., Sekino, Y., Tanaka, S., Mizui, T., Kishi, S., Shirao, T., 2003. Drebrin-dependent actin clustering in dendritic filopodia governs synaptic targeting of postsynaptic density-95 and dendritic spine morphogenesis. J. Neurosci. 23, 6586–6595.

Yuste, R., Bonhoeffer, T., 2001. Morphological changes in dendritic spines associated with long-term synaptic plasticity. Annu. Rev. Neurosci. 24, 1071–1089.

Ziv, N.E., Smith, S.J., 1996. Evidence for a role of dendritic filopodia in synaptogenesis and spine formation. Neuron 17, 91–102.

Neuroscience xx (2006) xxx

IN VIVO, COMPETITIVE BLOCKADE OF *N*-METHYL-D-ASPARTATE RECEPTORS INDUCES RAPID CHANGES IN FILAMENTOUS ACTIN AND DREBRIN A DISTRIBUTIONS WITHIN DENDRITIC SPINES OF ADULT RAT CORTEX

S. FUJISAWA,[a] T. SHIRAO[b] AND C. AOKI[a]*

[a]*Center for Neural Science, New York University, 4 Washington Place #809, New York, NY 10003, USA*

[b]*Department of Neurobiology and Behavior, Gunma University Graduate School of Medicine, 3-39-22 Showamachi, Maebashi 371, Japan*

Abstract—*In vitro* studies have demonstrated that prolonged *N*-methyl-D-aspartate receptor (NMDAR) blockade triggers a homeostatic up-regulation of NMDARs at synapses. Such upregulation can also be seen within 30 min *in vivo* in adult rats, implicating trafficking of reserve pools of NMDARs. Here, we evaluated the involvement of filamentous actin (F-actin), the major cytoskeletal component in spines, in this rapid *in vivo* homeostatic response, using biotinylated phalloidin as its probe. We also immuno-labeled spines for drebrin A, an F-actin-binding protein found at excitatory synapses and with a proposed role of modulating F-actin's cross-linking with one another and interactions with NMDARs. Quantitative 2-D analysis of ultrastructural images revealed that NMDAR blockade increased filamentous actin labeling per spine by 62.5% ($P<0.005$). The proportion of dendritic spines immuno-labeled for drebrin A also increased significantly, from 67.5% to 85% following NMDAR blockade ($P<0.001$), especially among larger spines. The frequency distributions of spine widths and postsynaptic density lengths were not affected by the D-(+)-2-amino-5-phosphonopentanoic acid (D-APV) treatment. However, the average postsynaptic density length was reduced by 25 nm among the fewer, drebrin A immuno-negative spines, indicating that drebrin A confers stability to synapse size. We propose that, in a homeostatic *in vivo* response, increases of drebrin A and F-actin within spines can enhance NMDAR trafficking by reducing cytoskeletal rigidity within the spine cytoplasm without changing the overt morphology of axo-spinous synapses. Alternatively or in addition, the cytoskeletal redistribution within spine cytoplasm may be triggered by the D-APV-induced, homeostatic up-regulation of NMDAR.

Key words: F-actin, drebrin, activity-dependent, trafficking, electron-microscopy, immunocytochemistry.

Dendritic spines exhibit high concentrations of cytoskeletal proteins, such as filamentous actin (F-actin) (Capani et al., 2001), and these proteins are believed to be involved in activity-dependent organization of synaptic molecules. For example, Fukazawa et al. (2003) showed that F-actin in spines is essential in long-term potentiation (LTP)-induced trafficking of alpha-amino-3-hydroxy-5-methyl-4-isoxazole propionic acid (AMPA) receptors. However, the involvement of cytoskeleton in activity-dependent trafficking of *N*-methyl-D-aspartate subtype of glutamate receptors (NMDARs) is not as well understood. Previous *in vitro* studies showing that NMDARs increase within dendritic spines in response to long-term NMDAR blockade (Rao and Craig, 1997; Turrigiano, 1999; Barria and Malinow, 2002; Carpenter-Hyland et al., 2004). Our laboratory has shown that a 30-minute *in vivo* application of an NMDAR antagonist, D-(+)-2-amino-5-phosphonopentanoic acid (D-APV), also produces a significant increase in the number of pre- and post-synaptic NR2A subunits and a concurrent decrease of synaptic NR2B subunits (Aoki et al., 2003; Fujisawa and Aoki, 2003). This rapid, homeostatic regulation of NMDAR may be achieved by trafficking of receptors along cytoskeletal tracts that connect the postsynaptic density (PSD) to the cytoplasm of spine heads and dendritic shafts. The current study examined D-APV-induced changes in the amount of two major cytoskeletal proteins within spines, namely, F-actin and the F-actin-binding protein, drebrin A.

F-actin functions as part of the PSD anchor for synaptic proteins, including NMDARs and drebrin. The disruption of F-actin drastically alters the localization of these molecules within spines (Adam and Matus, 1996; Allison et al., 1998, 2000), indicating that F-actin is also involved in intra-spine trafficking and endo/exocytosis of receptors (Kaech et al., 2001; Zhou et al., 2001; Qualmann et al., 2004). Reorganization of actin cytoskeleton is, in turn, initiated by changes in synaptic activity (van Rossum and Hanisch, 1999). Influx of extracellular Ca^{2+} via activation of NMDARs causes stabilization of F-actin (Star et al., 2002) and spine morphology (Ackermann and Matus, 2003; Brunig et al., 2004). Strong stimulation of NMDARs, however, induces massive depolymerization of F-actin and eventual collapse of dendritic spines (Rosenmund and Westbrook, 1993; Halpain et al., 1998). We surmised that F-actin within spines might be increased by the 30-min NMDAR blockade, and this promotes the intra-spinous trafficking of NMDARs.

*Corresponding author. Tel: +1-212-998-3926; fax: +1-212-995-4011.
E-mail address: chiye@cns.nyu.edu (C. Aoki).

Abbreviations: AMPA, alpha-amino-3-hydroxy-5-methyl-4-isoxazole propionic acid; BSA, bovine-serum albumin; DAB, diaminobenzidine; D-APV, D-(+)-2-amino-5-phosphonopentanoic acid; EM, electron microscopy/electron microscope; F-actin, filamentous actin; L-APV, L-(+)-2-amino-5-phosphonopentanoic acid; LTP, long-term potentiation; NMDAR, *N*-methyl-D-aspartate receptor; PB, phosphate buffer; PBS, phosphate buffer saline; PSD, postsynaptic density; SIG, silver-intensified gold.

0306-4522/06$30.00+0.00 © 2006 IBRO. Published by Elsevier Ltd. All rights reserved.
doi:10.1016/j.neuroscience.2006.03.009

We also hypothesized that receptor trafficking might be facilitated by the dissociation of NMDARs from the cytoskeletal anchors. α-Actinin-2 is known to anchor NMDARs onto actin cytoskeleton (Wyszynski et al., 1997; Dunah et al., 2000). An increase of another F-actin-binding protein, drebrin A, would competitively displace α-actinin-2 from F-actin, thus freeing receptors from cytoskeletal anchors and allowing them to relocate (review by Shirao and Sekino, 2001). Thus, we predicted that NMDAR blockade would increase intra-spinous levels of drebrin A and this event facilitates NMDAR trafficking within spines. Here, we report that our findings concur with these predictions about drebrin A and F-actin.

EXPERIMENTAL PROCEDURES

In vivo blockade of NMDARs in the cerebral cortex

We used tissues from brains of four animals prepared in our previous NMDAR-blockade experiments and prepared brains from four additional animals, using an alternative fixative (described below). *In vivo* application of NMDAR antagonist was as described previously (Aoki et al., 2003; Fujisawa and Aoki, 2003). Briefly, adult male Sprague–Dawley rats were anesthetized with 50 mg/kg of Nembutal. After stabilizing their heads in a stereotaxic apparatus, bilateral craniotomy and durotomy was performed over the medial parietal cortex. A small piece of Gelfoam (approximately 5 mm^2) soaked in 5 mM D-APV (Sigma, St. Louis, MO, USA) was placed above the durotomy site ($\sim$2 mm in length) in one hemisphere. The contralateral hemisphere received an equal-sized piece of Gelfoam soaked in an equal concentration of the inactive enantiomer, L-(+)-2-amino-5-phosphonopentanoic acid (L-APV) (Sigma). Both drugs were dissolved in artificial cerebrospinal fluid (115 mM NaCl, 3.3 mM KCl, 1 mM $MgSO_4$, 2 mM $CaCl_2$, 25.5 mM $NaHCO_3$, 1.2 mM NaH_2PO_4, 5 mM lactic acid, and 25 mM glucose). The drug application lasted for 30 min. All surgical procedures were in accordance with the National Institutes of Health Guide for the Care and Use of Experimental Animals and were approved by the NYU Animal Care and Use Committee. Care was taken to minimize the number of animals used and their suffering.

Tissue processing for ultrastructural analysis

At the end of drug application, the animals were perfused transcardially, first for 30 s with saline containing 300 USP units/ml of heparin (Henry Shine, NY, USA), followed immediately with the aldehydes. The perfusate was either 4% paraformaldehyde (EMS, Hatfield, PA, USA), mixed with 1% glutaraldehyde (EMS; therein called "glutaraldehyde-fixed") and dissolved in 0.1 M phosphate buffer (PB) (Aoki et al., 2003; Fujisawa and Aoki, 2003), or 4% paraformaldehyde alone (therein called "paraformaldehyde-fixed"). The brain was dissected out of the skull, and cut into 40 μm-thick sections using a vibratome. This procedure yielded approximately 20 vibratome sections that contained the cortical neuropil residing directly under the drug-soaked Gelfoam. All of these vibratome sections were stored, free-floating, in 0.01 M PB with 0.9% sodium chloride (phosphate buffer saline, PBS) and 0.05% sodium azide, at 4 °C.

Ultrastructural localization of F-actin and drebrin A for electron microscopy (EM)

F-actin was detected by its binding to biotinylated phalloidin (Molecular Probes, Eugene, OR, USA), while drebrin A was detected immunocytochemically using a well-characterized antibody (Aoki et al., 2005). First, the sections were freeze-thawed (see Aoki et al., 2003) in order to enhance penetration of histological reagents, then incubated in 1% hydrogen peroxide in PBS for 30 min and washed in PBS in order to minimize background labeling. Subsequently, the sections were incubated in 1% bovine-serum albumin in PBS (PBS–BSA) for 30 min in order to block non-specific binding of phalloidin or of the anti-drebrin A antibody.

We detected F-actin using silver-intensified gold (SIG) as the label. This label is non-diffusible and discrete, thus amenable to quantification and precise localization within single spines (Aoki et al., 2003). The sections were incubated in biotinylated phalloidin (Molecular Probes), diluted 1:20 in PBS–BSA with 0.05% sodium azide for 3 days at room temperature. After washes in PBS, tissues labeled with phalloidin were further incubated in a 1:100 dilution of 0.8 nm gold-conjugated goat anti-biotin antibody (EMS) for 3 h. Following post-fixation with 1% glutaraldehyde, the colloidal gold particles were intensified with silver (SIG), using the IntensEM Kit (Amersham, Arlington Heights, IL, USA). This procedure enlarges the gold particles to sizes detectable under the EM. Tissues labeled with phalloidin underwent osmium-free tissue processing to minimize loss of SIG labels (see Phend et al., 1995; Aoki et al., 2003).

The vibratome sections allotted for drebrin A immuno-labeling were processed for HRP–diaminobenzidine (DAB)-based labeling. HPR-DAB-based labels are diffusible and enzymatically amplified, thereby allowing for better detection of antigens. This label was chosen over SIG, because we wanted to optimize detection of the protein within spines, more than the precise localization or quantification within single spines. The tissues were incubated in PBS–BSA–azide solution containing a 1:1000 dilution of the anti-drebrin A antibody for 3 days at room temperature. After washes in PBS, these sections were incubated in a 1:200 dilution of secondary antibody, biotinylated goat anti-rabbit IgG (Vector, Burlingame, CA, USA) for 30 min, followed by PBS washes. Tissues were then incubated in the avidin–biotin complex solution (Elite Kit, Vector) for 30 min. Bound antibodies were visualized by the peroxidase reaction, using 0.3% 3,3′-DAB HCl in PBS with 0.01% hydrogen peroxide as a substrate. After washing in PBS, drebrin A-labeled tissues were fixed using 1% osmium tetroxide for 1 h.

Cytochemical control sections for both F-actin and drebrin labeling underwent the same procedures in parallel, except that they were incubated in PBS–BSA–azide without phalloidin or the drebrin A antibody.

The phalloidin- and drebrin A-labeled sections were dehydrated through incubations in ethanol and acetone, and then embedded in EMBed 812 (EMS). Drug-treated areas of the brain were determined by slight indentations of the cortex that resulted from craniotomy. Small areas of cortex ($\sim$1 mm in diameter) from the region immediately below the craniotomy were embedded in Beem capsules (2 vibratome sections from each animal). Previous studies showed that the D-APV-induced NMDAR redistribution was restricted to a 2 mm diameter of surface area immediately below the craniotomy (Aoki et al., 2003), and a depth extending down to layer 2 (Fujisawa and Aoki, 2003). The quantitative EM analysis in the current study was restricted to this zone showing the NMDAR trafficking. Each capsule was coded so that the experimental condition of each vibratome section would be unknown to the experimenter until the data analysis stage.

EM

Labeled tissues were cut into approximately 80 nm-thick sections using an ultramicrotome before examination under the EM (JEOL 1200XL, Japan). Conventional EM negatives or a digital camera (Hamamatsu CCD Camera, Japan; AMT, Danvers, MA, USA) were used to capture EM images from at least two grids per capsule. These images were taken in a systematically random

order for unbiased sampling, and in close proximity (within 5 μm) to the tissue–Epon interface, where labeling was most intense. At least two grids from each hemisphere from each animal were examined under the EM. For every animal, 40~80 pictures were taken for each experimental condition at 20,000~30,000× magnification. During the process of picture taking and the subsequent data collection, the experimenter had no knowledge of the treatment condition of the tissues being examined.

Data sampling: DAB and SIG labeling

We tallied the synapses in the electron micrographs in the order encountered. Asymmetric synapses were identified by the juxtaposition of two plasma membranes, with the presynaptic terminals containing synaptic vesicles, and the opposing profiles containing electron-dense PSDs.

Control tissues received no exposure to biotinylated phalloidin, but were incubated in a solution containing gold-conjugated anti-biotin antibodies. These displayed an extremely low level of non-specific, background labeling. Only one or two particles were observed within 20 μm^2 of the tissue captured by any single digital picture, and none of them fell on top of a synapse. Therefore, in F-actin-labeled tissues, a synapse was categorized as "labeled" if it contained even a single SIG particle within either the pre- or postsynaptic profile. In labeled synapses, the number of SIG particles within the pre- and postsynaptic profiles was recorded.

For drebrin-labeled tissues, synapses were categorized into one of three tiers, according to the intensity of the DAB reaction product. If the labeling filled the entire profile and was of strong intensity, the profile was categorized as "intensely labeled." If the labeling was discretely concentrated to a small area within the profile, or if it was of lighter intensity, the profile was categorized as "lightly labeled." Synapses with no detectable peroxidase reaction product were categorized as "not labeled."

Data sampling: spine widths and PSD lengths

In order to determine whether the 30-min D-APV blockade of NMDARs causes a change in the size of spines and synapses, we undertook a quantitative morphometric analysis. The ultra-thin sections used for these measurements were the same ones that had undergone immunolabeling for drebrin A. All of the tissue used for morphological analysis had undergone drebrin A-immunocytochemistry, followed by osmium tetroxide fixation. This set of tissue was chosen, because osmium post-fixation minimized tissue shrinkage. A minimum of two grids were used from each of the seven D-APV and the seven L-APV-treated hemispheres. As stated previously, these were derived from a systematically random selection of vibratome sections.

For measurements of spine widths and PSD lengths, we identified axo-spinous synapse profiles by the presence of PSDs, the spine apparatus and by the lack of mitochondria and microtubules in the postsynaptic profile. While we understand that there are large dendritic protrusions containing mitochondria and microtubules (Li et al., 2004), we excluded postsynaptic structures with these organelles, so that we could be sure to exclude dendritic shafts, many of which would be GABAergic and only sparsely spiny (White, 1989). Thus, by excluding the potentially GABAergic postsynaptic profiles from the sample, we were able to focus our analysis to excitatory synapses formed upon glutamatergic neurons (i.e. glutamate-to-glutamate connections). Synapses for which only a part of the spine was visible in the micrograph were also excluded from this analysis.

For each analyzable postsynaptic spine encountered within a single plane of section, we measured a drawn line that coursed parallel to the PSD at the widest point of the spine. The distance from one to the other end of the PSD darkening was measured using an Accutracker pen (Precision Technology Devices, IL, USA), taking care to follow the PSD's curvature. The lengths of these lines in nanometers were calculated according to the magnification of the micrographs taken.

Unlike a 3-D morphometric analysis, such as the disector method, the 2-D analysis introduces two forms of bias: greater sampling of larger spines than of smaller ones, and inability to verify that spine widths are being measured at their widest points (Mouton, 2002). Indeed, a limited 3-D analysis of a dozen randomly encountered spines indicated that spine width measurements differed by about 20% compared with the outcome from 2-D analysis (data not shown). However, our aim was not to determine the absolute values of spine diameters or PSD lengths, but to determine whether the D-APV treatment caused a population shift in the size of synapses and spines, relative to the values observed within the L-APV-treated hemispheres. Moreover, we wished to use the same sample for analyzing whether the D-APV treatment had different effects upon drebrin A-immunoreactive versus drebrin A-negative spines. Since immunoreactivity is strongly influenced by the depth from the vibratome surface, we opted to sample widely and more efficiently using single-plane sections at portions that captured the resin-vibratome interfaces, rather than to perform 3-D reconstructions. Care was taken to use matched final magnifications to view and capture images from the D- and L-APV tissues.

Data analysis

In order to determine whether the proportion of F-actin- or drebrin-labeled synapses was different between the L-APV- and D-APV-treated tissues, we calculated the percentage of labeled synapses for every 20 synapses encountered. Student's *t*-test was used to determine the significance of differences between mean percentages of L- vs. D-APV tissues. Additionally, we also performed a Freeman-Tukey transformation method (Freeman and Tukey, 1950) of converting binomial data set into normal distributions. The results of this statistical test were similar to the *t*-test and thus are not shown.

When analyzing the differences in the number of F-actin-labeled SIG particles within single synapses, we grouped animals according to the aldehyde used for brain fixation. The two groups were 4% paraformaldehyde alone (will be referred to as the "paraformaldehyde-fixed tissue") and 4% paraformaldehyde plus 1% glutaraldehyde ("glutaraldehyde-fixed tissue"). The frequency distributions of average SIG particles per synapse were skewed heavily to the right regardless of the fixative used. Therefore, instead of using a parametric test to compare data from L- vs. D-APV tissues, we performed the non-parametric, Mann-Whitney *U* test. The group statistics were calculated by averaging the percent-changes from the L-APV data for each animal. The significance of the differences in percent-changes was tested using single-sample *t*-test, since the distributions were normal (data not shown).

The frequency distributions of spine widths and PSD lengths were normal, and therefore these sets of data from L-APV tissues and D-APV tissues were statistically compared using the Student's *t*-test.

Multiple linear regressions were performed to determine the degree of correlation between spine widths and PSD lengths.

RESULTS

NMDAR blockade induces an increase in the proportion of synapses labeled for F-actin using phalloidin

The cortical surfaces of adult rats were treated with a competitive NMDAR antagonist, D-APV, over one hemisphere and with its inactive enantiomer, L-APV, on the

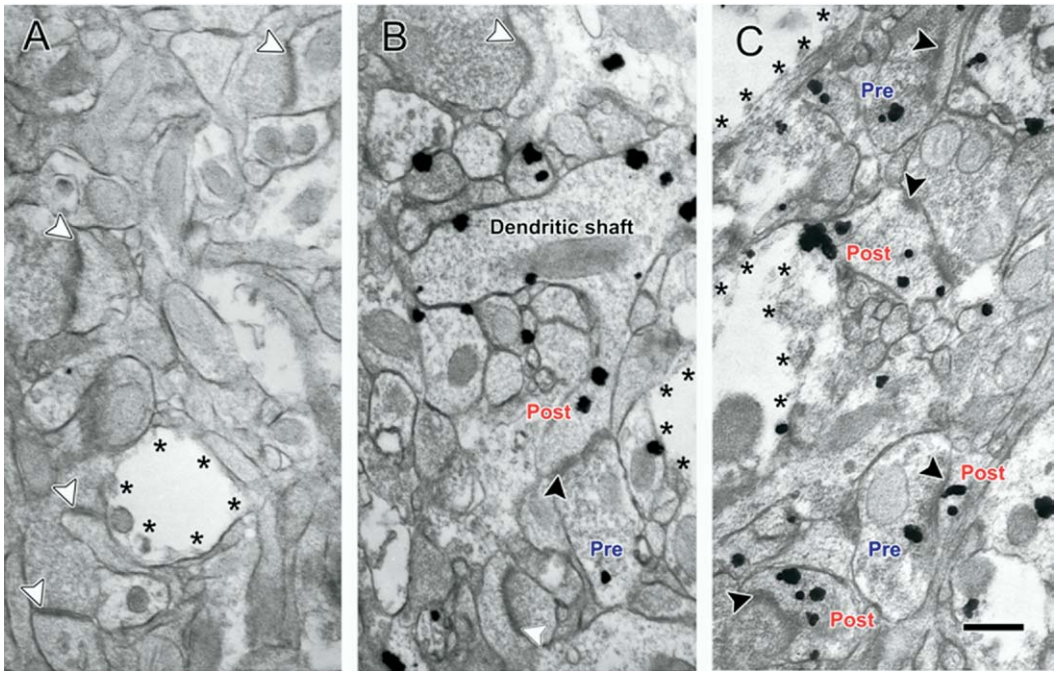

Fig. 1. Electron micrographs show phalloidin-labeling of F-actin in presynaptic axon terminals and postsynaptic spines of L-APV- and D-APV-treated tissues. The micrographs in these figures were derived from tissues of a paraformaldehyde-fixed animal, sampled strictly along the tissue-Epon interface (asterisks on the Epon-side). Arrowheads, indicating synapses, reside in the presynaptic terminals and point to PSDs. White arrowheads point to unlabeled synapses. Black arrowheads point to labeled synapses; i.e. those with one or more SIG particles in pre- and/or postsynaptic terminals. Post, postsynaptic spine; Pre, presynaptic axon terminal. Scale bar=200 nm. (A) Cytochemical control tissue from D-APV-treated hemisphere, incubated in a buffer lacking biotinylated phalloidin but containing gold-conjugated anti-biotin antibody. There was very little SIG labeling; none of them were found at synapses. (B) Pharmacological control, L-APV-treated tissue. Phalloidin labels were found in dendritic shafts, spines and axon terminals. Those found in dendritic spines were tallied as "postsynaptic labels," while those of the axon terminals were tallied as "presynaptic labels." In this example, two out of three synapses within this field show no detectable phalloidin-binding sites. (C) D-APV-treated tissue. More synapses were labeled with SIG particles and each labeled synapse contained more particles, compared with the L-APV-treated tissue.

contralateral hemisphere for 30 min. Aldehyde-fixed brain tissues from these animals were labeled for F-actin, using biotinylated phalloidin. Phalloidin was visualized with SIG particles, and their presence at drug-infused synapses in layer I of the cortex was determined by EM. Fig. 1B and C show examples of L- and D-APV-infused areas respectively, taken from one of four paraformaldehyde-fixed animals. Tissues from glutaraldehyde-fixed animals (n=3) exhibited relatively less labeling. In both types of tissues, SIG particles were observed in dendritic spines and axon terminals, as well as in dendritic shafts.

Since no synapse exhibited background SIG particles when phalloidin was omitted from the incubation cocktail (Fig. 1A), we were able to categorize a synapse as "labeled" (black arrowheads in Fig. 1), even if it contained only one SIG particle within its pre- or postsynaptic profile. When we calculated the average percentage of labeled synapses for every 20 synapses encountered in the L-APV-treated hemisphere, the paraformaldehyde-fixed tissues contained more synapses labeled with phalloidin (40.3±1.8% S.E.M.) than the glutaraldehyde-fixed tissues (24.5±2.1% S.E.M.; Fig. 2). Presumably, this difference in labeling reflects differences in accessibility of the phalloidin binding site brought about by the different fixation conditions. In both glutaraldehyde- (t=4.78, df=63, P<0.001) and paraformaldehyde-fixed tissues (t=3.64, df=91, P<0.001), the proportion of F-actin-labeled synapses in the D-APV-treated area was increased significantly, compared with the L-APV-treated area, using Student's t-test (Fig. 2). This indicated that more synapses reached

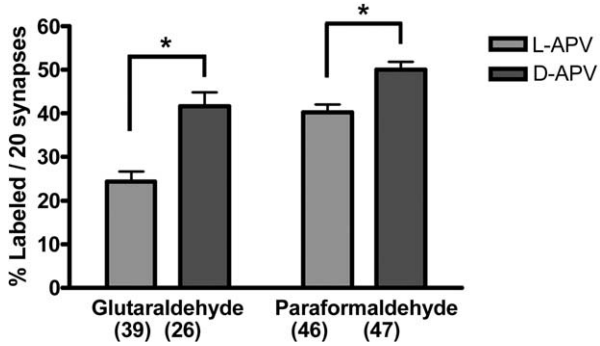

Fig. 2. The proportion of phalloidin-labeled synapses increases after D-APV application. For every 20 synapses encountered, the percentage of immuno-labeled synapses was calculated. The bar graphs show the mean percentage with S.E.M. as error bars. The numbers in parentheses below the bars correspond to the N for that data set. The distributions were compared between L-APV and D-APV treatments of single animals. Student's t-test showed significant increase in the proportion of labeled synapses, in both glutaraldehyde- and paraformaldehyde-fixed tissues. * Indicates P<0.001.

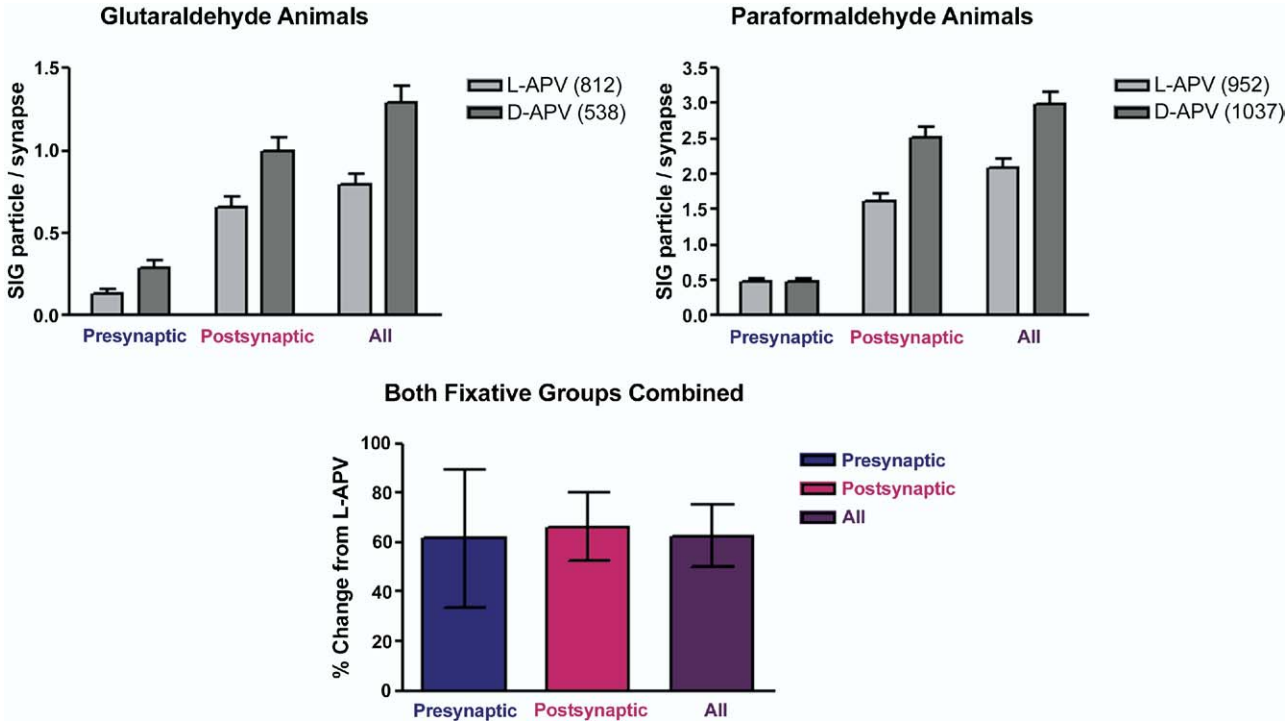

Fig. 3. The number of SIG particles labeling F-actin in the synaptic subcellular domains is greater in the D-APV-treated tissues. Top two graphs (A and B) represent the average number of SIG particles found within presynaptic profile, postsynaptic profile and across both micro-domains of each synapse ("All"). Data in graph A were taken from tissues of animals perfused with 4% paraformaldehyde–1% glutaraldehyde mixture ($n=3$). Data in graph B were from paraformaldehyde-fixed animals ($n=4$). Error bars show the standard error of means across synapses. Lighter-colored bars are data from L-APV-treated tissues from each animal, and darker-shaded bars are those from D-APV-treated tissues. The total number of synapses examined for both tissues is shown in parentheses next to the legend. Statistical analysis comparing L- and D-APV-treated tissues was performed for each micro-domain of each animal separately, using the non-parametric Mann-Whitney *U* test. Single asterisk indicates $P<0.001$. Panel C combines the data from both groups of data, by averaging the percent change from L-APV from all of the glutaraldehyde- and paraformaldehyde-fixed animals examined ($n=7$). Single-sample *t*-test was used to determine whether the changes were significantly different from zero; single star denotes $P<0.005$.

threshold level for F-actin detection, following the D-APV application.

NMDAR blockade induces an increase in the average number of F-actin labels within single synapses

We suspected that an increase in the number of synapses with detectable levels of F-actin reflects an increase in the amount of spinous F-actin within single synaptic profiles. Since SIG particles are quantifiable, we calculated the average number of SIG particles found within the following ultrastructural domains: within the presynaptic axon terminal, within the postsynaptic dendritic shaft or spine, and combined across both domains ("all"; Fig. 3). For each category, the average number of SIG particles per synapse was compared between the L- and D-APV-treated areas.

In glutaraldehyde-fixed brain tissues (Fig. 3A), SIG particles were less numerous in the presynaptic domain than in the postsynaptic domain. Comparisons across the drug treatments revealed a 63.3% greater density of SIG particles in the "all" category of the D-APV condition, relative to the L-APV condition ($z=5.15$, $df=1348$, $P<0.001$, Mann-Whitney *U* test). The D-APV condition exhibited an increase of SIG particles in the "presynaptic" ($z=2.16$, $df=1348$, $P<0.05$) and "postsynaptic" ($z=3.98$, $df=1348$, $P<0.001$) micro-domains of synapses as well.

As seen in the glutaraldehyde-fixed tissue, the paraformaldehyde-fixed tissue (Fig. 3B) also exhibited less SIG particles in the presynaptic domain. Comparisons across the drug-treatment conditions revealed that SIG particles were significantly greater within postsynaptic profiles of the D-APV condition ($z=4.51$, $df=1987$, $P<0.001$), but not significantly different within presynaptic terminals ($z=0.49$, $df=1987$, $P>0.05$). In the combined "all" category, a significant increase by 43.1% followed the D-APV application ($z=4.25$, $df=1987$, $P<0.001$).

In order to analyze the overall trend across both fixative groups, the data from all animals ($n=7$) were combined by taking an average of percent-changes induced by the D-APV treatment, relative to the L-APV data, from each animal (Fig. 3C). Using single-sample *t*-test, we found a significant increase of SIG counts in the "postsynaptic" category (66.3%; $t=4.8$, $df=6$, $P<0.005$) and the "all" category (62.5%; $t=4.98$, $df=6$, $P<0.005$). Presynaptic counts also increased by the drug treatment, but the changes were too variable to be statistically significant ($t=2.19$, $df=6$, $P>0.05$). The data suggest that NMDAR blockade induces a greater, more consistent increase of

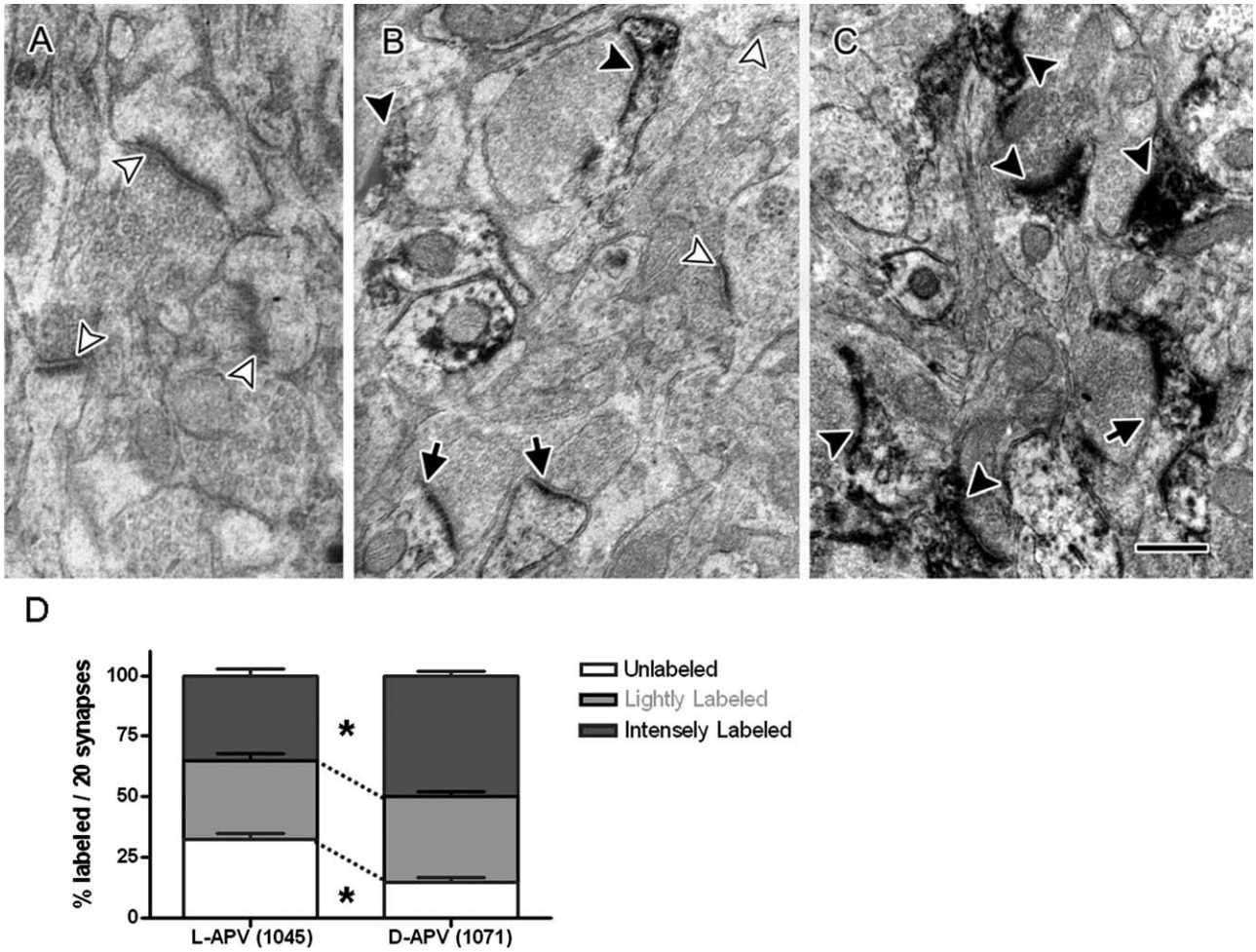

Fig. 4. D-APV treatment induces significant increases in drebrin A-labeled spines. All micrographs were taken from a representative animal. As with phalloidin-labeled tissues, pictures were taken along the tissue–Epon interface. All arrows indicating synapses are in presynaptic terminals, pointing at PSDs. White arrowheads point to unlabeled synapses; black arrows to lightly-labeled synapses; and black arrowheads to intensely-labeled synapses. Drebrin A labeling, when present, was always found within the postsynaptic profile and was never found presynaptically. (A) Control tissues incubated in a buffer without the primary antibody but otherwise treated identically to experimental tissue. No synapse was labeled by DAB (white arrows). (B) L-APV-treated tissue. Most synapses were labeled with DAB, but many of them were only lightly labeled (black arrows). (C) D-APV-treated tissue. There were more intensely labeled synapses (black arrowheads). (D) Each bar represents the proportion of unlabeled (white), lightly-labeled (gray) and intensely-labeled (dark gray) spines among all spines encountered (indicated in parentheses on the *x* axis). The proportion of unlabeled spines was significantly reduced within D-APV tissues, while the proportion of intensely-labeled synapses was significantly increased. Asterisk indicates $P<0.001$ by Student's *t*-test.

F-actin labels within postsynaptic profiles compared with presynaptic terminals.

NMDAR blockade increased the proportion of drebrin A-immunoreactive spines

We next evaluated whether the D-APV-induced increase of F-actin was accompanied by changes in drebrin A, an adult isoform of an F-actin-binding protein. In four glutaraldehyde-fixed animals, we immuno-labeled drebrin A with an isoform-specific antibody and visualized it with an immuno-peroxidase reaction product (Fig. 4B and C). There was not a single synapse whose presynaptic terminal was labeled for drebrin A but the majority of postsynaptic spines were immunolabeled. The average percentage of synapses lacking any immuno-labeling (white arrowheads in Fig. 4A and B) for every 20 synapses encountered was 32.5% in the L-APV-treated tissues and 15.0% in the D-APV-treated tissues. This decrease following D-APV treatment was statistically significant by the Student's *t*-test (Fig. 4D; $t=6.00$, $df=100$, $P<0.001$).

The peroxidase immuno-reaction product was categorized to be "intensely labeled" or "lightly labeled" depending on the extent and intensity of labeling within spines. Fig. 4 shows examples of intensely-labeled spines where the entire profile is filled with dark reaction product (Fig. 4B and C, black arrowheads). A lightly-labeled profile was so categorized when the reaction product was either only partially filled or was less intense (Fig. 4B and C, black arrows). Since the intensely- and lightly-labeled spines occurred within close proximity of one another, it is unlikely that this heterogeneity in the intensity of labeling resulted from varied degrees of penetration of immuno-reagents.

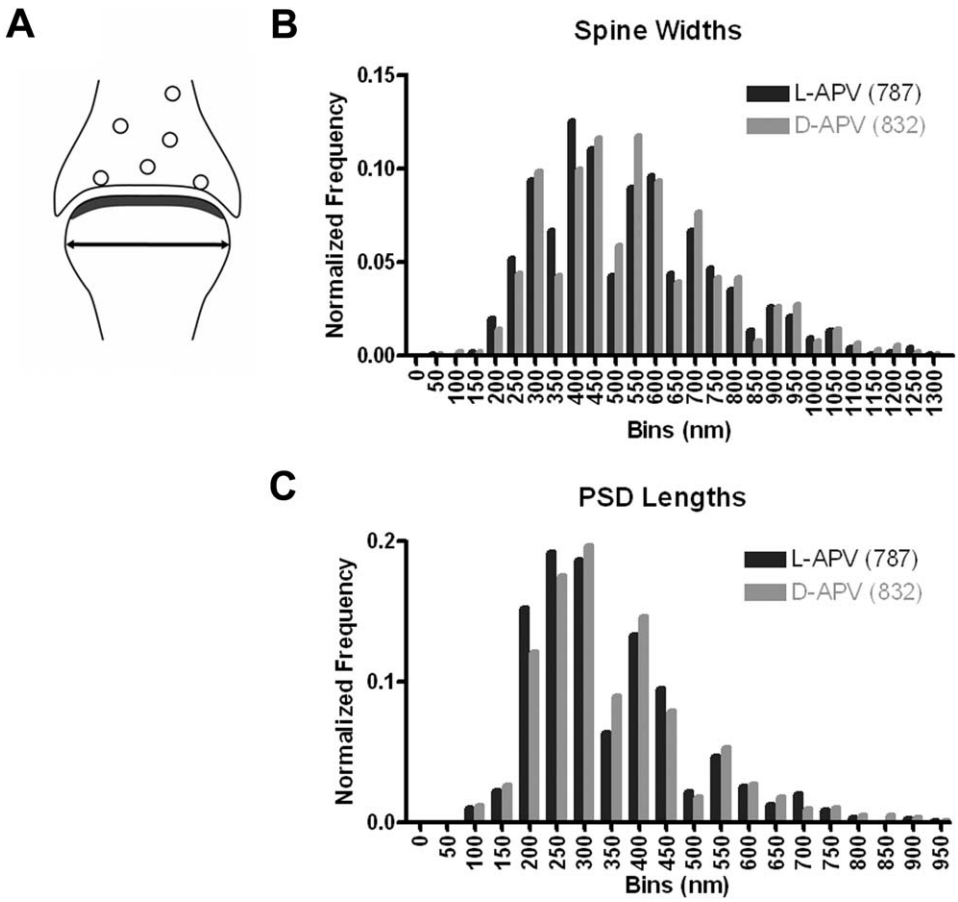

Fig. 5. D-APV treatment did not cause enlargement of spine heads or lengthening of PSDs. (A) Schematic drawing of how spine widths were measured on electron micrographs taken from glutaraldehyde- and osmium-fixed, drebrin immuno-labeled tissue. All spines encountered, whether or not drebrin A-labeled, were included in the sample. A line parallel to the PSD and postsynaptic membrane was drawn at the widest part of the spine head (arrow). Then length of this line was measured in nanometers. Additionally, the length of the PSD was measured by following any curvatures that were present along the synaptic cleft. (B, C) Normalized frequency distributions of spine widths and PSD lengths, respectively, binned by 50 nm. The numbers in parentheses in the legend represent the *N* for each group. There were no statistical differences in frequency distributions from the L- and D-APV tissues.

Rather, this heterogeneity is more likely to reflect varied amounts of drebrin A within spines, or differences in drebrin A's conformation that allow more antigenic sites to be available for antibody binding.

The proportion of intensely-labeled synapses was determined for every group of 20 randomly encountered synapses. Analysis of these groups revealed a significant increase in the proportion of intensely-labeled synapses following D-APV application ($t=4.79$, $df=100$, $P<0.001$; Fig. 4D). On the other hand, the proportion of lightly-labeled synapses did not change ($t=0.79$, $df=100$, $P>0.05$), suggesting that D-APV-induced increase in the number of drebrin A-immuno-positive synapses was due almost entirely to an increase of the intensely-labeled synapses.

NMDAR blockade does not induce morphological changes

Following an LTP-inducing protocol, an increase of F-actin within dendritic spines is accompanied by an increase in the volume of those spines (Matsuzaki et al., 2004). Although our pharmacological treatment was not an LTP-inducing paradigm, we also observed an increase of F-actin within spines. Thus, we sought to determine whether D-APV induced changes in the apparent size of dendritic spine profiles and PSD profiles. 2-D analysis was chosen over 3-D analysis, so as to maximize the sample size within the zone that was both D-APV-treated and immunolabeled. (Further discussion of the rationale for this approach appears under "Experimental Procedures.")

Altogether we measured 1619 spine profiles. In L-APV-treated tissue, the average spine width (drebrin A-labeled and unlabeled, combined) was 538.5 nm (±7.6 nm S.E.M.) and ranged from 58.8 nm to 1323.5 nm. The mean spine width in the D-APV tissue was 551.8 nm (±7.4 nm S.E.M.) and ranged from 58.8 nm to 1323.5 nm (Fig. 5B). Student's *t*-test revealed that there is no significant difference in the spine-width distribution between the L-APV and the D-APV tissues ($t=1.24$, $df=1617$, $P>0.05$).

Analysis of PSD lengths from the same sample of spines showed that D-APV application did not induce any change in this parameter either ($t=0.87$, $df=1617$, $P>0.05$). The average PSD length in the L-APV tissue was

345.3 nm (±5.0 nm S.E.M.), ranging from 88.2 nm to 941.2 nm. In the D-APV tissue, PSD lengths had the same range of distribution, and the average length was 351.4 nm (±4.9 nm S.E.M.) (Fig. 5C).

Correlation between spine widths and PSD lengths was significant in the L-APV tissues (r^2=0.589, P<0.001), as tested by multiple regression analysis. As expected, the correlation between these two values remained significant in the D-APV tissues (r^2=0.567, P<0.001).

Spines containing drebrin A-immunoreactivity are larger and the larger spines are more likely to gain drebrin A-immunoreactivity following the NMDAR blockade

Although the average size of synapses remained the same, a possibility remained that a size change occurred within the subpopulation distinguishable by drebrin A-immunoreactivity.

We first noted that, in L-APV tissues, drebrin A immuno-positive spines were larger (567.4±9.9 nm S.E.M.) and had longer PSDs (371.7±6.2 nm S.E.M.) than those lacking drebrin A immunoreactivity (490.7±11.4 nm S.E.M. for spine widths; 301.4±7.1 nm S.E.M. for PSD lengths). These differences were significant, as tested by the Student's t-test (t=4.93, df=785, P<0.001 for spine widths; t=6.99, df=785, P<0.001 for PSD lengths). Similarly significant differences were found in spine widths and PSD lengths in the D-APV tissues (t=5.13, df=830, P<0.001 for spine widths; t=7.04, df=830, P<0.001 for PSD lengths).

NMDAR blockade induced a small reduction in the average spine width of drebrin A-negative synapses (25.2 nm reduction), compared with those in L-APV tissues, but this difference did not reach statistical significance (t=−1.27, df=427, P>0.05). The drug application also reduced the average PSD length of drebrin A-negative synapses by 27.4 nm, and this change reached statistical significance (t=−2.23, df=427, P<0.05). The PSD lengths of drebrin A-positive spines decreased following D-APV treatment, but to a smaller extent (by 5.6 nm). Widths of these drebrin A-immunoreactive spines were unaffected by the NMDAR blockade, increasing only by 0.8 nm. These results suggested that the drebrin A-positive spines are resistant to the D-APV-induced decrease of spine and PSD sizes.

Seeing that the D-APV treatment induced no significant overall changes in spine widths or PSD lengths, but did cause an increase in the proportion of spines with drebrin A-immunoreactivity, we then asked whether drebrin A-immunoreactivity increased similarly across spines of different sizes. To address this question, we categorized spines into two: those with diameter greater than 700 nm and those with diameter less than 700 nm. A comparison across the two size groups revealed that larger spines were more likely to contain drebrin A, as seen within the L-APV tissue (t=4.23, df=38, P<0.001). D-APV-induced increase of drebrin A-immunoreactivity was greater among the larger spines (by 61.1%) than the smaller spines (by 54.5%). Altogether, these observations indicated that larger spines are more likely to be drebrin A-immunoreactive and are also more likely to gain drebrin A-immunoreactivity following NMDAR blockade.

DISCUSSION

Previously, our laboratory showed that 30-minutes of *in vivo* NMDAR blockade causes trafficking of the NR2A subunits of NMDARs into the synaptic area and of the NR2Bs away from synapses (Aoki et al., 2003; Fujisawa and Aoki, 2003). In the present study, we have demonstrated that the same manipulation also causes changes in the distribution of cytoskeletal proteins, especially within the larger spines, without causing overt changes in the size of spines or PSDs.

NMDAR blockade alters cytoskeletal distribution: postsynaptic impact

We have shown that both the number of synapses labeled with phalloidin and the density of labeling within single synaptic profiles significantly increased following NMDAR blockade (Figs. 2 and 3). How might the increased F-actin level contribute to the homeostatic up-regulation of NMDARs? Compared with AMPA receptors, relatively little is known about the trafficking of NMDAR within spines (Wu et al., 2002; Schulz et al., 2004; Wierenga et al., 2005). F-actin allows vesicles to traffic via myosin motor proteins (Baker and Titus, 1998; Wu et al., 2002) and these myosin motor proteins have been localized to spines (Morales and Fifkova, 1989; Walikonis et al., 2000). Although NMDARs have not been identified as cargoes, Naisbitt et al. (2000) have shown that PSD-95, a scaffolding protein often associated with NMDARs, is trafficked along F-actin via myosin-V. For trafficking up to the spine but not within spines, Hirokawa's group has identified KIF-17-containing motor protein complexes that carry NR2B subunits along microtubules in the dendrites (Setou et al., 2000; Guillaud et al., 2003). Taken together, the increased F-actin observed within D-APV-blocked spines may facilitate the movement of NMDAR-containing vesicles within spines relatively more than in dendritic shafts.

NMDAR blockade alters cytoskeletal distribution: presynaptic impact

We have demonstrated here that D-APV induces an increase of F-actin within terminals, albeit to a lesser degree than within spines. Perhaps the lack of postsynaptic NMDAR activity is reported back to the presynaptic terminal via retrograde signaling, and the presynaptic terminal increases F-actin in order to maintain homeostasis. How might axonal F-actin be involved in the maintenance of homeostasis?

F-actin's role within axon terminals remains unclear (Doussau and Augustine, 2000; Halpain, 2003). Some studies suggest that neurotransmitter vesicles are trafficked along actin filaments via myosin (Evans et al., 1998). F-actin may also be involved in vesicle recycling (Shupliakov et al., 2002), scaffolding of vesicles (Sankaranarayanan et al., 2003) and/or vesicular release (Cole et al., 2000). Increased levels of F-actin in the terminals may enhance these vesicular func-

tions and, together, increase neurotransmitter release as a response to NMDAR blockade.

Increased F-actin in terminals may also facilitate the trafficking of presynaptic NMDARs. NMDARs are present in the axon terminals as autoreceptors (Woodhall et al., 2001; Sjostrom et al., 2003), and we have seen changes in the distribution of these receptors within axons following D-APV applications (Aoki et al., 2003; Fujisawa and Aoki, 2003).

NMDAR blockade may create a plastic cytoskeletal environment via drebrin A

Drebrin A is the adult form of an F-actin-binding protein that is found exclusively in postsynaptic compartments of excitatory synapses (Fig. 4B and C, also see Aoki et al., 2005). In this study, we have shown that 30 min of NMDAR blockade causes a significant increase in the proportion of synapses immuno-labeled for drebrin A (Fig. 4D). This increase is likely to reflect the influx of drebrin A from dendritic shafts. De novo synthesis of drebrin A is less likely, since the D-APV treatment was brief. It is possible that conformational changes have also taken place, yielding enhanced immunoreactivity of the protein.

What does the observed increase of drebrin A immunolabeling signify? Firstly, drebrin A competes with α-actinin-2 for actin-binding. α-Actinin-2 is another dynamic PSD protein (Nakagawa et al., 2004) with binding sites for both F-actin and NMDARs (Wyszynski et al., 1997; Dunah et al., 2000). If α-actinin-2 anchors synaptic NMDARs onto the actin cytoskeleton, and if the observed increase of drebrin A (due to increased protein level or possibly also due to conformational changes) leads to greater displacement α-actinin-2 from the actin cytoskeleton, this disruption may free NMDARs to be trafficked into or out of the synaptic zone (review by Shirao and Sekino, 2001).

Besides linking NMDARs to the cytoskeleton, α-actinin-2 also has an actin cross-linking activity (Dunah et al., 2000; Gimona et al., 2002). With drebrin preventing α-actinin-2 from bundling the actin filaments (Ishikawa et al., 1994), the actin cytoskeleton may be more mobile and plastic, thereby allowing for increased trafficking of NMDARs within spines.

Drebrin also competes with tropomyosin for actin-binding (Ishikawa et al., 1994). Tropomyosin, when bound to actin, protects actin filaments from actin-destabilizing agents. Since increased drebrin A levels should reduce the number of tropomyosin-actin complex, we suggest that actin cytoskeleton in D-APV-treated spines could be more susceptible to severing. Perhaps this is a necessary condition to allow filaments to break free of a rigid organization and then enhance motility of NMDARs within spines.

An increase of drebrin is associated with various types of plasticity. For example, increased levels of drebrin are observed in the stimulated layers of the hippocampus after *in vivo* LTP induction (Fukazawa et al., 2003). Conversely, cultured hippocampal neurons with decreased levels of drebrin A expression fail to exhibit the D-APV-induced elevation of NMDARs within spines (Takahashi et al., 2005). Drebrin A is also known to be highly expressed in spines that are just maturing (Takahashi et al., 2003; Aoki et al., 2005). In contrast, drebrin is found in low amounts in brains of Alzheimer's or Down syndrome patients (Harigaya et al., 1996; Hatanpaa et al., 1999; Shim and Lubec, 2002). Our present finding leads us to believe that there is a yet unknown cascade within spines that forms a tight link between cytoskeletal changes via drebrin A and synaptic strength modifications.

NMDAR blockade does not trigger enlargement of spines, but larger spines exhibit greater cytoplasmic plasticity

Since increases in F-actin labeling and over-expression of drebrin A are both known to promote morphological plasticity in spines (Hayashi and Shirao, 1999; Takahashi et al., 2003; Matsuzaki et al., 2004; Mizui et al., 2005), we predicted that the size of spines may change following D-APV application. However, this was not the case. When spine widths and PSD lengths were measured from micrographs, we observed that, despite the apparent increases in cytoskeletal proteins, D-APV application did not induce morphological changes in spines. If anything, the D-APV treatment caused a slight decrease of PSD lengths. This size reduction was measurable only among the population of spines lacking drebrin A. Since the D-APV treatment increased the population of drebrin A-immunoreactive spines, drebrin A may have conferred morphological stability upon an increasing sub-population of spines. These PSD-length reductions among the drebrin A-negative spines did not result in a significant shift in the overall size of spines and PSDs, presumably because the drebrin A-negative spines are much fewer in number. A separate study from our laboratory supports the idea that drebrin A may have a stabilizing influence upon spines (Mahadomrongkul et al., 2005). Together, these findings indicate that drebrin A may stabilize overt morphology, such as the size of spines and PSDs, while also redirecting the intracellular organization of F-actin toward a state favoring trafficking of synaptic proteins, such as the NR2A and NR2B subunits of NMDARs.

There are a number of explanations for why overt morphological changes did not accompany increases in cytoskeletal proteins in this study. One possibility is the one we alluded to earlier, namely that the increases in the cytological detection of the proteins may have been caused by conformational changes, with or without changes in the overall levels of F-actin or of drebrin A. One approach that is tailored more toward measuring protein levels is Western blot analyses. However, studies comparing Western blot data with EM immunocytochemical analyses of spine proteins indicate that neither is a good predictor of the other (Harigaya et al., 1996; Rodrigues et al., 2004; Mahadomrongkul et al., 2005). Such differences in outcomes might be expected, since Western blot analyses cannot exclude proteins residing at subcellular domains outside of spines, while EM-ICC cannot distinguish altered levels of protein detection derived from conformational changes versus protein level changes.

Another explanation for the lack of apparent changes in spine widths is that 2-D analyses fail to detect changes

in spine shapes. However, this explanation seems unlikely, because we could already detect small changes (25 nm, 7.5% change) in PSD lengths within a sample size of 429, or roughly one-quarter of the sample size of all spines encountered. This sample size was likely to have been large enough to minimize the variance of the data (Umbriaco et al., 1994) and detect changes, if there were any.

It is possible that the amount of increases in cytoskeletal proteins triggered by NMDAR blockade is much less than those evoked by LTP-inducing protocols. What we have shown is that changes in the intracellular environment of spines may be separable from the overt changes in spine shape or size.

Molecular steps leading to cytoskeletal reorganization must be explored

Other studies have also shown that prolonged changes in NMDAR activity lead to cytoskeletal reorganization. Matus's group has shown that influx of Ca^{2+} via NMDAR stimulation leads to reduced spine motility (Brunig et al., 2004), and conversely, others have pointed to a link between reduced NMDAR activity and increased spine motility (Fischer et al., 2000; Burrone et al., 2002; Star et al., 2002; Ackermann and Matus, 2003). Together, we hypothesize that decreased levels of NMDAR-mediated synaptic activity may be the trigger that initiates cytoskeletal changes. In the case of the current study, this reorganization may facilitate or be required for trafficking of NMDARs.

Since AMPA-to-NMDA receptor ratio is maintained well following LTP in cortical synapses (Watt et al., 2000), the mechanism regulating NMDAR trafficking may overlap with that for trafficking of AMPA receptors that occur during the late phase of LTP. Matsuzaki's (2004) group and others (Toni et al., 2001; Okamoto et al., 2004) have repeatedly shown that LTP induction increases spine size and F-actin content. This cytoskeletal plasticity seems to be crucial in trafficking of AMPA receptors for the maintenance LTP (Fukazawa et al., 2003). Perhaps accelerated polymerization of actin is required whenever there is an increased targeting of receptors into spine heads, regardless of how receptor trafficking is triggered (by LTP or by smaller changes associated with homeostasis). However, molecular mechanisms that initiate cytoskeletal reorganization are not well understood and await further research.

Acknowledgments—We would like thank Anita Disney and Yuko Sekino for critical reading of the article. We would also like to thank Larry Malone for his help with the statistics. This study was supported by: Grants-in-Aid (12053209) for Scientific Research (T.S.); R01-NS41091, R01-EY13145 (C.A.); P30 EY13079 (J. A. Movshon and C.A.).

REFERENCES

Ackermann M, Matus A (2003) Activity-induced targeting of profilin and stabilization of dendritic spine morphology. Nat Neurosci 6:1194–1200.

Adam G, Matus A (1996) Role of actin in the organisation of brain postsynaptic densities. Brain Res Mol Brain Res 43:246–250.

Allison DW, Chervin AS, Gelfand VI, Craig AM (2000) Postsynaptic scaffolds of excitatory and inhibitory synapses in hippocampal neurons: maintenance of core components independent of actin filaments and microtubules. J Neurosci 20:4545–4554.

Allison DW, Gelfand VI, Spector I, Craig AM (1998) Role of actin in anchoring postsynaptic receptors in cultured hippocampal neurons: differential attachment of NMDA versus AMPA receptors. J Neurosci 18:2423–2436.

Aoki C, Fujisawa S, Mahadomrongkul V, Shah PJ, Nader K, Erisir A (2003) NMDA receptor blockade in intact adult cortex increases trafficking of NR2A subunits into spines, postsynaptic densities, and axon terminals. Brain Res 963:139–149.

Aoki C, Sekino Y, Hanamura K, Fujisawa S, Mahadomrongkul V, Ren Y, Shirao T (2005) Drebrin A is a postsynaptic protein that localizes in vivo to the submembranous surface of dendritic sites forming excitatory synapses. J Comp Neurol 483:383–402.

Baker JP, Titus MA (1998) Myosins: matching functions with motors. Curr Opin Cell Biol 10:80–86.

Barria A, Malinow R (2002) Subunit-specific NMDA receptor trafficking to synapses. Neuron 35:345–353.

Brunig I, Kaech S, Brinkhaus H, Oertner TG, Matus A (2004) Influx of extracellular calcium regulates actin-dependent morphological plasticity in dendritic spines. Neuropharmacology 47:669–676.

Burrone J, O'Byrne M, Murthy VN (2002) Multiple forms of synaptic plasticity triggered by selective suppression of activity in individual neurons. Nature 420:414–418.

Capani F, Martone ME, Deerinck TJ, Ellisman MH (2001) Selective localization of high concentrations of F-actin in subpopulations of dendritic spines in rat central nervous system: a three-dimensional electron microscopic study. J Comp Neurol 435:156–170.

Carpenter-Hyland EP, Woodward JJ, Chandler LJ (2004) Chronic ethanol induces synaptic but not extrasynaptic targeting of NMDA receptors. J Neurosci 24:7859–7868.

Cole JC, Villa BR, Wilkinson RS (2000) Disruption of actin impedes transmitter release in snake motor terminals. J Physiol 525 (Pt 3): 579–586.

Doussau F, Augustine GJ (2000) The actin cytoskeleton and neurotransmitter release: an overview. Biochimie 82:353–363.

Dunah AW, Wyszynski M, Martin DM, Sheng M, Standaert DG (2000) Alpha-actinin-2 in rat striatum: localization and interaction with NMDA glutamate receptor subunits. Brain Res Mol Brain Res 79:77–87.

Evans LL, Lee AJ, Bridgman PC, Mooseker MS (1998) Vesicle-associated brain myosin-V can be activated to catalyze actin-based transport. J Cell Sci 111 (Pt 14):2055–2066.

Fischer M, Kaech S, Wagner U, Brinkhaus H, Matus A (2000) Glutamate receptors regulate actin-based plasticity in dendritic spines. Nat Neurosci 3:887–894.

Freeman MF, Tukey JW (1950) Transformations related to the angular and the square root. Ann Math Stat 21:607–611.

Fujisawa S, Aoki C (2003) In vivo blockade of N-methyl-D-aspartate receptors induces rapid trafficking of NR2B subunits away from synapses and out of spines and terminals in adult cortex. Neuroscience 121:51–63.

Fukazawa Y, Saitoh Y, Ozawa F, Ohta Y, Mizuno K, Inokuchi K (2003) Hippocampal LTP is accompanied by enhanced F-actin content within the dendritic spine that is essential for late LTP maintenance in vivo. Neuron 38:447–460.

Gimona M, Djinovic-Carugo K, Kranewitter WJ, Winder SJ (2002) Functional plasticity of CH domains. FEBS Lett 513:98–106.

Guillaud L, Setou M, Hirokawa N (2003) KIF17 dynamics and regulation of NR2B trafficking in hippocampal neurons. J Neurosci 23: 131–140.

Halpain S (2003) Actin in a supporting role. Nat Neurosci 6:101–102.

Halpain S, Hipolito A, Saffer L (1998) Regulation of F-actin stability in dendritic spines by glutamate receptors and calcineurin. J Neurosci 18:9835–9844.

Harigaya Y, Shoji M, Shirao T, Hirai S (1996) Disappearance of actin-binding protein, drebrin, from hippocampal synapses in Alzheimer's disease. J Neurosci Res 43:87–92.

Hatanpaa K, Isaacs KR, Shirao T, Brady DR, Rapoport SI (1999) Loss of proteins regulating synaptic plasticity in normal aging of the human brain and in Alzheimer disease. J Neuropathol Exp Neurol 58:637–643.

Hayashi K, Shirao T (1999) Change in the shape of dendritic spines caused by overexpression of drebrin in cultured cortical neurons. J Neurosci 19:3918–3925.

Ishikawa R, Hayashi K, Shirao T, Xue Y, Takagi T, Sasaki Y, Kohama K (1994) Drebrin, a development-associated brain protein from rat embryo, causes the dissociation of tropomyosin from actin filaments. J Biol Chem 269:29928–29933.

Kaech S, Parmar H, Roelandse M, Bornmann C, Matus A (2001) Cytoskeletal microdifferentiation: a mechanism for organizing morphological plasticity in dendrites. Proc Natl Acad Sci U S A 98: 7086–7092.

Li Z, Okamoto K, Hayashi Y, Sheng M (2004) The importance of dendritic mitochondria in the morphogenesis and plasticity of spines and synapses. Cell 119:873–887.

Mahadomrongkul V, Huerta PT, Shirao T, Aoki C (2005) Stability of the distribution of spines containing drebrin A in the sensory cortex layer I of mice expressing mutated APP and PS1 genes. Brain Res 1064:66–74.

Matsuzaki M, Honkura N, Ellis-Davies GC, Kasai H (2004) Structural basis of long-term potentiation in single dendritic spines. Nature 429:761–766.

Mizui T, Takahashi H, Sekino Y, Shirao T (2005) Overexpression of drebrin A in immature neurons induces the accumulation of F-actin and PSD-95 into dendritic filopodia, and the formation of large abnormal protrusions. Mol Cell Neurosci 30:149–157.

Morales M, Fifkova E (1989) In situ localization of myosin and actin in dendritic spines with the immunogold technique. J Comp Neurol 279:666–674.

Mouton P (2002) Principles and practices of unbiased stereology. Baltimore: Johns Hopkins University Press.

Naisbitt S, Valtschanoff J, Allison DW, Sala C, Kim E, Craig AM, Weinberg RJ, Sheng M (2000) Interaction of the postsynaptic density-95/guanylate kinase domain-associated protein complex with a light chain of myosin-V and dynein. J Neurosci 20:4524–4534.

Nakagawa T, Engler JA, Sheng M (2004) The dynamic turnover and functional roles of alpha-actinin in dendritic spines. Neuropharmacology 47:734–745.

Okamoto K, Nagai T, Miyawaki A, Hayashi Y (2004) Rapid and persistent modulation of actin dynamics regulates postsynaptic reorganization underlying bidirectional plasticity. Nat Neurosci 7: 1104–1112.

Phend KD, Rustioni A, Weinberg RJ (1995) An osmium-free method of epon embedment that preserves both ultrastructure and antigenicity for post-embedding immunocytochemistry. J Histochem Cytochem 43:283–292.

Qualmann B, Boeckers TM, Jeromin M, Gundelfinger ED, Kessels MM (2004) Linkage of the actin cytoskeleton to the postsynaptic density via direct interactions of Abp1 with the ProSAP/Shank family. J Neurosci 24:2481–2495.

Rao A, Craig AM (1997) Activity regulates the synaptic localization of the NMDA receptor in hippocampal neurons. Neuron 19:801–812.

Rodrigues SM, Farb CR, Bauer EP, LeDoux JE, Schafe GE (2004) Pavlovian fear conditioning regulates Thr286 autophosphorylation of Ca2+/calmodulin-dependent protein kinase II at lateral amygdala synapses. J Neurosci 24:3281–3288.

Rosenmund C, Westbrook GL (1993) Calcium-induced actin depolymerization reduces NMDA channel activity. Neuron 10:805–814.

Sankaranarayanan S, Atluri PP, Ryan TA (2003) Actin has a molecular scaffolding, not propulsive, role in presynaptic function. Nat Neurosci 6:127–135.

Schulz TW, Nakagawa T, Licznerski P, Pawlak V, Kolleker A, Rozov A, Kim J, Dittgen T, Kohr G, Sheng M, Seeburg PH, Osten P (2004) Actin/{alpha}-actinin-dependent transport of AMPA receptors in dendritic spines: role of the PDZ-LIM protein RIL. J Neurosci 24:8584–8594.

Setou M, Nakagawa T, Seog D-H, Hirokawa N (2000) Kinesin superfamily motor protein KIF17 and mLin-10 in NMDA receptor-containing vesicle transport. Science 288:1796–1802.

Shim KS, Lubec G (2002) Drebrin, a dendritic spine protein, is manifold decreased in brains of patients with Alzheimer's disease and Down syndrome. Neurosci Lett 324:209–212.

Shirao T, Sekino Y (2001) Clustering and anchoring mechanisms of molecular constituents of postsynaptic scaffolds in dendritic spines. Neurosci Res 40:1–7.

Shupliakov O, Bloom O, Gustafsson JS, Kjaerulff O, Low P, Tomilin N, Pieribone VA, Greengard P, Brodin L (2002) Impaired recycling of synaptic vesicles after acute perturbation of the presynaptic actin cytoskeleton. Proc Natl Acad Sci U S A 99:14476–14481.

Sjostrom PJ, Turrigiano GG, Nelson SB (2003) Neocortical LTD via coincident activation of presynaptic NMDA and cannabinoid receptors. Neuron 39:641–654.

Star EN, Kwiatkowski DJ, Murthy VN (2002) Rapid turnover of actin in dendritic spines and its regulation by activity. Nat Neurosci 5:239–246.

Takahashi H, Mizui T, Shirao T (2005) Down-regulation of drebrin A expression suppresses synaptic targeting of NMDA receptors in developing hippocampal neurones. J Neurochem. 97(S1):110–115. doi:10.1111/j.1471-4159.2005.03536x.

Takahashi H, Sekino Y, Tanaka S, Mizui T, Kishi S, Shirao T (2003) Drebrin-dependent actin clustering in dendritic filopodia governs synaptic targeting of postsynaptic density-95 and dendritic spine morphogenesis. J Neurosci 23:6586–6595.

Toni N, Buchs P-A, Nikonenko I, Povilaitite P, Parisi L, Muller D (2001) Remodeling of synaptic membranes after induction of long-term potentiation. J Neurosci 21:6245–6251.

Turrigiano GG (1999) Homeostatic plasticity in neuronal networks: the more things change, the more they stay the same. Trends Neurosci 22:221–227.

Umbriaco D, Watkins KC, Descarries L, Cozzari C, Hartman BK (1994) Ultrastructural and morphometric features of the acetylcholine innervation in adult rat parietal cortex: an electron microscopic study in serial sections. J Comp Neurol 348:351–373.

van Rossum D, Hanisch UK (1999) Cytoskeletal dynamics in dendritic spines: direct modulation by glutamate receptors? Trends Neurosci 22:290–295.

Walikonis RS, Jensen ON, Mann M, Provance DW Jr, Mercer JA, Kennedy MB (2000) Identification of proteins in the postsynaptic density fraction by mass spectrometry. J Neurosci 20:4069–4080.

Watt AJ, van Rossum MC, MacLeod KM, Nelson SB, Turrigiano GG (2000) Activity coregulates quantal AMPA and NMDA currents at neocortical synapses. Neuron 26:659–670.

White E (1989) Cortical circuits: synaptic organization of the cerebral cortex. Boston: Birkhauser.

Wierenga CJ, Ibata K, Turrigiano GG (2005) Postsynaptic expression of homeostatic plasticity at neocortical synapses. J Neurosci 25: 2895–2905.

Woodhall G, Evans DI, Cunningham MO, Jones RS (2001) NR2B-containing NMDA autoreceptors at synapses on entorhinal cortical neurons. J Neurophysiol 86:1644–1651.

Wu H, Nash JE, Zamorano P, Garner CC (2002) Interaction of SAP97 with minus-end-directed actin motor myosin VI. Implications for AMPA receptor trafficking. J Biol Chem 277:30928–30934.

Wyszynski M, Lin J, Rao A, Nigh E, Beggs AH, Craig AM, Sheng M (1997) Competitive binding of alpha-actinin and calmodulin to the NMDA receptor. Nature 385:439–442.

Zhou Q, Xiao M-Y, Nicoll RA (2001) Contribution of cytoskeleton to the internalization of AMPA receptors. Proc Natl Acad Sci U S A 98: 1261–1266.

(Accepted 6 March 2006)

Journal of Neurochemistry, 2006, **97** (Suppl. 1), 110–115 doi:10.1111/j.1471-4159.2005.03536.x

SPECIAL ISSUE

Down-regulation of drebrin A expression suppresses synaptic targeting of NMDA receptors in developing hippocampal neurones

Hideto Takahashi, Toshiyuki Mizui and Tomoaki Shirao

Department of Neurobiology and Behavior, Gunma University Graduate School of Medicine, Maebashi, Gunma, Japan

Abstract

Drebrin is a major F-actin-binding protein in the brain. We have recently demonstrated that drebrin A (neurone-specific isoform) clusters at synapses and governs targeting of the post-synaptic density 95 protein to synapses during development. To determine the role of drebrin A on excitatory synapse formation, we analysed whether the suppression of drebrin A expression affects filopodia-spine morphology and synaptic targeting of NMDA receptors in cultured hippocampal neurones. Suppression of developmentally programmed up-regulation of drebrin A by antisense treatment significantly decreased the density and width of filopodia-spines. Immunocytochemistry showed that the antisense treatment did not attenuate synaptic clustering of NMDA receptors under conditions that permitted spontaneous activities but inhibited the accelerated targeting of NMDA receptors into synapses by its antagonist D-(–)-2-amino-5-phosphonopentanoic acid. These results indicate that drebrin A up-regulation plays a pivotal role in spine morphogenesis and activity-dependent synaptic targeting of NMDA receptors.

Keywords: actin cytoskeleton, antisense oligonucleotide, dendritic spine, drebrin, NMDA receptor, synaptic targeting.
J. Neurochem. (2006) **97** (Suppl. 1), 110–115.

Drebrin A is a neurone-specific F-actin-binding protein and its expression is increased in parallel with synapse formation (see review, Shirao 1995). Drebrin A is found exclusively in dendrites and is particularly concentrated in dendritic spines (Aoki *et al*. 2005). Overexpression of drebrin A in mature neurones induces elongation of spines (Hayashi and Shirao 1999). Down-regulation of drebrin A expression during the process of spine morphogenesis suppresses the accumulation of spinal F-actin, the most prevalent cytoskeletal element in spines (Takahashi *et al*. 2003). These observations suggest that spine morphogenesis depends on the drebrin A accumulation in the spine.

Further, drebrin is necessary for synaptic clustering of a post-synaptic density (PSD) scaffold protein, PSD-95 (Takahashi *et al*. 2003). PSDs contain high concentrations of NMDA receptors (NMDARs) as well as PSD-95 (Kennedy 2000). As PSD-95 binds to the NMDAR subunits NR2A and NR2B (Niethammer *et al*. 1996), drebrin A might also regulate synaptic targeting of NMDARs via PSD-95.

In this study, we analysed whether down-regulation of drebrin A expression affects spine morphogenesis and synaptic targeting of NMDARs in developing hippocampal neurones. Our results indicate that developmentally programmed up-regulation of drebrin A expression is involved in the spine morphogenesis and activity-dependent synaptic targeting of NMDAR.

Materials and methods

Hippocampal cell culture and antisense treatment

Low-density cell cultures of hippocampal neurones were prepared by Banker's methods (Takahashi *et al*. 2003). D-(–)-2-amino-5-phosphonopentanoic acid (AP5; 50 μM) (Tocris, Ellisville, MO,

Received June 15, 2005; revised manuscript received August 18, 2005; accepted September 19, 2005.

Address correspondence and reprint requests to Tomoaki Shirao, Department of Neurobiology and Behavior, Gunma University Graduate School of Medicine, 3-39-22, Showamachi, Maebashi, Gunma, 371-8511, Japan. E-mail: tshirao@med.gunma-u.ac.jp

Abbreviations used: AOD, antisense oligonucleotides against drebrin A-specific exon; AP5, D-(–)-2-amino-5-phosphonopentanoic acid; DIV, days *in vitro*; NMDAR, NMDA receptor; PLSD, protected least significant difference tests; PSD, post-synaptic density; ROD, reversed antisense oligonucleotides against drebrin A-specific exon.

USA) was added to the culture medium from 14 days *in vitro* (DIV). Antisense oligonucleotides against drebrin A-specific exon (AOD; 10 μM) and reversed AOD (ROD; 10 μM) were used as described previously (Takahashi *et al*. 2003). ROD-treated neurones represented an immunostaining pattern of NR1 and synapsin I similar to untreated neurones (data not shown). Therefore, we used ROD-treated neurones as controls for the analysis of the synaptic targeting of NR1.

Western blot, F-actin staining and immunocytochemistry

Western blot, F-actin staining and immunocytochemistry were performed as described previously (Takahashi *et al*. 2003), with a minor modification. For immunocytochemistry, neurones were simultaneously fixed and permeabilized in methanol for 10 min at −20°C. We used mouse monoclonal anti-NR1 antibody (clone 54.1, PharMingen, San Diego, CA, USA), which recognizes all splice variants of NR1, and polyclonal anti-synapsin I antibody (Chemicon, Temecula, CA, USA). The acquisition of fluorescent images, analysis of captured images and preparation of images for presentation were performed as described previously (Takahashi *et al*. 2003).

Quantification

For quantification of spine morphology, spiny neurones with pyramidal morphology were selected from four independent cultures using phalloidin staining. The dendrites that existed between the cell soma and second branch point were selected for the analysis. Dendritic protrusions were selected as described previously (Takahashi *et al*. 2003). The maximum length and width of each protrusion were manually measured. For quantification of NR1 and PSD-95 clustering, we obtained the data from two independent cultures. NR1 and PSD-95 clusters were defined as a round stained region with a peak fluorescent intensity that was twofold greater than the averaged fluorescent intensity of dendrites. NR1 clusters were judged to be 'synaptic' when the NR1 clusters overlapped with synapsin I clusters at one or more pixels of each fluorescent imaging. Data were statistically analysed by Student's *t*-test for comparing between two groups or by ANOVA with a post-hoc test using Fisher's protected least significant difference tests (PLSD) for multiple comparisons, as applicable. All data are presented as the mean ± SEM.

Results

Down-regulation of drebrin A expression decreased the density and width of filopodia-spines of developing hippocampal neurones

Our previous studies have shown that developmental up-regulation of drebrin A expression in the cerebral cortex and hippocampus occurs after 1 week post-natal *in vivo* (Aoki *et al*. 2005). We first analysed whether drebrin A up-regulation occurs in the hippocampal neurones in low-density cultures similar to that *in vivo* (Fig. 1a). Western

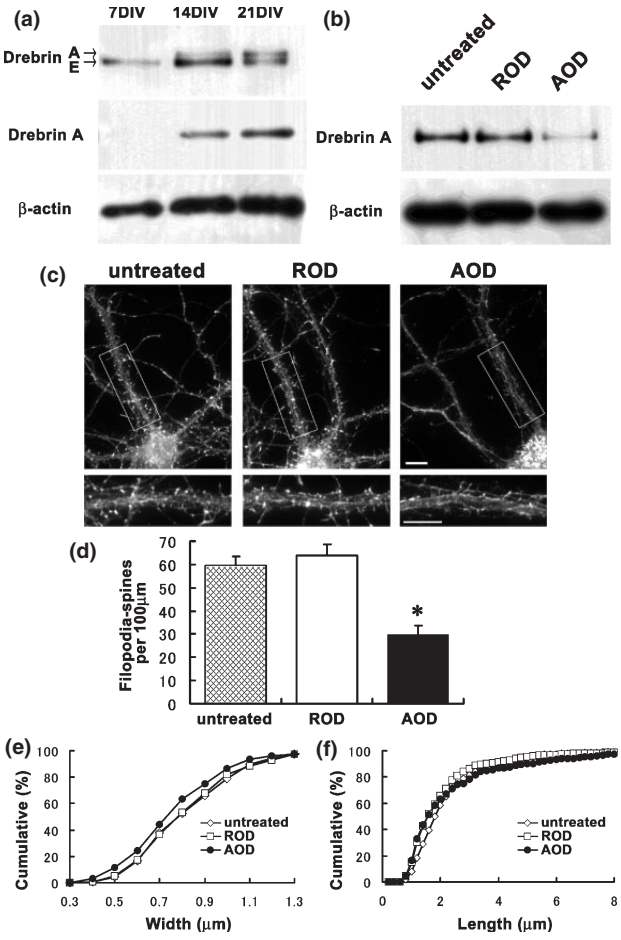

Fig. 1 Developmental up-regulation of drebrin A expression and effects of antisense oligonucleotides against drebrin A-specific exon (AOD) treatment on morphological characterization of filopodia-spines. (a) Proteins equivalent to 1/20 of a culture dish at 7, 14 and 21 days *in vitro* (DIV) were separated by sodium dodecyl sulphate–polyacrylamide gel electrophoresis, blotted onto the membrane and immunostained with antibodies specific to pan-drebrin (M2F6), drebrin A and β-actin. Immunoreactivity of drebrin A at 7 DIV is hardly detected. Note that drebrin A expression is up-regulated after 14 DIV. (b) Western blots showing a representative effect of AOD and reversed AOD (ROD) on expression of drebrin A and β-actin. 12-DIV neurones were cultured further for 2 days in the medium supplemented without antisense oligonucleotides (untreated) and in those with 10 μM ROD and 10 μM AOD. AOD treatment selectively inhibits the expression of drebrin A. ROD treatment has no effect on the expression of drebrin and β-actin. (c) F-actin labelling of untreated, ROD-treated or AOD-treated neurones. Top panels show grayscale images of F-actin labelling of untreated (left), ROD-treated (middle) and AOD-treated (right) neurones. Boxed regions in top panels are shown below at higher magnification. Scale bars, 10 μm (top panels) and 5 μm (bottom panels). (d) A histogram of filopodia-spine density (number of filopodia-spines/100 μm dendrite; mean + SEM) of each neurone group ($n = 20$ dendritic segments for each group; $^*p < 0.0001$) Fisher's protected least significant difference tests (PLSD). Cumulative frequency plots of filopodia-spine width (e) and length (f) of untreated, ROD-treated and AOD-treated neurones (961, 720 and 342 filopodia-spines from the 20 dendritic segments of untreated, ROD-treated and AOD-treated neurones, respectively). All morphometric measurements were performed using phalloidin staining.

blot using anti-drebrin antibody showed a single band at 7 DIV and double bands at 14 and 21 DIV. The upper band for drebrin corresponds to drebrin A and the lower band to drebrin E. Western blot using antibody specific to the drebrin A isoform also showed that drebrin A was hardly detected at 7 DIV. Faint and intense bands of drebrin A were detected at 14 and 21 DIV, respectively. Western blot using anti-β-actin antibody showed a slightly more intense band at 14 than at 7 DIV.

We have previously shown that AOD treatment (10 μM for 2 days from 12 DIV) significantly reduces drebrin A expression to 48% of untreated neurones but does not affect β-actin expression (Takahashi *et al*. 2003). ROD (control sense) treatment did not have any effect on either drebrin A or β-actin expression (Fig. 1b). In the present study, we performed phalloidin labelling at 14 DIV of untreated, ROD-treated and AOD-treated neurones (Fig. 1c), and analysed the density and morphology of dendritic protrusions emerging from dendrites (called filopodia-spines) of each treated neurone (Figs 1d–f). Filopodia-spine density in AOD-treated neurones (29.6 ± 3.9 filopodia-spines/100 μm, $n = 20$ dendritic segments) was significantly less than that in untreated (59.6 ± 3.4 filopodia-spines/100 μm, $n = 20$ dendritic segments) and ROD-treated (64.1 ± 4.6 filopodia-spines/100 μm, $n = 20$ dendritic segments) neurones ($p < 0.0001$) (Fig. 1d). There was no significant difference in the filopodia-spine density between untreated and ROD-treated neurones. Filopodia-spine width in AOD-treated neurones (0.72 ± 0.02 μm) was significantly less than that in untreated (0.79 ± 0.02 μm) and ROD-treated (0.80 ± 0.02 μm) neurones ($p < 0.05$) (Fig. 1e). However, there was no significant difference in filopodia-spine length among untreated (2.28 ± 0.13 μm), ROD-treated (2.16 ± 0.15 μm) and AOD-treated (2.61 ± 0.20 μm) neurones (ANOVA, $F = 1.96$, $p = 0.15$) (Fig. 1f).

Down-regulation of drebrin A expression inhibited synaptic clustering of NMDA receptors accelerated by chronic blockade of NMDA receptor activities

We analysed the effect of drebrin A down-regulation on synaptic clustering of NR1 subunit, which is the essential subunit for NMDARs. It has been reported that NR1 is not highly clustered at synapses under conditions of spontaneous activity but that chronic blockade of NMDARs causes an increase in synaptic NR1 clustering (Rao & Craig 1997). Therefore, we incubated 14-DIV ROD-treated (control) and AOD-treated neurones with or without the application of NMDAR antagonist AP5 (50 μM) for 48 h and then labelled them dually with anti-NR1 and anti-synapsin I antibodies (Fig. 2a).

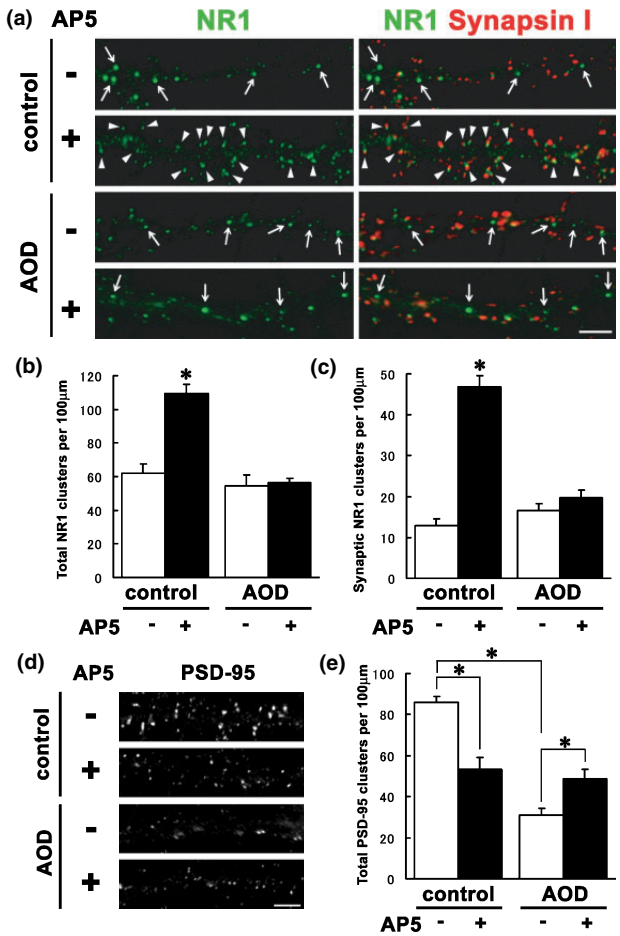

Fig. 2 Activity-dependent synaptic targeting of NR1 is inhibited by the suppression of drebrin A expression. Cultured hippocampal neurones (12 days *in vitro*) were incubated in the medium containing antisense oligonucleotides against drebrin A-specific exon (AOD) or reversed AOD (ROD) for 2 days and further incubated in the above medium supplemented with or without 50 μM D-(–)-2-amino-5-phosphonopentanoic acid (AP5) for another 2 days. The neurones were then double-labelled for NR1 and synapsin I. (a) Left panels show NR1 staining in ROD-treated (control) and AOD-treated neurones with or without AP5 exposure. Right panels show double labelling for NR1 (green) and synapsin I (red). In control neurones, AP5 exposure increased NR1 clusters, which were associated with synapsin I clusters (second top, arrowheads). In contrast, in AOD-treated neurones, AP5 exposure had no effect on NR1 clustering (bottom). Arrows indicate non-synaptic NR1 clusters. Scale bars, 5 μm. Quantitative analysis of densities of total (b) and synaptic (c) NR1 clusters in the ROD-treated (control) and AOD-treated neurones with or without AP5 exposure. Note that the density of total and synaptic NR1 clusters of the control neurones exposed to AP5 is significantly higher than those of three other neuronal groups ($n = 30$ dendritic segments for each group, $^*p < 0.0001$, Fisher's PLSD). (d) Post-synaptic density (PSD)-95 immunostaining in control and AOD-treated neurones with or without AP5 exposure. In control neurones, AP5 treatment decreases PSD-95 clustering. In contrast, in AOD-treated neurones, AP5 treatment increases PSD-95 clustering. (e) Quantitative analysis of density of total PSD-95 clusters of each treated group. Note that AP5 treatment induced a different response of PSD-95 from that of NR1 in both control and AOD-treated neurones ($n = 20$ dendritic segments for each group, $^*p < 0.0001$, Fisher's PLSD).

Without AP5 exposure, control neurones showed NR1 clusters along dendrites, which were hardly associated with synapsin I clusters (Fig. 2a, top, arrows). AOD-treated neurones without AP5 exposure also showed a similar immunostaining pattern of NR1 to that of control neurones (Fig. 2a, third top).

With AP5 exposure, control neurones increased the number of NR1 clusters, which were associated with synapsin I clusters (Fig. 2a, second top, arrowheads). These data indicate that the AP5 treatment accelerated synaptic targeting of NR1 clusters, which is consistent with a previous study (Rao and Craig 1997). In contrast, AOD-treated neurones with AP5 exposure kept showing NR1 clusters along dendrites, which were hardly associated with synapsin I clusters (Fig. 2a, bottom).

We determined the density of total and synaptic NR1 clusters in neurones following each of four conditions and statistically analysed the differences among them ($n = 30$ for each group, ANOVA with Fisher's PLSD) (Figs 2b and c). The density of total NR1 clusters of control neurones with AP5 exposure (109.5 ± 5.5 clusters/100 μm) is significantly higher than those of other neurones (control neurones without AP5, 62.0 ± 5.6; AOD-treated neurones without AP5, 54.5 ± 6.7; AOD-treated neurones with AP5, 56.3 ± 2.8 clusters/100 μm) ($p < 0.0001$) (Fig. 2b). The density of synaptic NR1 clusters of control neurones with AP5 exposure (46.8 ± 2.8 clusters/100 μm) is also significantly higher than those of other neurones (control neurones without AP5, 12.9 ± 1.6; AOD-treated neurones without AP5, 16.5 ± 1.8; AOD-treated neurones with AP5, 19.7 ± 2.0 clusters/100 μm) ($p < 0.0001$) (Fig. 2c). These quantitative data also showed that AOD treatment did not affect the density of total and synaptic NR1 clusters in the absence of AP5. In contrast, AOD treatment inhibited the AP5 inducing increase of the density of total and synaptic NR1 clusters.

Post-synaptic density 95 binds to NR2A and NR2B of the NMDAR subunits (Niethammer *et al*. 1996). In mature hippocampal neurones, NMDAR blockade does not affect the distribution of PSD-95 but induces a redistribution of NMDARs to synaptic sites previously containing PSD-95 (Rao & Craig 1997). We have previously shown that synaptic PSD-95 clustering depends on prior drebrin clustering, which is triggered by drebrin A up-regulation in developing hippocampal neurones (Takahashi *et al*. 2003). Therefore, we determined the density of total PSD-95 clusters in neurones following each of four conditions used in the NMDAR experiments here and statistically analysed the differences among them ($n = 20$ for each group, ANOVA with Fisher's PLSD) (Figs 2d and e). Control neurones without AP5 exposure had a large number of PSD-95 clusters (86.1 ± 2.8 clusters/100 μm). On the other hand, control neurones with AP5 exposure had a significant number (53.4 ± 5.8 clusters/100 μm) of PSD-95 clusters but a smaller number of PSD-95 clusters than control neurones without AP5 exposure ($p < 0.0001$). AOD-treated neurones without AP5 exposure also had a smaller number (30.9 ± 3.3 clusters/100 μm) of PSD-95 clusters than control neurones without AP5 exposure ($p < 0.0001$), which is consistent with our previous study (Takahashi *et al*. 2003). Interestingly, AOD-treated neurones with AP5 exposure had a larger number (48.7 ± 4.5 clusters/100 μm) of PSD-95 clusters than AOD-treated neurones without AP5 exposure ($p < 0.001$). These data indicate the possibility that synaptic clustering of NMDAR accelerated by AP5 exposure is independent of the molecular interaction between PSD-95 and NMDARs.

Discussion

In this study, we suppressed the developmentally programmed up-regulation of drebrin A in cultured hippocampal neurones by AOD treatment, so as to analyse the role of drebrin A on spine morphogenesis and synaptic targeting of NMDARs. The AOD treatment decreases filopodia-spine density and width, indicating that drebrin A up-regulation is necessary for formation and/or maintenance of filopodia-spines during development. Synaptic clustering of NMDARs is accelerated by AP5 treatment and this acceleration was also inhibited by the AOD treatment. AOD treatment has no effect on synaptic targeting of NMDARs under conditions of spontaneous activity. These data indicate that drebrin A plays a pivotal role in spine morphogenesis and activity-dependent alteration of synaptic NMDAR clustering.

Down-regulation of drebrin A causes the reduction in density and width of filopodia-spines. Our previous study has shown that down-regulation of drebrin A inhibits clustering of drebrin, F-actin and PSD-95 at synapses on filopodia-spines (Takahashi *et al*. 2003). These data indicate that drebrin A is necessary for spine formation. However, our recent study has shown that overexpression of drebrin A does not promote spine formation in immature neurones, although it accumulates F-actin and PSD-95 into dendritic protrusions (Mizui *et al*. 2005). These data suggest that drebrin A plays a role in spine maintenance as well as spine formation. In fact, drebrin A expression in fibroblasts induces cytochalasin D-resistant actin structures at their adhesion plaques (Ikeda *et al*. 1996). The dendritic spine is also a type of specialized adhesion machinery with the accumulation of cytochalasin D-resistant F-actin (Allison *et al*. 1998). Taken together, it is suggested that the ability of drebrin A to accumulate spinal proteins and stabilize F-actin contributes to spine formation and/or spine maintenance.

NMDA receptor clusters can already be observed at 1 week *in vitro* (Rao *et al*. 1998), prior to the expression of drebrin A. Such NMDAR clusters are localized on dendritic shafts but not in spines. After 1 week *in vitro*, when drebrin A expression is up-regulated, NMDAR clusters change their localization from shafts to spines. The present study demonstrates that AOD treatment inhibits AP5-accelerated

synaptic clustering of NR1 without altering the NR1 clusters under conditions of spontaneous activity. This indicates that drebrin A is involved in synaptic targeting of NMDAR clusters, rather than NMDAR cluster formation itself.

D-(–)-2-amino-5-phosphonopentanoic acid exposure increased the density of both total and synaptic NR1 clusters in control neurones. These results raise two possibilities: (i) that AP5 exposure increases NR1 clustering itself and the density of synaptic clusters passively increased thereafter and (ii) that AP5 exposure specifically promotes targeting of NR1 into synapses. The present study shows that AP5 exposure increases synaptic NR1 cluster density to 359 ± 21% (n = 30) of control neurones without AP5 exposure, whereas AP5 exposure increases non-synaptic NR1 cluster density to only 128 ± 11% ($p < 0.0001$). Therefore, our data support the second possibility. In AOD-treated neurones, AP5 exposure leads to no significant change in synaptic NR1 (119 ± 12% of AOD-treated neurones without AP5 exposure) and non-synaptic NR1 (96 ± 11%) cluster density. Taken together, it is suggested that down-regulation of drebrin A inhibits AP5-accelerated targeting of NR1 into synapses.

One possible explanation for the suppression of AP5-accelerated NMDAR clustering by AOD treatment is the reduction of filopodia-spine density, rather than a direct effect of AOD upon NMDAR cluster targeting to synapses. However, this possibility is unlikely because the present study shows that ROD-treated (control) neurones with AP5 exposure increase synaptic NR1 cluster density to 359 ± 21% (n = 30) of control neurones without AP5 exposure. Here, we assume the hypothetical condition that all synapses locate on filopodia-spines, which maximizes the effect of filopodia-spine loss on synaptic targeting of NR1. As the AOD treatment causes filopodia-spine density to decrease to about 50% of control neurones (see Fig. 1d), if the NR1 clustering were to remain the same then AOD-treated neurones with AP5 exposure should increase NR1 cluster density to about 180% of AOD-treated neurones without AP5 exposure, which is 50% of the control neurones' AP5-induced change. However, the present study shows that the increase of synaptic NR1 cluster density of AOD-treated neurones by AP5 exposure is 119 ± 12% (n = 30). This is significantly lower than the above estimated percentage, even in this assumption ($p < 0.0001$, t-test). Therefore, it is clear that drebrin A down-regulation reduces NR1 cluster density by inhibition of synaptic targeting of NMDARs rather than just by filopodia-spine loss.

How does drebrin A regulate synaptic targeting of NR1 clusters? As far as we know, there are no data showing a direct interaction between drebrin and NMDARs. It has been reported that PSD-95 binds to NR2A and NR2B NMDAR subunits (Niethammer *et al*. 1996). As we have shown that drebrin A down-regulation inhibits synaptic clustering of PSD-95 in developing hippocampal neurones (Takahashi *et al*. 2003), drebrin may indirectly regulate synaptic targeting of NMDARs via PSD-95. However, PSD-95 mutant mice represent normal synaptic localization of NMDARs (Migaud *et al*. 1998). Further, overexpression of PSD-95 does not promote synaptic targeting of NMDARs (El-Husseini *et al*. 2000), although it has been reported that overexpression of PSD-95 enhances excitatory synapse size and reduces the number of inhibitory synaptic contacts (Prange *et al*. 2004). In addition, we here show that AP5 treatment in control neurones accelerates synaptic clustering of NMDAR but diminishes PSD-95 clustering and that AP5 treatment in AOD-treated neurones has no effect on synaptic clustering of NMDAR but enhances PSD-95 clustering. These data do not support the idea that drebrin regulates synaptic targeting of NMDARs via PSD-95.

It is known that activity-dependent alterations in NMDAR trafficking play a role in a homeostatic form of plasticity 'synaptic scaling' (Perez-Otano and Ehlers 2005). The present study clearly demonstrates that down-regulation of drebrin A does not affect NMDAR distribution under conditions of spontaneous activity but affects NMDAR accumulation under conditions of homeostatic synaptic scaling. Thus, it is suggested that drebrin A is a strong candidate governing homeostatic synaptic scaling.

Acknowledgements

We thank Dr Chiye Aoki for useful comments and Tomoko Takahashi for preparing hippocampal cultures. This work was supported in part by Grants-in-Aid for Scientific Research (1253209 and 17023008) from the Ministry of Education, Culture, Sports, Science and Technology of Japan.

References

Allison D. W., Gelfand V. I., Spector I. and Craig A. M. (1998) Role of actin in anchoring postsynaptic receptors in cultured hippocampal neurons: differential attachment of NMDA versus AMPA receptors. *J. Neurosci.* **18**, 2423–2436.

Aoki C., Sekino Y., Hanamura K., Fujisawa S., Mahadomrongkul V., Ren Y. and Shirao T. (2005) Drebrin A is a postsynaptic protein that localizes in vivo to the submembranous surface of dendritic sites forming excitatory synapses. *J. Comp. Neurol.* **483**, 383–402.

El-Husseini A. E., Schnell E., Chetkovich D. M., Nicoll R. A. and Bredt D. S. (2000) PSD-95 involvement in maturation of excitatory synapses. *Science* **290**, 1364–1368.

Hayashi K. and Shirao T. (1999) Change in the shape of dendritic spines caused by overexpression of drebrin in cultured cortical neurons. *J. Neurosci.* **19**, 3918–3925.

Ikeda K., Kaub P. A., Asada H., Uyemura K., Toya S. and Shirao T. (1996) Stabilization of adhesion plaques by the expression of drebrin A in fibroblasts. *Brain Res. Dev. Brain Res.* **91**, 227–236.

Kennedy M. B. (2000) Signal-processing machines at the postsynaptic density. *Science* **290**, 750–754.

Migaud M., Charlesworth P., Dempster M. *et al.* (1998) Enhanced long-term potentiation and impaired learning in mice with mutant postsynaptic density-95 protein. *Nature* **396**, 433–439.

Mizui T., Takahashi H., Sekino Y. and Shirao T. (2005) Overexpression of drebrin A in immature neurons induces the

accumulation of F-actin and PSD-95 into dendritic filopodia, and the formation of large abnormal protrusions. *Mol. Cell. Neurosci.* **30**, 149–157.

Niethammer M., Kim E. and Sheng M. (1996) Interaction between the C terminus of NMDA receptor subunits and multiple members of the PSD-95 family of membrane-associated guanylate kinases. *J. Neurosci.* **16**, 2157–2163.

Perez-Otano I. and Ehlers M. D. (2005) Homeostatic plasticity and NMDA receptor trafficking. *Trends Neurosci.* **28**, 229–238.

Prange O., Wong T. P., Gerrow K., Wang Y. T. and El-Husseini A. (2004) A balance between excitatory and inhibitory synapses is controlled by PSD-95 and neuroligin. *Proc. Natl. Acad. Sci. USA* **101**, 13 915–13 920.

Rao A. and Craig A. M. (1997) Activity regulates the synaptic localization of the NMDA receptor in hippocampal neurons. *Neuron* **19**, 801–812.

Rao A., Kim E., Sheng M. and Craig A. M. (1998) Heterogeneity in the molecular composition of excitatory postsynaptic sites during development of hippocampal neurons in culture. *J. Neurosci.* **18**, 1217–1229.

Shirao T. (1995) The roles of microfilament-associated proteins, drebrins, in brain morphogenesis: a review. *J. Biochem. (Tokyo)* **117**, 231–236.

Takahashi H., Sekino Y., Tanaka S., Mizui T., Kishi S. and Shirao T. (2003) Drebrin-dependent actin clustering in dendritic filopodia governs synaptic targeting of postsynaptic density-95 and dendritic spine morphogenesis. *J. Neurosci.* **23**, 6586–6595.

